



HAL
open science

Disruption of Amygdala Tsc2 in Adolescence Leads to Changed Prelimbic Cellular Activity and Generalized Fear Responses at Adulthood in Rats

Fanny Joly, Pauline Jeckel, Martin Kriebel, Sanket Raut, Nicole El Massioui, Cyrille Vaillend, Luke Johnson, Hansjürgen Volkmer, Valérie Doyère

► **To cite this version:**

Fanny Joly, Pauline Jeckel, Martin Kriebel, Sanket Raut, Nicole El Massioui, et al.. Disruption of Amygdala Tsc2 in Adolescence Leads to Changed Prelimbic Cellular Activity and Generalized Fear Responses at Adulthood in Rats. *Cerebral Cortex*, 2022, 32 (20), pp.4619-4639. 10.1093/cercor/bhab506 . hal-03582450

HAL Id: hal-03582450

<https://cnrs.hal.science/hal-03582450v1>

Submitted on 7 Nov 2022

HAL is a multi-disciplinary open access archive for the deposit and dissemination of scientific research documents, whether they are published or not. The documents may come from teaching and research institutions in France or abroad, or from public or private research centers.

L'archive ouverte pluridisciplinaire **HAL**, est destinée au dépôt et à la diffusion de documents scientifiques de niveau recherche, publiés ou non, émanant des établissements d'enseignement et de recherche français ou étrangers, des laboratoires publics ou privés.



Disruption of amygdala Tsc2 in adolescence leads to changed prelimbic cellular activity and generalized fear responses at adulthood in rats

| | |
|-------------------------------|---|
| Journal: | <i>Cerebral Cortex</i> |
| Manuscript ID | CerCor-2021-00504.R1 |
| Manuscript Type: | Original Article |
| Date Submitted by the Author: | 07-Dec-2021 |
| Complete List of Authors: | Joly, Fanny; Paris-Saclay Institute of Neuroscience, Cognitive and Network Neurosciences Jeckel, Pauline; Natural and Medical Sciences Institute at the University of Tübingen, Molecular cell biology Kriebel, Martin; Natural and Medical Sciences Institute at the University of Tübingen, Department of Molecular Biology, Natural and Medical Sciences Institute (NMI) Raut, Sanket; University of Tasmania College of Health and Medicine, School of Psychological Science El Massioui, Nicole ; Paris-Saclay Institute of Neuroscience, Cognitive and Network Neurosciences Vaillend, Cyrille; Paris-Saclay Institute of Neuroscience, Cognitive and Network Neurosciences Johnson, Luke R.; University of Tasmania College of Health and Medicine, School of Psychological Science; Uniformed Services University, Psychiatry Volkmer, Hansjürgen; Natural and Medical Sciences Institute at the University of Tübingen, Molecular cell biology Doyère, Valérie; Paris-Saclay Institute of Neuroscience, Cognitive and Network Neurosciences; NYU Langone Health, Child and Adolescent Psychiatry |
| Keywords: | Adolescence, Amygdala, Fear conditioning, Medial prefrontal cortex, Tuberos Sclerosis Complex 2 |
| | |

SCHOLARONE™
Manuscripts

Disruption of amygdala *Tsc2* in adolescence leads to changed prelimbic cellular activity and generalized fear responses at adulthood in rats

Fanny Joly¹, Pauline Jeckel² Martin Kriebel², Sanket Raut³, Nicole El Massioui¹, Cyrille Vaillend¹, Luke R. Johnson^{3,4}, Hansjürgen Volkmer² & Valérie Doyère^{1,5}

¹Université Paris-Saclay, CNRS, Institut des Neurosciences Paris-Saclay, 91400, Saclay, France

²Natural and Medical Sciences Institute at the University of Tübingen, Markwiesenstr. 55, 72770 Reutlingen, Germany

³School of Psychological Sciences, College of Health and Medicine, University of Tasmania, Launceston, TAS, 7250, Australia

⁴Centre for the Study of Traumatic Stress, Department of Psychiatry, Uniformed Services University School of Medicine, Bethesda, MD, 20814, USA

⁵NYU Child Study Center Department of Child and Adolescent Psychiatry, New York University Langone School of Medicine, New York, USA

Corresponding authors:

Fanny Joly, Université Paris-Saclay, CNRS, Institut des Neurosciences Paris-Saclay (NeuroPSI), UMR9197, Saclay, 91400, France; jolyheno.fanny@gmail.com

Valérie Doyère, Université Paris-Saclay, CNRS, Institut des Neurosciences Paris-Saclay (NeuroPSI), UMR9197, Saclay, 91400, France; valerie.doyere@universite-paris-saclay.fr

Abstract – 200 words limitation

Adolescence constitutes a period of vulnerability in the emergence of fear-related disorders (FRD), as a massive reorganization occurs in the amygdala-prefrontal cortex (PFC) network, critical to regulate fear behavior. Genetic and environmental factors during development may predispose to the emergence of FRD at the adult age, but the underlying mechanisms are poorly understood. In the present study, we tested whether a partial knock-down of tuberous sclerosis complex 2 (*Tsc2*, *Tuberin*), a risk gene for neurodevelopmental disorders, in the basolateral amygdala (BLA) from adolescence could alter fear-network functionality and create a vulnerability ground to FRD appearance at adulthood. Using bilateral injection of a lentiviral vector expressing a miRNA against *Tsc2* in the BLA of early (PN25) or late adolescent (PN50) rats, we show that alteration induced specifically from PN25 resulted in an increased c-Fos activity at adulthood in specific layers of the prelimbic cortex, a resistance to fear extinction and an overgeneralization of fear to a safe, novel stimulus. A developmental dysfunction of the amygdala could thus play a role in the vulnerability to FRD emergence at adulthood. We propose our methodology as an alternative to model the developmental vulnerability to FRD, especially in its comorbidity with *TSC2*-related autism syndrome.

Key words (up to 5, alphabetic order): Adolescence, Amygdala, Fear Conditioning, Medial prefrontal cortex, Tuberous Sclerosis Complex 2

Introduction

Nowadays, fear-related disorders (FRD) such as anxiety or post-traumatic stress disorder (PTSD) affect a large amount of worldwide population (up to 33.7% for anxiety disorders or 6% for PTSD) (Atwoli et al. 2015; Bandelow and Michaelis 2015), with debilitating symptoms such as exaggerated fear responses, fear-extinction deficits and overgeneralization of fear (Rauch et al. 2006; Liberzon and Sripada 2007; Fenster et al. 2018). In FRD, an imbalanced functionality of the fear circuitry, in particular between the amygdala and the medial prefrontal cortex (mPFC), has been highlighted. Human and laboratory-rodent studies show that adults suffering from PTSD, anxiety, or phobias display a disruption of amygdala's activity (Pavliša et al. 2006; Bremner et al. 2007; Shin and Handwerker 2009; Morey et al. 2012; Neves et al. 2019) associated with a dysfunctional mPFC (Shin and Handwerker 2009; Whitaker et al. 2014). The fear network has the particularity to undergo an asynchronous development, especially between the early maturing amygdala, a major hub underlying associative fear learning (Gründemann and Lüthi 2015), and the late maturing medial prefrontal cortex (mPFC), which modulates fear expression and its maintenance in memory (Ledoux 1996; LeDoux 2000; Sierra-Mercado et al. 2011). While the amygdala reaches its adult-like maturational state and functionality before adolescence (Bouwmeester et al. 2002; Cressman et al. 2010; Uematsu et al. 2012), the mPFC is not fully mature until adulthood (Tottenham and Gabard-Durnam 2017). Moreover, the amygdala-prefrontal networks undergoes deep maturational changes during adolescence until adulthood, making the network sensitive to disruption at these crucial periods (Burghy et al. 2013; Scherf et al. 2013; Arruda-Carvalho et al. 2017; Zimmermann et al. 2019). Hence, the adolescence period constitutes a window of vulnerability to genetic and environmental factors, where a stressful event appearing during these intense maturational processes may lead to the appearance of emotional and cognitive disorders at adult age, in particular in fear-related disorders (Tsoory et al. 2007; Cloitre et al. 2009; Chaby et al. 2020).

Although the majority of the world population has been exposed at least once in their lifetime to a stressful event, not all individuals will develop FRD, suggesting singular genetic

1
2
3 and/or environmental vulnerabilities (Koenen et al. 2009; Klengel and Binder 2015; Sharma et
4 al. 2016). Understandably, the lack of knowledge regarding the initial subjects' Amygdala-
5 Prefrontal (AP) network functionality, or their anatomical and functional features, makes
6 difficult to identify what could have predisposed them to FRD. A genetic and/or environmental
7 disruption of the early maturing amygdala's activity at adolescence could have influenced the
8 development of a balanced activity in the late-maturing PFC, resulting in emotional disorders
9 appearance at adulthood (Márquez et al. 2013; Hermans et al. 2014; Cisler et al. 2016;
10 Johnson et al. 2018; Kaiser et al. 2018). An intriguing observation is the genetic case of
11 tuberous sclerosis (TSC) disease, in which a loss-of-function mutations of the *Tsc2* gene (Li
12 et al. 2004; Hoeffler and Klann 2010) may induce alteration in cortico-limbic structures and
13 functions (Kim et al. 2010; Maximo et al. 2014; Ha et al. 2015; Top et al. 2016), with a
14 heightened risk to develop FRD compared to the general population at adult age, especially if
15 the diseased individuals presents a co-occurrence of spectrum autism disorder (Haruvi-
16 Lamdan et al. 2020; Rumball et al. 2020, Kerns et al. 2014; Rosen et al. 2018; Hollocks et al.
17 2019; Nimmo-Smith et al. 2020; Rodriguez-Seijas et al. 2020, Kopp et al. 2008; Boronat et al.
18 2013; de Vries et al. 2018, 2020; Ehninger et al. 2008; Ehninger and Silva 2011; Haji et al.
19 2020) . This highlights the importance of a proper balanced brain development in the regulation
20 of emotional behavior at adult age.

21
22 In human suffering of FRD, whether a developmental imbalance in the AP network, due
23 to an initial malfunction of amygdala and/or mPFC, resulting from genetic and/or environmental
24 causes, may be a predisposal factor for FRD appearance at the adult age remains an open
25 question. To address this question, we have developed an alternative rat model of
26 developmental fear-network malfunction based on a viral construct designed to induce a partial
27 knock-down of *Tsc2* expression (*Tsc2*-KD) in glutamatergic CaMKII-positive neurons,
28 selectively in the basolateral amygdala (BLA) from early or late adolescence. This strategy
29 intends to help circumscribe the potential origin of certain alterations in brain development or
30 structures' activity that may lead to FRD in adulthood. It has been shown that heterozygous
31 *TSC2* mutation in human (Marcotte et al. 2012; Im et al. 2016) may trigger imbalance of

1
2
3 neuronal excitability and disrupted synaptic plasticity, or disruption of axonal growth and
4
5 formation (Choi et al. 2008; Hisatsune et al. 2021; Reis et al. 2021). In the present work, we
6
7 used this model to determine the extent to which an alteration of *Tsc2/mTOR* pathway in the
8
9 amygdala during the highly vulnerable period of adolescence could modulate emotional
10
11 behavior and mPFC activity later in adult age, and thus participate to the development of fear-
12
13 related disorders as assessed by using a fear-conditioning paradigm.

14
15
16 We report that rats whose amygdala was disrupted from early adolescence present
17
18 symptoms of fear-related disorders at adulthood, i.e., a resistance to fear extinction and an
19
20 overgeneralization of fear, associated with a basal hyper-activity in layers of mPFC generally
21
22 implicated in fear behavior modulation. Thus, our strategy constitutes an interesting alternative
23
24 to model how a modulation of a signaling pathway crucial for brain development in the
25
26 amygdala while the AP network is still developing may be a predisposal factor for the genesis
27
28 of emotional and cognitive disorders at adulthood.
29
30
31
32
33
34
35
36
37
38
39
40
41
42
43
44
45
46
47
48
49
50
51
52
53
54
55
56
57
58
59
60

Materials and Methods

Animals

A total of eighty-nine male Sprague Dawley rats (Envigo, France) was used. Rats were housed in Plexiglas cages (three to four per cage) in a 12/12h light-dark cycle (7am-7pm) with controlled temperature ($21 \pm 2^\circ\text{C}$) and hygrometry ($55 \pm 5\%$), and water and food *ad libitum*. Cages were enriched with tunnels, wood sticks and two types of litter (wood chip and sawdust), allowing them to dig and hide. All rats were handled and weighed daily. Experimental procedures were conducted in accordance with the guidelines established by the European Communities Council Directive (2010/63/EU Council Directive Decree) and the Paris-Centre et Sud Ethical Committee (CEEA N°59). All efforts were made to reduce the number of rats used and to minimize their suffering.

Two groups of different ages were used: Forty-four rats were late adolescents, weighing 280 ± 20 g at arrival in our facility, underwent surgery at postnatal day 50 (PN50) and constituted the “PN50_inj” group. Forty-five rats were young adolescents at the time of surgery and constituted the “PN25_inj” group. In the PN25_inj group, rats were either purchased after weaning; weighing 70 ± 10 g at their arrival, or for eleven of them were born in the laboratory from four gestating females (arrival in our facility at 7 days of gestation weighing 280 ± 20 g at arrival). Gestating females were in a separate room and housed alone in a cage until pups weaning. Cage litters were supplemented with cellulose paper, and breeding-specific food was given to mother and pups to provide them all the nutrients necessary for gestation and growth. Four weeks after birth, rats were weaned and separated from their mother and female siblings, and randomly assigned to an experimental group. **We verified that breeding condition had no significant effect on behavior for PN25-injected animals (not shown).**

Preparation and culture of primary neurons

Cultures of rat primary hippocampal or cortical neurons were prepared from E18 rat embryos as described recently (Kriebel et al. 2020). In brief, cells were isolated by trypsin digestion followed by trituration of the corresponding tissues and seeded in serum-free MEM with B27 supplement (ThermoFisher Scientific) on polyethylenimine (PEI) coated 96-well SENSOPATE microplates (Greiner Bio-One) at a density of 2.0×10^5 cells/cm². Cultures were maintained at 37°C, 5 % CO₂ in serum-free MEM with B27 supplement. A 50 % medium change was performed every other day.

Viral preparation and viral efficiency analysis

The lentiviral preparations were produced at the Natural and Medical Sciences Institute at the University of Tübingen (NMI; Reutlingen, Germany). The vector backbone used for both control and *Tsc2*-specific knockdown constructs has been described previously (Kriebel et al. 2020) (<https://doi.org/10.3389/fnmol.2020.00043>) and is summarized in **Fig. 1A**. For the identification of injection sites, all lentiviral vectors expressed the Enhanced Green Fluorescent Protein (EGFP) protein under the control of a synapsin promoter. KD lentiviruses also expressed a microRNA (miRNA) specific for *Tsc2* mRNA/protein (tuberin), under the control of the Ca⁺⁺-Calmoduline Kinase II (CaMKII) promoter. The miRNA targeted a specific mRNA sequence of the tuberin in order to diminish *Tsc2* expression levels in CaMKII producing cells, thus creating a constitutive and CaMKII-restricted knock-down of *TSC2*. Two target sequences for the *Tsc2*-miRNAs were used: Vector 1 (*Vir1_Tsc2*) sequence was TCATAGCCATGTGGTTCATTA; vector 2 sequence (*Vir2_Tsc2*) was GGATGGATGTTGGCTTGTCCT. As a control, a lentiviral vector expressing a negative control miRNA from pcDNATM6.2-GW/miR-neg (Thermo Fisher Scientific, USA) was constructed (*Vir_ctrl*). Titers of corresponding lentiviral suspensions were at least 5×10^7 Transduction Units (TU)/ml. Vector knock-down (KD) efficiency on *Tsc2* protein level was first evaluated in vitro by quantitative immunocytochemistry in primary hippocampal neurons, based on the intensity of anti-*Tsc2* immunoreactivity (IR) in somata of successfully

1
2
3 transduced neurons (i.e., EGFP-positive neurons). For this purpose, cultures of primary rat
4 hippocampal neurons transduced with lentiviral suspensions at DIV 3 at MOIs up to 10 were
5 fixed at DIV14 using 4 % paraformaldehyde/PBS for 10 min at room temperature. After
6 blocking and permeabilisation for 30 min at room temperature in 0.2 % Triton X-100/PBS
7 containing 1 x Blocking Reagent for ELISA (Merck), neuronal cultures were incubated
8 overnight at 4°C with primary antibodies diluted in blocking solution. After washing in PBS,
9 fluorescently labeled secondary antibodies (1:500; Cy3-coupled goat anti-rabbit (Dianova) and
10 Alexa Fluor 647-coupled goat anti-chicken (ThermoFisher Scientific)) were added, followed by
11 an incubation for 2 h at room temperature. Cell nuclei were stained with Hoechst Dye 33258
12 (1:1000 in PBS; Merck). The following primary and secondary antibodies were used: rabbit
13 anti-Tuberin/*TSC2* (D93F12; Cell Signaling Technology, Danvers, MA, Cat. No. 4308),
14 polyclonal chicken anti-MAP2 (Thermo Fisher Scientific, Waltham, MA, USA, Cat. No. PA1-
15 10005).

16
17
18 Stained *in vitro* cultures of primary hippocampal neurons were documented by means of
19 spinning disk confocal fluorescence microscopy (Cell Observer SD equipped with a 63x Plan-
20 Aplanachromat oil immersion objective, Carl Zeiss Microscopy GmbH). Acquisition settings
21 (excitation, emission) were kept constants for all experimental groups. Protein expression of
22 *Tsc2* (tuberin) in successfully transduced, EGFP-positive neurons was quantified using ZEN 2
23 (Carl Zeiss Microscopy GmbH). A region of interest (ROI) of maximum diameter was selected
24 from all confocal z-planes of recorded EGFP-positive neuronal somata. Within each ROI, the
25 mean fluorescence intensity was quantified using ZEN's measure function. KD efficiency was
26 also confirmed at the mRNA level, evaluated by qRT-PCR using duplicate samples from rat
27 primary cortical neurons transduced by the vectors, as previously described (Kriebel et al.
28 2011, 2020; Saha et al. 2017) (**Fig. 1**).

Surgery and viral infusion

According to the growth chart of Sprague Dawley rats provided by animal provider (Envigo, France), the PN50_inj rats had surgery at 300 ± 10 g and PN25_inj rats at 100 ± 5 g.

Surgery preparation

Twenty minutes before surgery, rats were isolated in a cage under a heating lamp. PN50 animals received a subcutaneous injection of the analgesic tolfedine (Tolfedamic Acid, 4 mg/kg), followed by anesthesia with an intraperitoneal (i.p) injection of a mix of ketamine (Imalgene® 1000, 70 mg/kg) and Metedomidine (domitor®, 0.5 mg/kg) diluted in 0.9% NaCl. According to veterinary recommendations, PN25 rats received the same anesthesia protocol with a dose reduced by 2/3 compared to PN50 rats to limit overdose risks. When necessary, a half dose of ketamine/metedomidine was supplemented at mid-surgery. The rat's body temperature was controlled and maintained during surgery with a warming pad, and the eyes were protected from dryness by calboprol creme (OcryGel). At the end of surgery, the wound was closed with surgical staples (Michel 100, 7.5 x 1.75 mm) after applying lidocaine/prilocaine ointment (Anesderm Gé) to limit pain during waking up. Rats were awakened with an intramuscular injection of Atipamezole (Antisedan®, 1 mg/kg for PN50 and 0.67 mg/kg for PN25) diluted in 0.9 % NaCl, and returned to home cage once fully awake.

Viral infusion

Rats were randomly assigned into different experimental groups, with no more than 2 early adolescents from the same litter in a viral condition group. Once rats were placed in a stereotaxic apparatus (Stoelting, USA), a midline incision was made onto the scalp and holes were made in the skull with a dental drill (Bravo Micromotor portable III, Hager Worldwide) for bilateral injection of the lentiviral preparation into the BLA. Cannulae (26G; Phymep, C3115I)

1
2
3 were slowly lowered at the following stereotaxic coordinates for PN50 rats (Anteroposterior
4 (AP): -2.64 mm; Mediolateral (ML): \pm 4.6 mm relative to Bregma ; Dorsoventral (DV): -6.8 mm
5 relative to the surface of the brain) (Paxinos and Watson 2009)), and for PN25 rats (AP: -2.9
6 mm; ML: \pm 4.8 mm relative to Bregma ; DV: -6.8 mm relative to the surface of the brain)
7 (Khazipov et al. 2015). Five minutes after reaching final coordinates, injections were performed
8 using a 10 μ l Hamilton Syringe (Hamilton 801 N) with an automated pump (Harvard Apparatus,
9 Pump II Elite, Harvard Bioscience, Inc) delivering 2 μ l of lentiviral preparation bilaterally at 0.05
10 μ l/min. The cannulae were progressively withdrawn from the brain 10 min after the end of the
11 infusion.
12
13
14
15
16
17
18
19
20
21
22
23

24 **Behavioral assessment: Fear conditioning**

25 *Apparatus*

26
27
28
29
30
31
32 Four identical conditioning chambers (30 x 25 x 30 cm, Coulbourn Instruments, USA) were
33 used, enclosed within a sound-isolation cubicle with a ventilation fan producing a background
34 noise of 60 dB. All rats were pseudo-randomly assigned to each conditioning chamber so that
35 every chamber received the same number of *Vir_ctrl*, *Vir1_Tsc2*, or *Vir2_Tsc2* animals.
36
37 Protocols were designed using the Graphic State 3.02 software (Coulbourn Instruments, USA).
38
39 Two different contexts were used in distinct phases of the experiment. For context A, each
40 chamber was equipped with a grid floor for delivery of electrical footshocks, a red light located
41 at the top right corner and a speaker at the top left corner of the box. The context B took place
42 in the same conditioning chambers, but with a green light, peppermint odor (Sigma-Aldrich, ref
43 77411) and a smooth floor with wood litter. Between rats, each chamber was cleaned with
44 water and cellulose tissue, and wood litter was changed. Between days, each chamber was
45 cleaned with 70° ethanol. Each chamber was equipped with an infrared camera (Coulbourn
46 Instruments, USA) placed above the conditioning chamber and connected to a television
47
48
49
50
51
52
53
54
55
56
57
58
59
60

1
2
3 screen and a DVD recorder. Infrared cues (Coulbourn Instruments, USA) lighted up during the
4
5 tone presentations to allow the experimenter to recognize the tone periods for off-line scoring.
6
7

8 9 *Protocol*

10
11
12
13 Seven weeks after vector infusion, animals were tested for fear behavior using a Pavlovian
14
15 auditory fear conditioning paradigm constituted of five sessions spaced by 24 h. Each session
16
17 lasted from 30 min to 70 min depending on the protocol step, and the intertrial interval (ITI,
18
19 from the end of a stimulus to the onset of the next one) of 3 min \pm 1.5 min was presented in
20
21 pseudorandom order in each session. At the start of each session, there was a variable period
22
23 of time, from 2 to 5 min (3 min in average among the 5 sessions), before apparition of the first
24
25 tone.
26
27

28
29
30 *Habituation:* On Day 1, familiarization to the Context and Tone was achieved by the delivery
31
32 of 5 conditioned stimuli alone (CS: 30s, 4 kHz, 80 dB) in Context A.
33
34

35
36
37 *Fear Learning:* On Day 2, classical fear conditioning was assessed in context A. During this
38
39 phase, rats received 7 CS paired with an electric foot-shock (unconditioned stimulus, US, 0.5
40
41 mA, 0.5s) delivered immediately at the end of the CS presentation.
42
43

44
45
46 *Extinction and Extinction Recall:* On Day 3, 20 presentations of the CS alone were given in the
47
48 new Context B (extinction session), followed 24 h later (Day 4) by a session evaluating
49
50 extinction recall by means of 5 presentations of the CS alone, in context B as well.
51
52

53
54
55 *Renewal and Generalization:* On Day 5, renewal of fear was tested by placing the rats back in
56
57 the original learning context (context A) with 5 presentations of the CS alone. The
58
59 generalization of fear to a new tone was then tested, after 3 min, with 5 presentations of an
60
unknown and distinct tone (30s, 11 kHz, 75 dB).

Analysis

Fear intensity was evaluated by off-line quantification of freezing behavior, an instinctive reaction of tonic immobility in response to a threat in rodents, defined by an absence of movement, except respiratory (Blanchard and Blanchard 1969; Sigmundi et al. 1980). The percent time spent freezing to the context alone and during the 30s tones was manually recorder for each session; the experiment and scoring was done blind regarding experimental groups. Due to a technical issue, the freezing behavior could not be scored for some rats (PN50_inj groups on Day 1: 2 *Vir_ctrl* and 4 *Vir1_Tsc2*; PN25_inj groups on Day 3, between tone 6 to tone 15: 1 *Vir_ctrl* and 5 *Vir1_Tsc2*). As a result, fear memory and extinction during Day 3 was statistically assessed by analyzing freezing behavior during the first 5 trials and the last 5 trials, respectively.

Biochemical and molecular studies

Seven weeks after fear conditioning, rats were deeply anesthetized with a high dose of sodium pentobarbital (i.p., Dolethal, 1ml/100g; diluted 1/3 in 0.9% NaCl) and then perfused intracardially at 25 rpm with 300 ml Phosphate buffered saline (PBS, 0.1 M), followed by 300 ml of 4 % paraformaldehyde at room temperature (RT). The brains were removed and stored in the same fixative solution for 24 h at 4°C, and then successively immersed for three consecutive days in 12%, 16% and 18% saccharose solution in Phosphate buffer (PB, 0.1 M). Brains were then frozen in Isopentane at -40°C during 3 min and stored at -20°C until sectioning. Coronal sections (40 µm thick) were cut using a cryostat (Thermo Scientific Microm HM 560) at -18°C ± 2°C. Each section was individually placed in a well of a 48 multi-well plate containing AMARAL solution (Glycerol, Ethylen Glycol, Distilled water, PB 0.1 M) at 4°C until treatment. Each section containing the BLA was placed on a microscope glass slide, floating in PBS (0.1 M), in order to observe tissue quality, coordinates, and EGFP expression by epifluorescence microscopy (Olympus BX60 with x4 objective, Explora Nova Software). Rats

1
2
3 for which the BLA presented no EGFP fluorescence (no vector transduction), holes caused by
4 injection, or having main EGFP signal outside the BLA due to misplaced injection, were
5 excluded from the entire experiment. At the end, a total of nineteen rats injected at PN50 and
6 ten rats injected at PN25 were excluded from the results, whatever their viral condition. In sum,
7 twenty-five animals injected at PN50 (*Vir_ctrl* or *Vir1_Tsc2*) and thirty-five animals injected at
8 PN25 (*Vir_ctrl*, *Vir1_Tsc2* or *Vir2_Tsc2*) were conserved for behavioral and histological
9 analyses.
10
11
12
13
14
15
16
17
18
19

20 *Detection of EGFP, Tsc2 and p70S6K-p by Immunofluorescence studies*

21 22 23 24 *Protocol*

25
26
27
28 For analysis of *Tsc2*/EGFP expression by immunofluorescence, forty sections from PN25_inj
29 rats and seventy section from PN50_inj rats correctly injected with *Vir_ctrl* or *Vir1_Tsc2* were
30 chosen depending on the highest immunostaining quality and presenting the denser viral
31 diffusion specifically into the BLA (PN25: 8 amygdalae from 5 *Vir_ctrl* rats; and 6 amygdalae
32 from 5 *Vir1_Tsc2* rats; PN50 : 8 amygdalae from 5 *Vir_ctrl* rats; and 9 amygdalae from 6
33 *Vir1_Tsc2* rats). They were washed 3 x 10 min in PBS 0.1 M, then once in PBS 0.1 M/Triton
34 0.5%, and washed again in PBS 0.1 M (3 x 10 min). Then, slices were incubated individually
35 in 250 µl of a blocking solution containing 1% Bovine Serum Albumin (BSA, Sigma Aldrich,
36 A9647-50G), 5% Normal Goat Serum (NGS, Eurobio, CAECHV00-0U) and 0.1% Triton in PBS
37 0.1 M, for 1h at RT. Sections were then co-incubated with the primary antibodies against EGFP
38 (Chicken anti-GFP, 1:1000 dilution, Ab13970) and against *Tsc2* protein (Rabbit anti-Tuberin–
39 N terminal, 1:100 dilution, Abcam, ab189304) diluted in the blocking solution for 24 h at 4°C
40 on a rotor plate. The following day, sections were washed in PBS 0.1 M (3 x 10 min), co-
41 incubated in 300 µl of a mix of secondary antibodies, i.e., a Goat anti-chicken Alexa Fluor 488
42 (1:400, Thermofisher A11039) and a Goat anti-rabbit Alexa Fluor 546 (1:400, Thermofisher
43 A11035) diluted in a blocking solution (BSA 2%, NGS 2% in PBS 0.1 M), during 45 min on a
44
45
46
47
48
49
50
51
52
53
54
55
56
57
58
59
60

1
2
3 rotor plate at RT, covered by aluminum foil to protect fluorophores from light. Sections were
4 then washed in PBS 0.1 M (3 x 10 min) and mounted on Trajan glass slides (Series 3
5 Adhesives, Trajan, T7611), embedded with Fluoromount® Aqueous Mounting Medium (Sigma
6 Aldrich, F4680) and stored at 4°C protected from light.
7

8
9
10 For analysis p70S6K-p/EGFP expression, a similar immunofluorescence protocol was used.
11
12 Twenty-nine sections from PN25_inj rats injected with *Vir_ctrl*, *Vir1* and *Vir2_Tsc2* and ninety
13 sections from PN50_inj rats injected with *Vir_ctrl* or *Vir1_Tsc2* were chosen (PN25: 13
14 amygdalae from 9 *Vir_ctrl* rats; 9 amygdalae from 7 *Vir1_Tsc2* rats; and 14 amygdalae from 8
15 *Vir2_Tsc2* rats. PN50: 7 amygdalae from 6 *Vir_ctrl* rats; and 12 amygdalae from 8 *Vir1_Tsc2*
16 rats). Slices were co-incubated with the primary antibodies against the phosphorylated form of
17 protein p70S6K (p70S6K-p; Phospho-p70 S6 Kinase (Thr389) (108D2) Rabbit mAb #9234,
18 Cell Signaling, dilution 1:500) and the primary antibody against EGFP (Chicken anti-GFP,
19 1:1000 dilution, Ab13970). The following day, after washing, slices were co-incubated in 300
20 µl of a mix of secondary antibodies as described above.
21
22
23
24
25
26
27
28
29
30
31
32
33

34 *Analysis*

35
36
37
38 The intensity of Tuberin (red) and EGFP (green) IR was measured in BLA cells using the
39 ImageJ software (ImageJ 1.53c, Wayne Rasband, NIH, USA). Images were acquired using a
40 Zeiss confocal microscope (Zeiss LSM700) using a 10x objective. The fluorescence intensity
41 of each cell within the BLA was thus measured in separate red and/or green channels. For
42 EGFP/Tuberin analysis, in order to individualize every cell in each channel, a duplicate layer
43 of either Tuberin (red) or EGFP (green) fluorescent image was used, each converted into
44 binary 8-bit image (grey); the background was subtracted with a threshold adjusting algorithm,
45 and an automatic contour of each Tuberin(+) and/or EGFP(+) cell was drawn and analyzed
46 with the “Analyze Particle” function of ImageJ. For each channel, each particle (cell) was
47 labeled with a unique number and was added to the ROI manager.
48
49
50
51
52
53
54
55
56
57
58
59
60

1
2
3 The mean grey intensity of each cell was calculated from RGB images using the
4 “Analyze/Measure” function in ImageJ. To determine which Tuberin (+) cell was also EGFP
5 (+), reflecting colocalization of the two markers in transduced neurons, the initial EGFP image
6 was taken, and the ROI manager corresponding to the Tuberin (red) channel was
7 superimposed on the EGFP (green) image. Every particle drawn that perfectly overlaid with an
8 EGFP (+) cell was counted as a Tuberin(+)-EGFP(+) colocalization. For every analyzed rat, at
9 least 1mm² of BLA tissue has been analyzed.
10
11
12
13
14
15
16
17

18 For p70S6K-p/EGFP analysis, the p70S6K-p protein expression was counted as the
19 number of p70S6K-p fluorescent punctate (red channel) in every EGFP(+) cells (green
20 channel), and expressed as the numbers of punctate per 100µm² of area measured in
21 EGFP(+)-corresponding cells, normalized per cell. Images were acquired using a Zeiss
22 confocal microscope (Zeiss LSM700) using a 20x objective. The same protocol as described
23 above for Tuberin/EGFP analysis was done, and numbers of punctate were measured using
24 the “Analyze Particles” function in ImageJ. For each rat, at least 1mm² of BLA tissue has been
25 analyzed.
26
27
28
29
30
31
32
33
34
35
36

37 **Detection of c-Fos(+) cells by immunohistochemistry**

38 *Protocol*

39
40
41
42
43
44
45 Three EGFP(+) BLA sections were taken from each rat injected with *Vir1_Tsc2* or *Vir_ctrl*. In
46 addition, three tissue sections from the prefrontal cortex were chosen depending on their
47 anteroposterior (AP) coordinates (for Methods, see Bergstrom et al. 2011; Jacques et al. 2018)
48 from AP 2.8 to AP 2.6 mm relative to Bregma in order to maximize the mPFC cellular activity
49 analysis through the antero-posteriority axis. Briefly, sections containing prelimbic (PL) and
50 infralimbic (IL) cortices at 3 different AP were chosen based on the shape and length of the
51 *corpus callosum*, measured as the Ferret Length (Jacques et al. 2018). For each AP, the Ferret
52 length had to be statistically not different between subjects and between experimental
53
54
55
56
57
58
59
60

1
2
3 conditions, but it had to be statistically different between APs. Sorting the sections with this
4 method allowed us to measure specifically differences in c-Fos(+) cells density at a given AP
5 and for a specific microanatomical zone. Sections of the three structures (BLA, PL and IL) were
6 treated for immunohistochemistry (IHC) at the same time, ran in 3 series (most anterior, middle
7 and posterior slices).
8
9
10
11
12

13
14 Sections stored in AMARAL at 4°C were washed in PBS 0.1 M (3 x 10 min) at RT using
15 a rotor plate, then incubated 10 min in a mix of 20% Methanol, 77% distilled water (dH₂O) and
16 3% H₂O₂ in order to deactivate endogenous peroxidases. Sections were then washed in dH₂O,
17 then in PBS 0.1 M for 5 min and finally in PBS 0.1 M with 0.2% Triton once for 10 min. Each
18 section was then incubated in 1.5 ml of a blocking solution containing PBS 0.1 M, 0.2% Triton
19 and 5% NGS (Normal Goat Serum, Eurobio, CAECHV00-0U) for 1h at RT using a rotor plate.
20 Finally, sections were individually incubated for 48 h on a rotor plate at 4°C in 1.5 ml of a
21 primary antibody against c-Fos (Rabbit anti-c-Fos, 1:3000, Proteintech, Euromedex, ref: PR-
22 26192-1-AP) diluted in the blocking solution. Sections were then successively washed in PBS
23 0.1 M-Triton 0.2% (3 times 10 min each), incubated individually in 1.5 ml of goat anti-rabbit
24 IgG (H+L) biotinylated secondary antibody (1:400, Eurobio, BA-1000) in blocking solution for
25 90 min at RT using a rotor plate, washed in PBS 0.1 M-Triton 0.2% for 10 min, incubated 90
26 min in the ABC kit (Kit Vectastain Elite ABC HRPO, Vector Lab, dilution 1:800) prepared 30
27 min before, and washed again in PBS 0.1 M-Triton 0.2% for 10 min. Immunohistochemistry
28 revelation was finally performed using a Vector SG Peroxidase Substrate Kit (Substrat SG
29 HRP, Eurobio, SK-4700). Sections of mPFC and BLA were individually incubated in 1.5 ml of
30 the Substrate kit solution, and the revelation was stopped at desired coloration (about 4 min
31 for mPFC and 8 min for BLA). Reaction was stopped by transferring slices in dH₂O and storing
32 them in PB 0.1 M at 4°C for 24 h. Sections were then mounted on Trajan glass slides,
33 dehydrated in acetone (2 x 5 min), immersed in xylene (2 x 5 min), immediately embedded
34 with Eukitt (Chem Lab, Belgium, ref CL0405030500) and stored at 4°C protected from light.
35
36
37
38
39
40
41
42
43
44
45
46
47
48
49
50
51
52
53
54
55
56
57
58
59
60

Analysis

Image preparation for quantification of c-Fos(+) cells

Histology images were taken with an Olympus BX 60 optic microscope using a x4 objective. We first excluded from analysis the sections presenting unreliable staining (heterogeneous staining in the structures due to folding of the tissue during process), no staining or damaged tissue. (BLA : *Vir_ctrl* : PN50 $n = 13$; PN25 $n = 10$; *Vir1_Tsc2* PN50; $n = 12$; PN25; $n = 10$). Then, for the mPFC, sections with extreme AP coordinates were excluded, and only PL and IL staining at AP 2.7 and 2.6 were common to most of the stained slices among animals. (AP 2.6: *Vir_ctrl*; PN50, $n = 8$; PN25, $n = 11$; *Vir1_Tsc2*; PN50, $n = 8$; PN25; $n = 13$; AP 2.7: *Vir_ctrl*; PN50, $n = 8$; PN25, $n = 10$; *Vir1_Tsc2*; PN50, $n = 8$; PN25; $n = 16$). Two control sections, one from mPFC and one from BLA, incubated in the blocking solution without primary antibody did not show any specific or confounding unspecific background staining.

For c-Fos(+) cells counting, images were acquired using an optic microscope (Olympus BX 60) with a 10x objective in a vertical mosaic manner, forming a vertical grid of 2x4 images for mPFC and with a square 2x2 design for BLA. Individual images were stitched using the Grid/Collection Stitching plugin in Fiji (Fiji software, (Schindelin et al. 2012)); Grid/collection stitching plugin (Preibisch et al. 2009) to form a single image. The image scale was set, and the contours of PL, IL and BLA were done manually in Fiji, using anatomical landmarks to determine the sizes and edges of the target structures. Typical landmarks in mPFC were the sizes and shapes of the caudate putamen and corpus callosum. For BLA, the lateral ventricle size, external capsule fiber aspect or optical fiber size were relevant anatomical anchors to isolate proper structure contours (for further methods, see (Bergstrom et al. 2011; Jacques et al. 2018)); from Paxinos and Watson, 2009 (Paxinos and Watson 2009).

Cell counting in mPFC and BLA

Areas of each outlined structure were measured and c-Fos(+) cells in this area were manually counted in a semi-quantitative manner using the “multi point” tool in Fiji. Non-colored cells (grey intensity equal to background), particles with non-neuronal shape, and particles under 4 μm of diameter were excluded from counting.

Density heat map analysis of mPFC

Methods to create density heat maps have previously been detailed (Jacques et al. 2018). We followed this method with slight modifications as we used the Fiji software to calibrate counting areas, draw the structures contours and manually count c-Fos(+) cells. The density heat maps were created using a MATLAB script written by the experimenter (MathWork Simulink, Matlab 2019a, USA). Briefly, once all the c-Fos(+) neurons were counted in the calibrated and contoured counting area, their (x,y) coordinates were binned and transformed into matrices to measure the exact localization and density of c-Fos(+) cells. As previously shown (Jacques et al. 2018), the number of bins can be calculated based on experimenter parameters or using existing formulas. Here, we calculated bins density with the square root of the total number of cells in each condition. In order to compare conditions (Ctrl/Virus) and groups (PN25/PN50) at the same matrices resolution, we transformed every (x,y) data into matrices containing the same number of bins, corresponding to the number of bins calculated for the viral condition presenting the highest density of c-Fos(+) cells, thus providing the optimal matrices resolution. Once the final number of bins was defined, (x,y) coordinates of each structure were transformed into two matrices (30x30 for PL and 20x20 for IL), mirrored for both hemispheres, and averaged by conditions (Ctrl vs Virus), using MATLAB. Averaged matrices were then transformed into a binned color map, smoothed and scaled at the same density units to form a final density heat map.

Statistical analysis

Data are expressed as means \pm SEM. Parametric ANOVAs were used for most parameter analyses addressing interactions between several factors and repeated measures (RM). Parametric comparisons (paired and two-group comparison unpaired t-test), planned Helmert contrasts tests, mixed ANOVA with group (age and viral condition) as independent (between) factors and repeated measures (Two- and Three-Way ANOVAs) as dependent (within) factors, followed by Bonferroni *post-hoc* test, were performed using JASP (JASP Team (2020), version 0.13.1) and JAMOVI (The JAMOVI project (2020), version 1.2). In case of a non-respect of equality of variance, a Welch correction was done. The Two-Way ANOVAs and FDR (False Discovery Rate) analyses for the matrices were done using GraphPad Prism 7 (GraphPad Prism 7.00 for Windows, GraphPad Software, La Jolla California, USA). Principal component analysis was performed using Statview 5.0 software (SPSS, USA). Factor extraction was performed using an orthogonal rotation (Varimax) and the weight of each variable on each extracted factor was calculated. Linear regression was performed using XLSTAT software. For all analyses, the *alpha* level of significance was set at 0.05, excepting for FDR analysis which was set at 0.1.

Results

Lentiviral transduction efficiency

Before their use in behavioral experiments, the transduction efficacy of the two viral vectors, expressing a miRNA for partial knockdown of *Tsc2* (“knock-down” or “KD” vectors, “Vir_ *Tsc2*”) was chosen for a better representation of the human heterozygous *TSC2* mutation were analyzed and compared to a control vector (*Vir_ ctrl*) *in vitro*. Two *Tsc2* mRNA targeting vectors were applied to a subset of experiments to rule out off-target effects. (**Fig. 1A, B**, but also **Fig. S1** for outline of the lentiviral strategy). The qRT-PCR analyses from transduced primary cortical neurons in duplicates with *Vir1_ Tsc2* and *Vir2_ Tsc2* revealed respectively 52.07 % and 40.59 % decrease of *Tsc2* mRNA expression (**Fig. 1C**). Transduced primary hippocampal neurons with *Vir1* or *Vir2_ Tsc2* also showed a 20% significant decrease of *Tsc2* protein (tuberin) expression levels compared to cells transduced by the control vector (**Fig. 1D** Helmert contrast test, Ctrl vs [*Vir1*, *Vir2*] $t = 5.088$; $P < 0.001$), and no differences were observed between the two KD vectors, demonstrating that (1) all three lentiviral vectors efficiently transduced neurons *in vitro*, and (2) the two KD viruses successfully reduced *Tsc2* mRNA and tuberin levels *in vitro*.

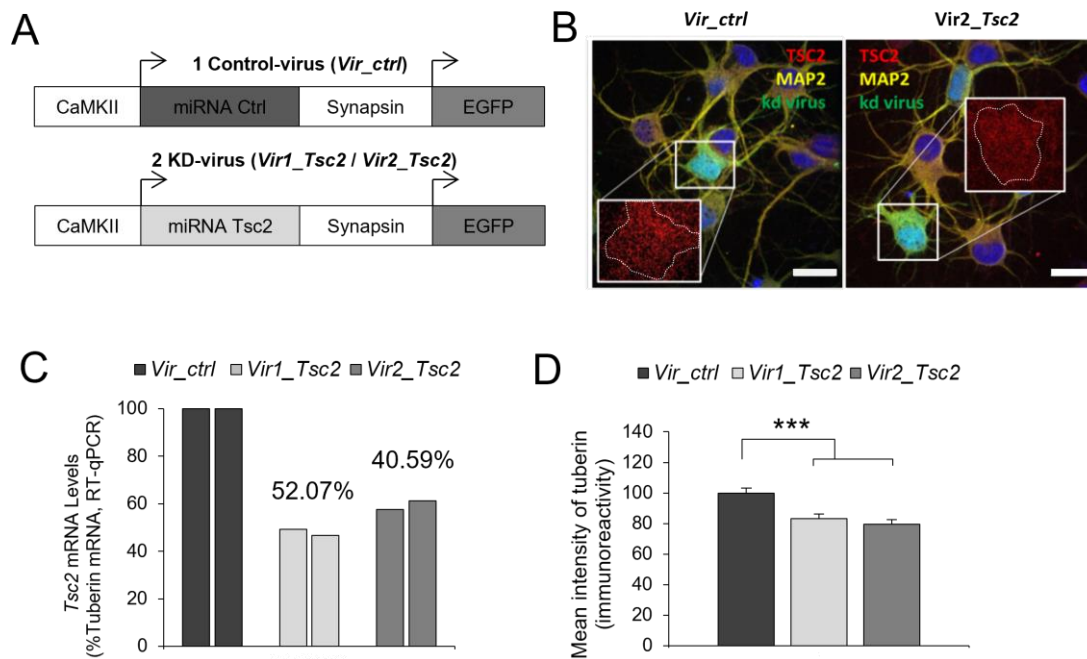
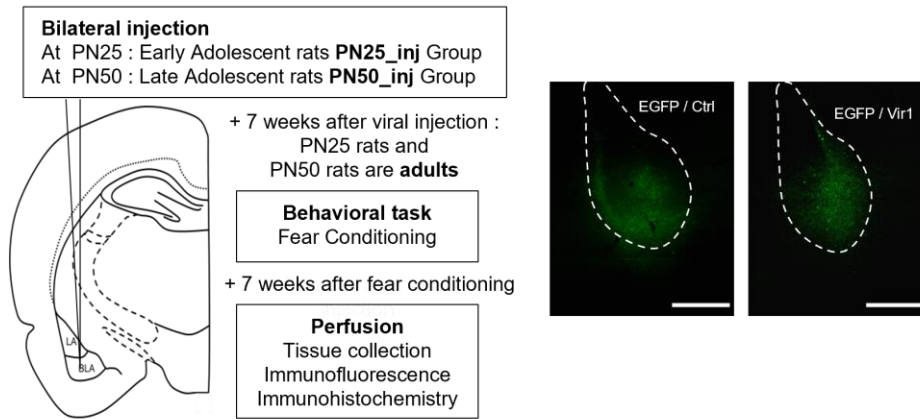


Figure 1. In vitro characterization of *Tsc2*-targeting virus efficiency. (A) Viral constructs. The diagrams show the lentiviral construction of the control virus (*Vir_ctrl*, up) and the two knock-down (KD) viruses targeting *Tsc2* (or tuberin) mRNA (*Vir1_Tsc2* and *Vir2_Tsc2*, down). The three constructions expressed EGFP protein under the control of a rat synapsin promoter, targeting neuronal cells; both *Vir1_Tsc2* and *Vir2_Tsc2* expressed a miRNA targeting *Tsc2* mRNA under control of a mouse CaMKII promoter, to constitutively decrease *Tsc2* protein expression and activate the mTOR pathway within CaMKII-expressing neuronal cells (see Fig. S1). (B) Sample images show immunoreactivity (IR) for tuberin (*Tsc2* protein) (red), the neuronal marker Microtubule Associated Protein 2 (MAP2, yellow) and the viral EGFP expressed by the knock-down virus (kd virus, green) in primary hippocampal neurons transduced by *Vir_ctrl* (left) or *Vir2_Tsc2* (right). Dotted lines represent a single cell contour. Colocalization between *TSC2*, MAP2 and EGFP is shown in cyan, DAPI nuclear stain in dark blue; the inset shows the punctuate IR of tuberin (red) in neuronal elements. Scale bar = 20 μ m (C) Tuberin expression levels in transduced primary cortical neurons. Histograms show the relative expression of *Tsc2* mRNA measured in duplicate cell cultures of primary cortical neurons transduced with the 3 viruses. *Tsc2* mRNA was detected by RT-qPCR and normalized to GAPDH reporter gene expression. *Tsc2* expression levels are presented as percent expression in neurons transduced by the control lentiviral vector. Mean percentage of mRNA changes compared to control are expressed above histograms. (D) Mean intensity of tuberin fluorescence measured in primary hippocampal neurons. Histograms show tuberin expression analyzed in neurons transduced with either *Vir_ctrl* or one of the two *Vir_Tsc2* KD lentiviruses and quantified by measuring the tuberin fluorescence signal intensity in transduced neurons. There was a significant decrease of tuberin levels in cells transduced by *Vir1_Tsc2* and *Vir2_Tsc2* compared to control (*Vir_ctrl*, $n = 70$; *Vir1_Tsc2*, $n = 68$; *Vir2_Tsc2*, $n = 63$). (Helmert contrast test, *Ctrl* vs [*Vir1*, *Vir2*], $t = 5.088$; $***P < 0.001$), and no differences were observed between the two KD vectors (Helmert contrast test, *Vir1* vs *Vir2*, $t = 0.848$; $P = 0.398$).

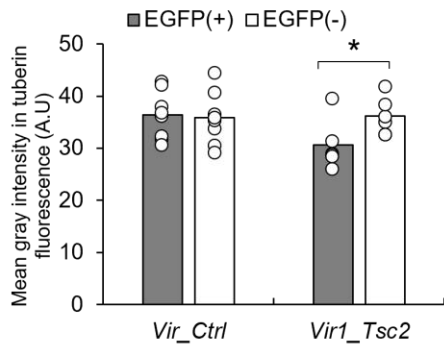
Given the highest decrease of *Tsc2* mRNA in cells transduced by the *Vir1* vector compared to *Vir2* in vitro, this KD-virus has been principally used for the entire behavioral and histological experiment. All lentiviral vectors (control or KD) expressed EGFP, allowing identification of transduced neurons (Fig. 2A). Thus, viral transduction efficacy was investigated ex vivo by immunofluorescence from brain tissues of animals infused at PN25 or PN50 by *Vir_ctrl* or *Vir1_Tsc2* vectors 14 weeks before in the basolateral amygdala (BLA, Fig. 2B, C). Dual-labelling of EGFP and tuberin showed a significant decrease of tuberin immunoreactivity (IR) in EGFP(+) cells in PN25_inj *Vir1_Tsc2* rats (Fig. 2B, Two-Way ANOVA, significant fluorescence x viral condition interaction $F(1,12) = 7.845$; $P = 0.016$; Bonferroni post-hoc,

1
2
3 EGFP(+) vs EGFP(-) for *Vir1_Tsc2* group, $P = 0.033$). Likewise, the same analysis done in
4
5 PN50_inj rats showed a significant decrease of tuberin IR in EGFP(+) cells of *Vir1_Tsc2*
6
7 animals (Fig. 2C, Two-Way ANOVA, significant fluorescence x viral condition interaction
8
9 $F(1,15) = 7.082$; $P = 0.018$; Bonferroni post-hoc, EGFP(+) vs EGFP(-) for *Vir1_Tsc2* group, P
10
11 = 0.039). Hence, these analyses validate the knock-down effect, as the KD lentivirus vector
12
13 was responsible for the decrease in tuberin expression in BLA cells *in vivo* for both groups of
14
15 age of injection.
16
17
18
19
20
21
22
23
24
25
26
27
28
29
30
31
32
33
34
35
36
37
38
39
40
41
42
43
44
45
46
47
48
49
50
51
52
53
54
55
56
57
58
59
60

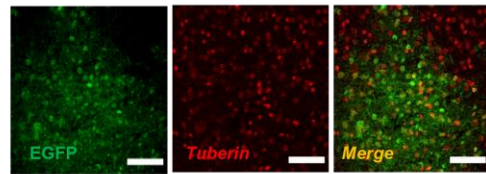
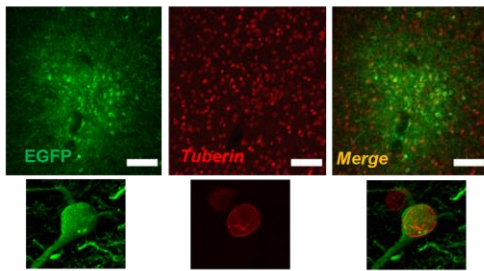
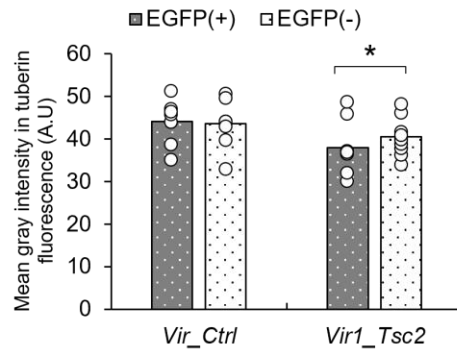
A



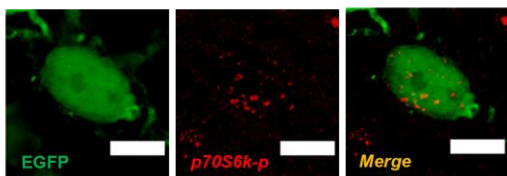
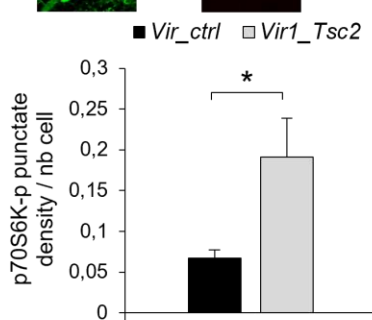
B



C



D



E

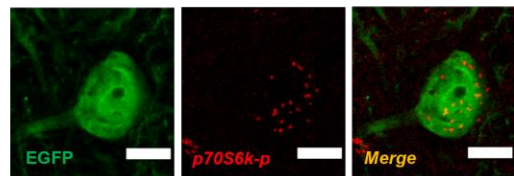
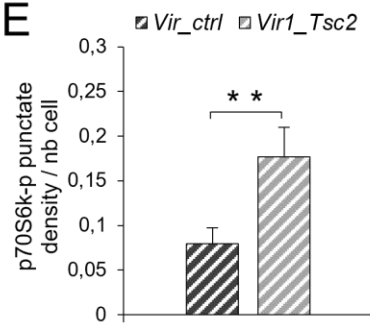


Figure 2. Ex vivo characterization of Tsc2-targeting virus efficiency. (A) Experimental procedure. Diagram (left) shows the procedure from lentiviral injection to tissue collection: Rats were bilaterally injected into the basolateral amygdala (BLA) with a lentiviral construction (*Vir_ctrl*, *Vir1_Tsc2* or *Vir2_Tsc2*) during postnatal development when early adolescent (at PN25), or late adolescent towards the end of brain development (PN50). We assessed fear behavior 7 weeks after lentiviral injection, i.e., once PN25_injected rats had reached the adult age (PN60) and PN50 rats a more mature age (PN90). Seven weeks after fear conditioning, brain tissue sections were collected, and immunofluorescence performed to appraise lentiviral efficiency in injected basolateral amygdalae. The sample images (right) show lentiviral transduction efficiency in BLA cells from PN25 rats injected with *Vir_ctrl* (left) and *Vir1_Tsc2* (right image). Scale bar = 100 μ m; Mosaic acquisition objective x10. (B) Semi-quantitative analysis of tuberin immunoreactivity in BLA from PN25_inj rats. Histograms show tuberin mean gray fluorescence intensity measured in cells colocalizing viral EGFP and tuberin fluorescence (EGFP(+)) or non-transduced cells expressing only tuberin (EGFP(-)) in BLAs of PN25 rats injected with *Vir_ctrl* or *Vir1_Tsc2*. Dots represent individual data. Sample images (down) show corresponding examples in a PN25_inj animal (tuberin: red; EGFP: green, Colocalization: Yellow, Scale bar = 100 μ m; objective x10). Miniatures below are individual neurons immunostained for tuberin (red), EGFP (green) or merged, objective x63. Note the significant decrease of tuberin fluorescence intensity selectively in EGFP(+) cells compared to EGFP(-) cells transduced with *Vir1_Tsc2* vector ($n = 6$ amygdalae), but not in those transduced with *Vir_ctrl* ($n = 8$); (* $P_{Bonf} = 0.033$). Dots on histograms represent each individuals. (C) Semi-quantitative analysis of tuberin immunoreactivity in BLA from PN50_inj rats. Histograms show tuberin mean gray fluorescence intensity measured in cells colocalizing viral EGFP and tuberin fluorescence (EGFP(+)) or non-transduced cells expressing only tuberin (EGFP(-)) in BLAs of rats injected at PN50 with *Vir_ctrl* or *Vir1_Tsc2*. Dots represent individual data. Sample images (down) show corresponding examples in a PN50_inj animal (tuberin: red; EGFP: green, Colocalization: Yellow, Scale bar = 100 μ m; objective x10). Note the significant decrease of tuberin fluorescence signal intensity selectively in EGFP(+) cells compared to EGFP(-) transduced with *Vir1_Tsc2* vector ($n = 9$ amygdalae), but not in those transduced with *Vir_ctrl* ($n = 8$); (* $P_{Bonf} = 0.039$). Dots on histograms represent individual data. (D) Semi-quantitative analysis of p70S6K-p fluorescent punctate in EGFP(+) cells of PN25_inj rats with *Vir_ctrl* or *Vir1_Tsc2*. Histograms show the density of punctate counted in cells co-expressing viral EGFP per number of cells. Note the significant elevation of p70S6K-p protein expression in BLA cells transduced by the KD-virus (*Vir1_Tsc2*, $n = 9$ amygdalae) compared to BLA cells transduced with the control vector (*Vir_ctrl*, $n = 13$ amygdalae; unpaired t-test *Vir_ctrl* vs *Vir1_Tsc2*, * $P = 0.031$). Sample images (below) show corresponding examples for each channel (p70S6K-p: red; EGFP: green ; Merge: yellow. Scale bar = 10 μ m; objective x40). (E) Semi-quantitative analysis of p70S6K-p fluorescent punctate in EGFP(+) cells of PN50_inj rats with *Vir_ctrl* or *Vir1_Tsc2*. Histograms show the density of punctate counted in cells co-expressing viral EGFP per number of cells. Note the significant elevation of p70S6K-p protein expression in BLA cells transduced by the KD-virus (*Vir1_Tsc2*, $n = 12$ amygdalae) compared to BLA cells transduced with the control vector (*Vir_ctrl*, $n = 7$ amygdalae; unpaired t-test *Vir_ctrl* vs *Vir1_Tsc2*, ** $P = 0.019$). Sample images (below) show corresponding examples for each channel (p70S6K-p: red; EGFP: green ; Merge: yellow. Scale bar = 10 μ m; objective x40).

Knowing that tuberous sclerosis complex is a negative regulator of mTOR, impairment of one of its components, hamartin (*Tsc1*) or tuberin (*Tsc2*), inhibits its activity. In order to control whether the KD-*Tsc2* resulted in the elevation of mTOR pathway's activity, a semi-quantitative analysis of phosphorylated p70S6K (p70S6K-p) protein expression, a well-known marker of mTOR activity (Fig. S1) was assessed on animals injected at PN25 or PN50 with *Vir_ctrl* or *Vir1_Tsc2* (Fig. 2C,D). Results showed that PN25 and PN50 animals injected with *Vir1_Tsc2* presented at adult age a significant elevation of p70S6K-p protein expression in EGFP-expressing cells *ex vivo* (Fig. 2D, unpaired t-test (Welch correction), $t(21)=8.69$; $P = 0.031$; Fig. 2E, unpaired t-test (Welch correction), $t(18)=15.957$; $P = 0.019$) suggesting here an increased mTOR activity after *Tsc2* mRNA knockdown since both time-points.

Also, no differences were observed in EGFP or background IR between the two sets of BLAs, reflecting a similar transduction rate between viral conditions (not shown) with a main EGFP localization into the BLA for animals injected at PN25 or PN50 with the control or KD viruses (Fig. S2B,C).

Behavioral outcomes of *Tsc2* partial inhibition in basolateral amygdala

Behavioral testing was undertaken in PN25_injected (PN25_inj) and PN50_injected (PN50_inj) rats 7 weeks after viral infusion, once they all had reached adulthood. The animals were tested on behaviors relying on the integrity of the networks involving the amygdala and the prefrontal cortex (i.e., fear conditioning and fear extinction paradigms). The data were analyzed using a Three-Way Repeated Measures (RM) ANOVA comparing freezing behavior during each trial or context Day (within-subject factor) and 2 x 2 between-subject factors: the age of viral injection (PN25 and PN50) and the viral condition (ctrl and knock-down *Vir1*). Thus, the following analyses were based on a (nTrial or Context Day) x Viral Condition x Age of injection design.

Statistical analysis of the freezing to context, measured before the first tone of each session, showed no difference between viral conditions, nor between ages at which the vector was injected, at any of the five days, but only a global day effect (**Fig. S3B, Table S1A**). Bonferroni *post hoc* analysis revealed a differential level of fear between Day 1 and all the other tested days ($P_{bonf} < 0.001$) and between Day 2 and all the other days ($P_{bonf} < 0.001$), revealing an increase in the level of fear to context for all animals after the fear learning session. Planned comparisons between freezing to context A before fear learning (Day 2) and freezing to the new context B at extinction day (Day 3) showed no differential generalization of fear to the new context (Day 2 vs Day 3, **Table S1A**), and no differences between viral conditions or ages of injection at Day 3 (**Table S1A**). However, a differential renewal of fear to the initial learning context (Day 4 vs Day 5) was revealed between ages of injection (PN25 and PN50) (Day 4 vs Day 5, **Fig. S3B, Table S1A**, Day x Age interaction, $P = 0.048$), which was due to a decreased level of fear to context B at the end of extinction testing for PN25_inj animals. Animals injected with the KD virus, whatever the age of injection, globally showed a lower percentage of freezing at the two testing days (Day 4 and 5) compared to animals injected with the control virus (Viral condition effect, $P = 0.043$). Bonferroni *post hoc* analyses revealed that PN25_injected rats, but not PN50_injected rats, showed an increase in freezing

1
2
3 between Day 4 and Day 5 (PN25_inj: $P_{\text{bonf}} < 0.001$; PN50_inj : $P_{\text{bonf}} = 0.434$). These results
4 revealed that PN25_inj rats showed a higher return of fear to the initial learning context,
5 regardless of the virus condition (Control and KD virus), suggesting a faster extinction to
6 context B and/or a stronger renewal of fear to the conditioning context. This may reflect an
7 impact of the surgical procedure and/or the anesthesia on a developing brain (i.e., PN25_inj
8 rats) that could influence fear behavior at adult age.
9
10
11
12
13
14

15
16 Freezing levels specific to the tone CS were different depending on the age at which the
17 KD virus was injected during distinct phases of the protocol (**Fig. 3B, Table S1B** for detailed
18 statistical analyses). During habituation (Day 1), there were no differences between viral
19 conditions or age of injection in the percent freezing to the CS, suggesting a comparable
20 unconditioned reaction between groups. During fear learning (Day 2), there was a rapid
21 increase in the percent freezing to the CS across repetitions of CS-US pairings, with a
22 significant Trial x Age interaction ($F(6,276) = 2.825$; $P = 0.025$). Bonferroni *post hoc* analysis
23 only pointed to slightly different kinetic curves depending on the ages of injection without
24 revealing differences between groups at any trial, reflecting successful fear learning for all viral
25 conditions or age of injection. As freezing increased rapidly between CS1 and CS2 for all
26 groups, there was no evidence of latent inhibition of fear learning due to pre-exposure to the
27 tone alone at Day 1, although it cannot be completely overruled. Overall, fear learning was
28 largely unaffected by pre-exposure to the tone, age of infusion and/or *Tsc2* inhibition. Long-
29 term fear memory, assessed through the analysis of the first five CS in a new context the next
30 day (Day 3, trials 1-5), differed depending on the age of injection, with PN25_injected rats
31 showing a lower level of freezing compared to PN50_injected rats (Age effect; ($F(1,46) = 6.289$,
32 $P = 0.016$). The level of fear extinction, as assessed through the analysis of the last five CS on
33 that day (Day 3, trials 16-20), revealed an effect of the Viral Condition ($F(1,46) = 4.222$, $P =$
34 0.046), with no effect of the age of lentiviral injection. These results indicate that rats with *Tsc2*-
35 KD in BLA showed a delayed, slowed rate of extinction compared to control, but similarly
36 whether rats had been injected during early or late adolescence. However, when the long-term
37 memory of extinction was assessed 24h later (Day 4, extinction recall), no differences between
38
39
40
41
42
43
44
45
46
47
48
49
50
51
52
53
54
55
56
57
58
59
60

1
2
3 ages or viral conditions were detected, with all animals presenting a high level of fear to tone
4
5 1 presentation, close to that observed at the beginning of Day 3. As the level of freezing was
6
7 still somewhat high at the last tone of Day 3 (tone 20), even for control animals, fear extinction
8
9 acquisition may have been incomplete for all groups, and a strong fear reminiscence effect
10
11 may have hidden any differential memory of extinction. Statistical analysis through tone
12
13 presentation at day 4 revealed further extinction, similar for all groups (Trial effect, $F(4,184) =$
14
15 $16.338, P < 0.001$). This was also true during the renewal test in the original context on Day 5,
16
17 during which only a global Trial effect was observed ($F(4,184) = 27.994, P < 0.001$), but no
18
19 significant main group effect and no significant group x trial interaction, indicating that the rats
20
21 did not differ in their CS-associated memory whatever the context they were tested in.
22
23
24
25
26
27
28
29
30
31
32
33
34
35
36
37
38
39
40
41
42
43
44
45
46
47
48
49
50
51
52
53
54
55
56
57
58
59
60

A

| | | |
|-----------------------------------|-------------------------------------|----------------------|
| Day 1 Habituation | 5 CS — 30 s 4 kHz | Context A |
| Day 2 Fear Learning | 7 CS — 30 s 7 US — 0.5 s, 0.5 mA | |
| Day 3 Fear Extinction | 20 CS — 30 s 4 kHz | Context B |
| Day 4 Extinction Recall | 5 CS — 30 s 4 kHz | |
| Day 5 Renewal | 5 CS — 30 s 4 kHz | Context A |
| Generalization | 5 new tone — 30 s 11 kHz | |

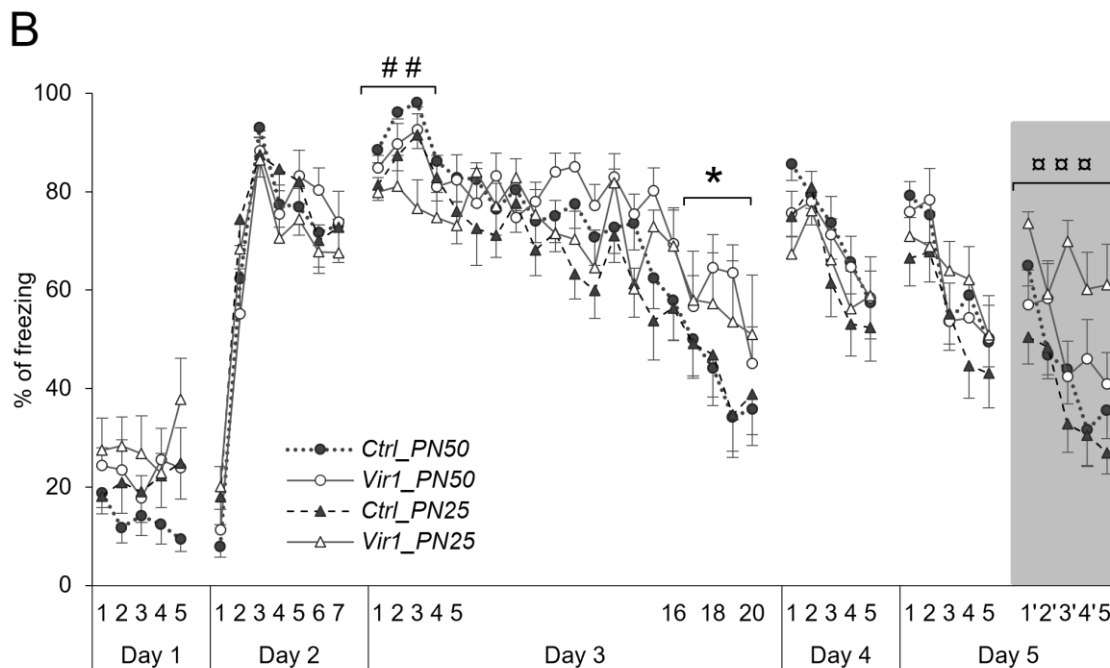


Figure 3. Delayed extinction and overgeneralization to a new tone in rats injected with *Vir1_Tsc2* at PN25. (A) Fear conditioning protocol. The protocol consisted in five consecutive days. Habituation (day 1) and Fear Learning (day 2) were conducted in context A, Extinction (day 3) and Extinction Recall (day 4) in context B. Fear Renewal (day 5) was performed in context A with presentation of the CS alone, followed 3 minutes later by generalization testing, consisting of five presentations of a new tone. **(B)** Rats injected with *Vir1_Tsc2* at PN25 displayed retarded fear extinction and fear overgeneralization. The percent freezing to the 30s tone was measured for each trial in groups of rats injected with KD (*Vir1_Tsc2*) and control (*Vir_ctrl*) viruses at PN25 or PN50, as indicated (*Vir_ctrl* PN25_inj, $n = 15$; *Vir1_Tsc2* PN25_inj, $n = 10$; *Vir_ctrl* PN50_inj, $n = 11$; *Vir1_Tsc2* PN50_inj, $n = 8$). Detailed statistics are provided in **Table S1**. The significant differences were an effect of the age of injection during the first 5 trials of Day 3 with a higher level of freezing for PN50_injected compared to PN25_injected rats, whatever the viral condition (Age effect, $^{##}P = 0.016$) an effect of viral condition for the last 5 trials of Day 3 (Viral condition effect, $^*P = 0.046$) revealing a higher level of freezing in *Tsc2*-KD rats regardless of the age of injection, and a (viral condition x age) interaction

1
2
3 during generalization testing (Day 5, highlighted in gray), revealing a higher level of freezing only in rats injected with *Vir1_Tsc2*
4 at PN25 (Bonferroni *post hoc* test, **** $P < 0.001$) compared to PN25 rats injected with *Vir_ctrl*.

5
6
7 In contrast, when fear generalization was assessed by presenting a distinct and unknown tone,
8
9 a differential level of fear was observed depending on the viral condition and age of injection
10
11 (**Fig. 3B**, Day 5 Trials 1' to 5'; Age x Viral Condition interaction, $F(1,46) = 7.25$, $P = 0.010$), due
12
13 to an apparent failure for rats to decrease fear responses during this part of the test, selectively
14
15 in those injected at PN25 with KD *Vir1_Tsc2* vector. Bonferroni *post hoc* analysis confirmed
16
17 this by revealing a significant difference between *Vir_ctrl* and *Vir1_Tsc2* conditions in
18
19 PN25_injected rats ($P_{bonf} < 0.001$), but not in PN50_injected rats, suggesting that only
20
21 PN25_injected rats with *Vir1_Tsc2* showed an overgeneralization of fear to a new tone. **As no**
22
23 **differential level of fear was observed to context A alone or to the tone CS on Day 5, it seems**
24
25 **unlikely that either could have played a role in the elevated fear responses to the new tones**
26
27 **observed for PN25_Vir1 rats. Hence, elevated generalization of fear observed in PN25 with**
28
29 **KD *Vir1_Tsc2* vector seems specific to the new tone presentation.**

30
31
32 In order to consolidate our conclusion that the knockdown of *Tsc2* in BLA was
33
34 responsible for alterations of fear behavior and discard a putative off-target effect of the virus,
35
36 we also tested in parallel the impact of the second KD lentivirus, *Vir2_Tsc2* when injected in
37
38 BLA of PN25 rats, by assessing fear conditioning, extinction and generalization following the
39
40 same protocol as in **Fig. 3A**. Immunofluorescence results showed a similar effect of *Vir2_Tsc2*
41
42 compared to *Vir1_Tsc2* on p70S6K-p activity elevation, confirming a successful effect on
43
44 *Tsc2*/mTOR's activity modulation (**Fig. S3A**). The behavioral results are shown in **Fig. S3C,D**.
45
46 For each phase of the protocol, a Helmert contrast test was used to compare *Vir_ctrl* vs
47
48 [*Vir1_Tsc2*, *Vir2_Tsc2*] on one hand, and *Vir1_Tsc2* vs *Vir2_Tsc2* on the other hand (See
49
50 **Table S2** for statistical details). Freezing to the context showed no differences between viral
51
52 conditions except in context B at the beginning of extinction recall session (Day 4), where
53
54 PN25_injected rats with *Vir2_Tsc2* showed a significantly higher level of fear than animals
55
56 injected with *Vir1_Tsc2* (**Fig. S3C; Table S2A**; Helmert Contrast Test $t(32) = -2.493$, $P =$
57
58 0.018). This higher level of fear might reflect an overgeneralization of fear to the safe context,
59
60

1
2
3 where the CS presentation alone during extinction in the new context transferred an aversive
4 value to this context.
5

6
7 Freezing levels to CS showed that the effects of *Vir2_Tsc2* were similar to *Vir1_Tsc2*
8 (see **Fig. S3D, Table S2B** for detailed statistical results), except for habituation (Day 1). On
9 that day, there was no significant difference between the two KD viral conditions and the control
10 virus, but *Vir1_Tsc2* injected rats showed a higher level of freezing to the unconditioned tone
11 compared to *Vir2_Tsc2* (Helmert contrast test, $P = 0.008$). However, fear learning (Day 2) was
12 comparable among groups, showing that they correctly and equally learnt the task. Importantly,
13 analyzing the level of freezing during the last five trials of extinction on Day 3 confirmed that
14 PN25 rats injected with a KD virus, *Vir1_Tsc2* and *Vir2_Tsc2*, showed a higher level of freezing
15 compared to animals injected with the control virus, indicating that both KD viral conditions
16 were associated with a delayed fear extinction (Helmert Contrast test, *Vir_ctrl* vs
17 [*Vir1_Tsc2*, *Vir2_Tsc2*], $t(32) = - 2.539$, $P = 0.016$), with no significant difference between
18 *Vir1_Tsc2* and *Vir2_Tsc2* injected animals. Analysis of generalization to a new tone on Day 5
19 (Tones 1'-5') indicated also no difference between *Vir1_Tsc2* and *Vir2_Tsc2*, and a significant
20 difference between these two groups of animals and the *Vir_ctrl* group ($t(32) = - 4.587$, P
21 < 0.001), confirming that rats injected with *Vir1_Tsc2* or *Vir2_Tsc2* into the BLA during
22 adolescence overgeneralized their fear to the new tone at the adult age.
23
24
25
26
27
28
29
30
31
32
33
34
35
36
37
38
39
40
41
42
43

44 Thus, *Vir2_Tsc2* injections in PN25 rats' BLA mostly altered fear behavior in the same
45 way as *Vir1_Tsc2* injected animals at PN25, as reflected by a poorer fear extinction and an
46 overgeneralization of fear to a new tone. This indicates that these behavioral outcomes were
47 not due to unspecific off-target effects and validates our model of *Tsc2* knock down effect
48 during brain development. As surgery or anesthetics may impact brain connectivity and
49 behavior (Pattwell et al. 2016), the ketamine administration took place lately in brain
50 development, and no signs of abnormal home-cage behavior (apathy, social interaction, food
51 and water intakes) nor behavioral deficits in fear learning and memory, suggesting little effect
52
53
54
55
56
57
58
59
60

1
2
3 of surgery on emotional state. In all, the behavioral results showed that a partial knockdown
4 (KD) of *Tsc2* into the BLA during early adolescence had a greater impact on behaviors
5 involving the fear circuit compared to a KD of *Tsc2* set out in a more mature brain. Indeed,
6
7 whereas both groups of age showed a higher fear to the tone CS at a late phase of extinction
8
9 learning, only rats injected with *Vir1_Tsc2* and *Vir2_Tsc2* at PN25 showed overgeneralization
10
11 of fear to an unknown tone in the initial learning context.
12
13
14

Basal neural activity changes following *Tsc2* partial inhibition in basolateral amygdala.

15
16
17
18
19 Knowing the functional role of the BLA – mPFC pathway in fear acquisition and extinction, the
20 behavioral outcomes unveiled in this study are congruent with a potential impact of BLA
21 modification on a still maturing mPFC, with a stronger impact when KD was induced from early
22 adolescence (PN25). Brains were taken for c-Fos immunohistochemistry (IHC) 7 weeks after
23 the fear conditioning protocol, from rats injected with *Vir_ctrl* or *Vir1_Tsc2*. Hence, BLA,
24 prelimbic (PL) and infralimbic (IL) parts of the mPFC were analyzed for c-Fos(+) IHC as
25 reflecting basal levels of neural activity (**Fig. 4A,B**). For these analyses, we considered each
26 hemisphere independently, given the bilateralism of injection (Cassell and Wright 1986).
27
28
29
30
31
32
33
34
35
36
37
38
39
40
41
42
43
44
45
46
47
48
49
50
51
52
53
54
55
56
57
58
59
60

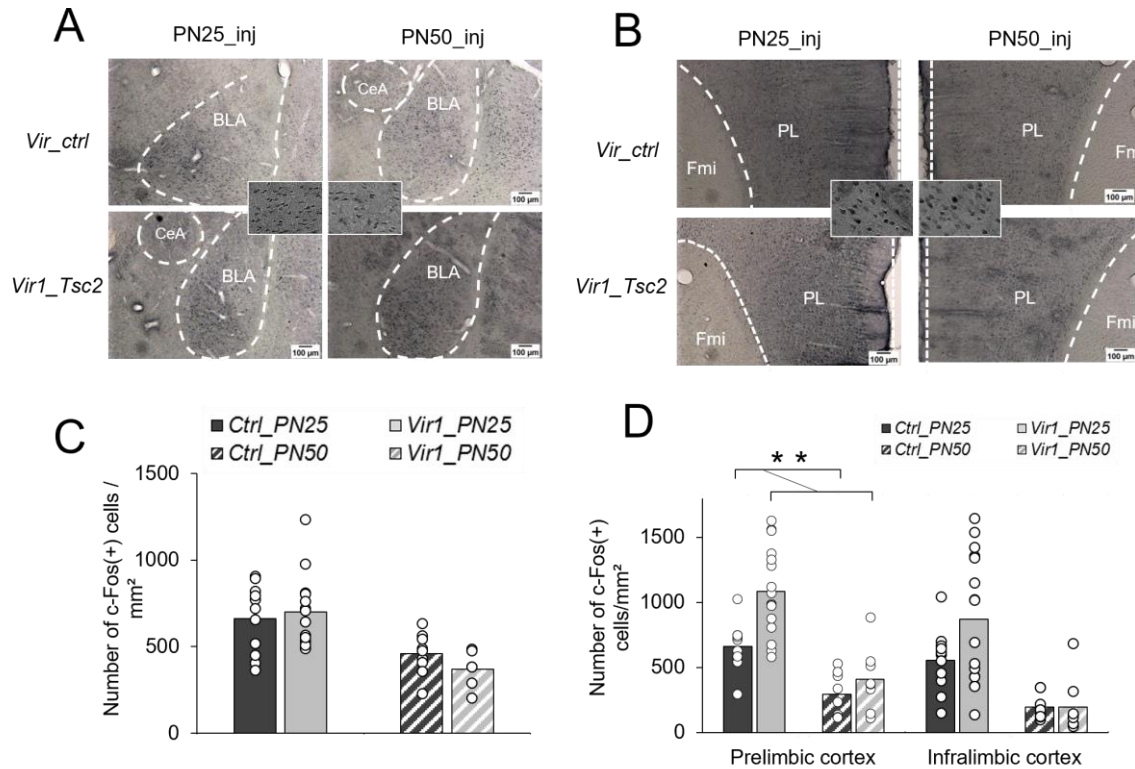


Figure 4. Basal neural activity was higher in prefrontal cortex later in adulthood in rats injected with KD_Tsc2 (Vir1) in the BLA at PN25. **(A)** Sample images of c-Fos immunostaining in basolateral amygdala in rats injected with *Vir_ctrl* or *Vir1_Tsc2* at PN25 (left panel) or PN50 (right panel). c-Fos(+) cells (black stain) were counted in basolateral amygdala near the site of injection. BLA: basolateral amygdala; CeA : Central Amygdala; Fmi : *Forceps minor corpus callosum*. **(B)** Sample images of c-Fos immunostaining in Prelimbic Cortex (PL) in rats injected with *Vir_ctrl* or *Vir1_Tsc2* at PN25 (left panel) or PN50 (right panel). c-Fos(+) cells (black stain) were counted in PL and infralimbic (IL, not shown) cortices. **(C)** Density of c-Fos(+) cells in basolateral amygdala (BLA) of rats injected at PN25 or PN50 with *Vir_ctrl* or *Vir1_Tsc2*. The histograms show the mean number of c-Fos(+) cells per square millimeter (*Vir_ctrl* PN25_inj, $n = 11$; *Vir1_Tsc2* PN25_inj, $n = 14$; *Vir_ctrl* PN50_inj, $n = 9$; *Vir1_Tsc2* PN50_inj, $n = 6$), near the site of injection. Dots represent individual data. No differences were observed between viral conditions in the number of c-Fos(+) into the BLA, but only a simple age effect, revealing a higher c-Fos(+) cells density in BLAs for animals injected at PN25. **(D)** Density of c-Fos(+) cells in prefrontal and infralimbic cortices of rats injected at PN25 or PN50 with *Vir_ctrl* or *Vir1_Tsc2*. The histograms show the mean number of c-Fos(+) cells per square millimeter in PL or IL cortices (*Vir_ctrl* PN25_inj, $n = 11$; *Vir1_Tsc2* PN25_inj, $n = 16$; *Vir_ctrl* PN50_inj, $n = 8$; *Vir1_Tsc2* PN50_inj, $n = 8$). Dots represent individual data. There was a significant effect of the age of injection on c-Fos expression for both PL and IL cortices, with a higher number of c-Fos(+) cells for PN25_inj rats compared to PN50_inj rats, and a significant effect of viral condition for PL cortex (Viral condition effect, $**P = 0.002$).

Density of c-Fos(+) cells in BLA and prefrontal cortex

Near the site of injection in the BLA, there was no difference in c-Fos(+) cell density between viral conditions (**Fig. 4C**, Viral condition, $F(1,36) = 0.201$, $P = 0.656$), but a significant higher number of c-Fos(+) cells in PN25_inj animals was observed (**Fig. 4C**, Age effect, $F(1,36) = 20.273$, $P < 0.001$; differences of 39% in c-Fos(+) cells density between PN25 and PN50_inj group irrespective of their viral condition).

In contrast, specific changes were detected in the prefrontal cortex. Viral injection resulted in a higher density of c-Fos(+) cells in the prefrontal cortex (PL) depending on the age

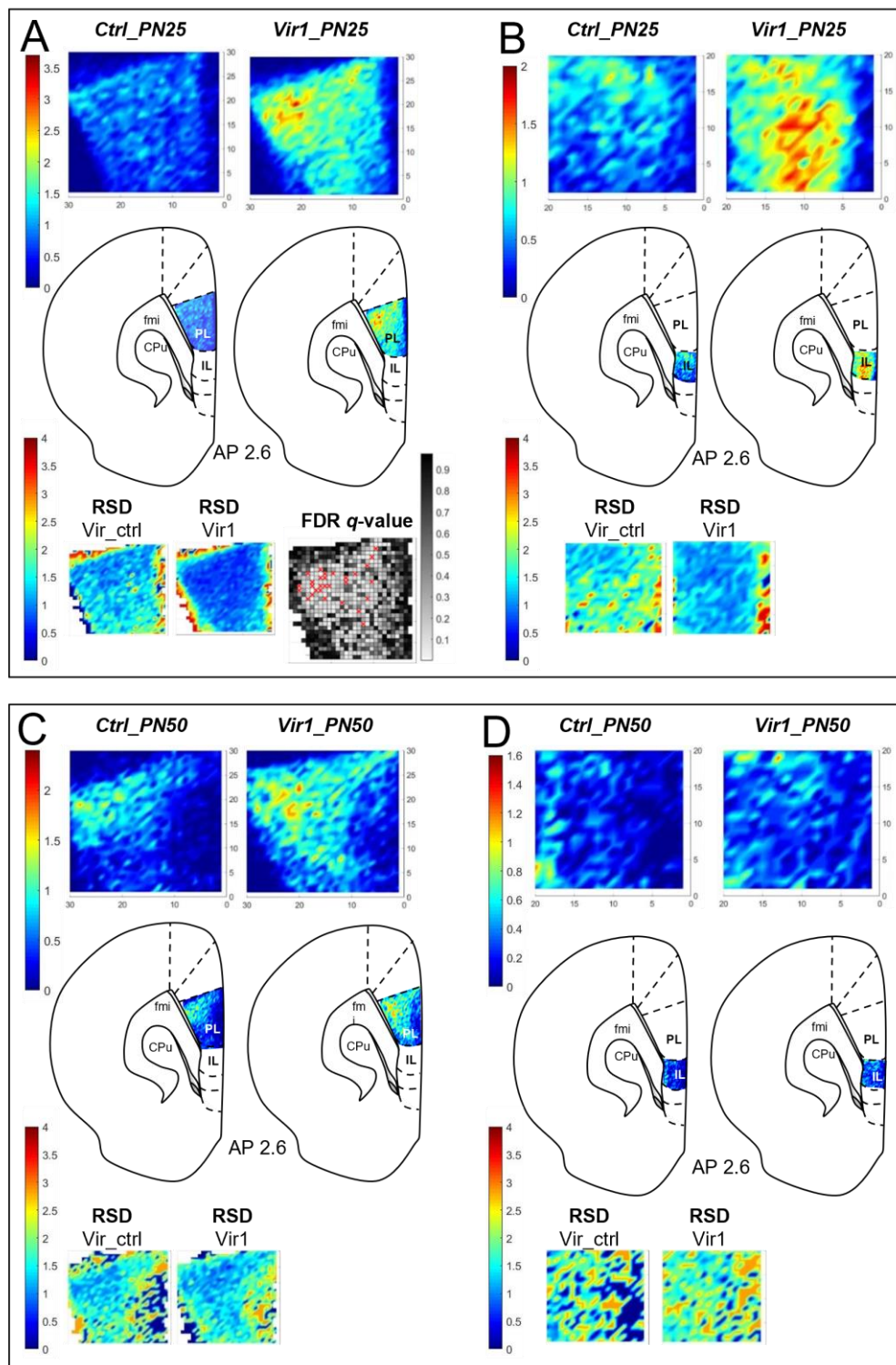
1
2
3 of injection or the viral condition (**Fig. 4D**, Two-Way ANOVA; Age effect $F(1,39) = 40.07$, $P <$
4 0.001 ; Viral condition effect $F(1,39) = 10.488$, $P = 0.002$; 40 % changes in c-Fos expression in
5 PL between PN25 and PN50_inj and 37 % changes in c-Fos expression in PL between Vir_ctrl
6 and Vir1_Tsc2 injected animals) with no significant Viral condition x Age interaction ($F(1,39) =$
7 3.482 , $P = 0.07$). The same tendency was observed for the infralimbic cortex (IL), but the viral
8 condition effect did not reach significance (Age effect $F(1,39) = 22.20$, $P < 0.001$; 27 % changes
9 in c-Fos expression in PL between PN25 and PN50_inj), suggesting a differential effect of
10 *Tsc2*-KD in BLA, PL and IL depending on the adolescence period (early or late). Knowing that
11 the trajectories of BLA-mPFC and PL-IL projections develop in a laminar-dependent manner,
12 we further investigated the distribution of the increased c-Fos activity within the prefrontal
13 cortex.
14
15
16
17
18
19
20
21
22
23
24
25
26
27
28
29

Spatial distribution of c-Fos(+) cells in PL and IL cortices

30
31 To analyze the spatial distribution of basal cell activity, we created a density heat map (HM)
32 representing the proportion of c-Fos(+) cells in PL or IL cortices at two anteroposterior (AP)
33 levels (AP 2.6 and AP 2.7 mm from Bregma), and analyzed them with a Two-Way RM ANOVA
34 (viral condition x XY coordinates) for each age of injection.
35
36
37
38
39

40 At AP 2.6 from PN25_inj rats, the HM evidenced changes in c-Fos(+) cells density in
41 PL cortex through a significant Viral Condition x XY Coordinates interaction (**Fig. 5A**, Viral
42 Condition x Coordinates interaction, $F(829,18260) = 1.375$, $P < 0.0001$), with significant
43 differences between viral conditions for 29 out of 830 tested bins (**Fig. 5A**, *post hoc* False
44 Discovery Rate (FDR), q -values comprised between $q < 0.0001$ and $q = 0.00868$). This
45 reflected that *Vir1_Tsc2* injected animals had a higher c-Fos(+) cell density selectively in bins
46 located in the deepest and middle layers of the PL structure. Interestingly, the analysis in IL
47 cortex also revealed a significant Viral Condition x XY Coordinates interaction (**Fig. 5B**,
48 $F(399,8778) = 1.191$, $P = 0.0062$), but among the 400 tested bins on FDR analysis, none
49
50
51
52
53
54
55
56
57
58
59
60

1
2
3 differed between viral conditions. So, as observed in the heat map, rats injected with *Vir1_Tsc2*
4
5 showed a global higher density in infralimbic cortex compared to *Vir_ctrl* animals.
6
7



8
9
10
11
12
13
14
15
16
17
18
19
20
21
22
23
24
25
26
27
28
29
30
31
32
33
34
35
36
37
38
39
40
41
42
43
44
45
46
47
48
49
50
51
52
53
54
55
56
57
58
59
60

Figure 5. Differential spatial distribution of basal cell activities in PL and IL cortices are induced by *Vir1_Tsc2* injection in BLA at early adolescence (PN25). (A) Density heat maps representing the mean distribution of c-FOS(+) cells in PL cortex at antero-posteriority of 2.6 mm from Bregma (AP 2.6) of adult rats injected into the BLA during early adolescence (PN25) (*Vir_ctrl*, $n = 11$ or *Vir1_Tsc2*, $n = 13$). Warmer colors indicate higher cell density (scales at left). Numbers beside x and y axis (0-30) represent the number of bins in each axis (30x30 bins). The "RSD heat maps" represent the Relative Standard Deviation (RSD) calculated for each bin for each viral condition, with warmer colors representing higher dispersion of data around the mean calculated in each bin (scale at left). The FDR q -value map (in black and white) represents the q -values obtained in each tested

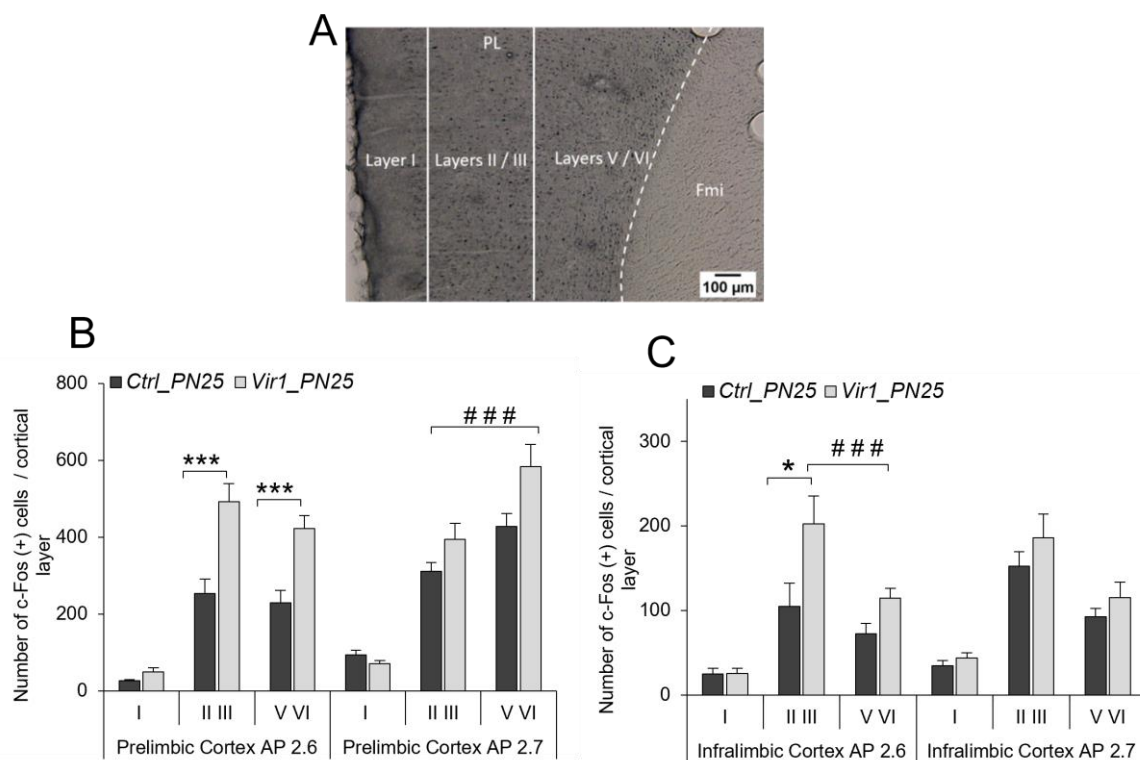
bin from a False Discovery Rate (FDR) statistical test, following a significant interaction in the Two-Way RM ANOVA of Density Heat Map; whiter colors represent q -values approaching significant differences (scale at right from $q = 0$ to 1); the 29 red crosses point to the significant differences detected between groups for each tested bin. **(B)** Density Heat Maps representing the distribution of c-FOS(+) cells in IL cortex at antero-posteriority 2.6 mm from Bregma (AP 2.6) of adult rats injected into the BLA during early adolescence with *Vir_ctrl* or *Vir1_Tsc2* and their relative RSD heat maps. Numbers beside x and y axis (0-20) represent the number of bins in each axis (20x20 bins). Note that density heat map color scales are different between PL and IL structures. **(C)** Density Heat Maps representing the mean distribution of c-Fos(+) cells counted in PL cortex at antero-posteriority of 2.6 mm from Bregma (AP 2.6) of rats injected into the BLA at late adolescence (PN50, *Vir_ctrl*, $n = 8$; *Vir1_Tsc2*, $n = 8$). Warmer colors indicate a higher cell density (scale at left) and their relative RSD heat maps below. Statistical tests revealed no interaction or differences between viral conditions. **(D)** Density Heat Maps representing the mean distribution of c-Fos(+) cells counted in IL cortex at antero-posteriority 2.6 mm from Bregma (AP 2.6) of rats injected into the BLA during late adolescence (*Vir_ctrl*, $n = 8$; *Vir1_Tsc2*, $n = 8$) and their relative RSD heat maps below. Statistical tests revealed no interaction or differences between viral conditions. Notice that Density Heat Map color scales differ between PL and IL cortices, but also with PN25_inj animals.

The analysis at AP 2.7 also confirmed a significant Viral Condition x XY Coordinates interaction in PL cortex of PN25_inj rats (**Table S3**, $P < 0.0001$), although *post hoc* FDR found only 2 significant bins among the 829 bins tested (**Fig. S4A**). Finally, differential results were obtained from infralimbic cortex at AP 2.7 (**Fig. S4B**) compared to AP 2.6, as we found no significant differences in c-Fos(+) cells density but only a significant XY coordinate effect (**Table S3**, $P < 0.0001$; 400 bins tested).

In PN50_inj animals, *Tsc2*-KD did not result in differences in c-Fos(+) cell density within PL or IL cortex at AP 2.6 (**Fig. 5C**, 852 bins tested; **Fig. 5D**, 396 bins), nor at AP 2.7 (PL 2.7 : **Fig. S4C**, 865 bins tested; IL 2.7: **Fig. S4D**, 394 bins; Statistical details in **Table S3**). In sum, this topographical analysis of c-Fos(+) cell density in PL or IL cortices unveiled that the spatial distribution of the effects of the vectors depended on the age at which the virus had been injected in the BLA.

To analyze whether the differences observed in c-Fos expression were specific to certain cortical layers, we sorted the total number of c-Fos(+) cells depending on their layers of origin in PL or IL cortices (**Fig. 6A**). This analysis revealed a significant Viral Condition x Layer interaction in PL cortex at AP 2.6 in rats injected in the BLA at PN25 (**Fig. 6B**, PL cortex AP 2.6, Viral Condition x Layer interaction, $F(2,44) = 7.729$, $P = 0.001$, **Table S4**), with a significant increase in the number of cells in middle (II III : *Vir_ctrl* vs *Vir1_Tsc2*, $P_{bonf} < 0.001$) and deep layers (V VI : *Vir_ctrl* vs *Vir1_Tsc2*, $P_{bonf} < 0.001$) in animals injected at PN25 with *Vir1_Tsc2*. Similar results were obtained at AP 2.7 (Viral Condition x Layer interaction, $F(2,48) = 4.147$, $P = 0.031$), with an increase in the number of cells in PL cortex at layers V VI compared to layers II III only in *Vir1_Tsc2* condition (II III vs V VI, *Vir1_Tsc2*, $P_{bonf} < 0.001$).

1
2
3 Interestingly, a significant Viral Condition x Layer interaction was also found in the IL cortex at
4 AP 2.6 (**Fig. 6C**, $F(2.44) = 5.395$, $P = 0.024$), with a significant increase in the number of cells
5 in layers II III (II III : *Vir_ctrl* vs *Vir1_Tsc2*, $P_{bonf} = 0.013$), for the *Vir1_Tsc2* condition, and an
6 increase in the number of cells at layers V VI compared to layers II III in *Vir1_Tsc2* condition
7 only (II III vs V VI, *Vir1_Tsc2*, $P_{bonf} = 0.001$). When the same analysis was performed for
8 PN50_inj animals, no differences were found between viral conditions, whatever the brain area
9
10
11
12
13
14
15
16 (**Fig. S5 A,B, Table S4**).



45
46
47
48
49
50
51
52
53
54
55
56
57

Figure 6. Differential increase in number of c-Fos(+) cells depending on cortical layers in PL and IL cortices in rats injected in the BLA with *Vir1_Tsc2* during early adolescence (PN25). (A) c-Fos immunostaining example image of a PL cortex from a PN25_inj rat with *Vir_ctrl* showing the cortical layers delimitations (Adapted from (van Eden and Uylings 1985; Van De Werd et al. 2010). Layer I is a thin layer almost acellular; Layers II III and V VI are thicker and densely marked. Cortical layers II to VI are hardly distinguishable with a c-Fos immunostaining, sizes proportions described in literature has been used to do proper delimitations. (B) Layers II III and V VI of PL cortex contained a higher number of c-Fos(+) cells in adult rats injected with *Vir1_Tsc2* at early adolescence (PN25). The histograms show the number of c-Fos(+) cells sorted depending on the origin belonging layers at Bregma 2.6 and 2.7 mm from most superficial (Layer I) to deeper (Layers V VI) layers. Rats injected with *Vir1_Tsc2* showed a significantly higher number of c-Fos(+) cells in both layers II III and V VI at AP 2.6 (*Vir_ctrl*, $n = 10$; *Vir1_Tsc2*, $n = 16$), and in layer V VI at AP 2.7 (Bonferroni *post-hoc* test, between Viral conditions, $***P_{bonf} < 0.001$; between layers for *Vir1_Tsc2*, $###P_{bonf} < 0.001$). (C) Layers II III of IL cortex contained a higher number of c-Fos(+) cells in rats injected with *Vir1_Tsc2* at early adolescence (PN25). The histograms show the number of c-Fos(+) cells in IL cortex sorted depending on their origin belonging layers at Bregma 2.6 mm and 2.7 mm. Rats injected with *Vir1_Tsc2* showed a significantly higher number of c-Fos(+) cells in layers II III at AP 2.6 (Bonferroni *post-hoc* test, between viral conditions, $*P_{bonf} = 0.024$; between layers for *Vir1_Tsc2*, $###P_{bonf} = 0.001$). (*Vir_ctrl*, $n = 11$; *Vir1_Tsc2*, $n = 13$).

58
59
60

Animals injected with the KD virus at early adolescence showed an increased basal activity at adulthood in specific layers in the prefrontal cortex and altered fear-related behaviors

1
2
3 when subjected to fear conditioning at adulthood, suggesting a potential relationship between
4 these two observations. In order to further determine possible correlations, we generated a
5 principal component analysis (PCA) and a correlation matrix including six variables from
6 behavioral and IHC experiments of PN25_inj rats: number of c-Fos(+) cells in PL or IL cortices
7 in Layers II III or V VI at AP2.6, and percent freezing at the end of extinction (Day 3, Tones 16-
8 20) or during generalization testing (Day 5, Tones 1'-5'). The PCA extracted two principal
9 components (factor 1 and 2) contributing to 78.39 % of the variance (**Fig. S6A**), which
10 comprised the number of c-Fos(+) cells in PL cortex and percent of freezing to tones 1'-5' at
11 generalization testing for Factor 1, and the number of c-Fos(+) cells in IL cortex for Factor 2
12 (**Fig. S6A,B**). Percent freezing during extinction equally contributed to the two factors.
13 Bartlett's sphericity test revealed that correlated variables respected homogeneity of variances
14 ($\chi^2(20) = 64.031, P < 0.0001$).

15
16 The associated correlation matrix pointed to a logical high correlation between number
17 of c-Fos(+) cells in middle and deep layers for both PL ($R^2 = 0.645, P = 0.001$), and IL ($R^2 =$
18 $0.742; P = 0.0002$) cortices (**Fig. S6C**), reflecting the anatomical and functional relationship in
19 cell activity between these two cortical layers in each structure. Interestingly, there was also a
20 significant correlation between the freezing level at generalization test and the number of c-
21 Fos(+) cells in layer II-III of PL cortex (**Fig. S6C, $R^2 = 0.37; p = 0.027$**), suggesting a relationship
22 between the specific increased generalization observed for PN25_inj animals and the elevated
23 basal cellular activity in middle layers of PL cortex. Given the 7 weeks elapsed between the
24 last fear tests and the brain's collection, it is unlikely that the changes in basal c-Fos occurred
25 as a long-term consequence of fear learning, although this cannot be completely ruled out.
26
27 **Rather, the correlation observed between our variables suggests that the specific elevation of**
28 **fear observed for PN25_inj animals during the generalization tests may have been a**
29 **consequence of the elevated basal cellular activity in middle layers of PL cortex at the time of**
30 **generalization testing and/or when animals experienced fear conditioning and extinction (Fig.**
31 **S7C). Whether a further elevation of cellular activity was elicited during fear conditioning or**
32 **generalization tests remains an open question.**

1
2
3
4
5
6
7
8
9
10
11
12
13
14
15
16
17
18
19
20
21
22
23
24
25
26
27
28
29
30
31
32
33
34
35
36
37
38
39
40
41
42
43
44
45
46
47
48
49
50
51
52
53
54
55
56
57
58
59
60

Discussion

What predisposes to the emergence of fear-related disorder when a trauma or a stressing event is experienced during adulthood is still unclear, and early life insults in combination with genetic factors likely play a role (Henigsberg et al. 2019; Chaby et al. 2020; Rumball et al. 2020). A dysfunctional amygdala-prefrontal (AP) network's activity is a potential predisposal source, since massive maturation is still undergoing until adulthood under the control of the early functional amygdala, a detector/regulator of adverse events (Gee et al. 2013; Hwang et al. 2014; Tottenham and Gabard-Durnam 2017; VanTieghem and Tottenham 2018).

In the present study, we used a lentiviral methodology in rats, which mimics changes in *Tsc2* seen in TSC patients and intended to produce mTOR dysregulation and altered connectivity within the amygdala and between amygdala and cortical structures. We showed that a partial knock-down of the *Tsc2* mRNA in the BLA at early adolescence in rat (PN25) is associated with selective behavioral alterations in a fear conditioning paradigm assessed at adult age and long-term modification of adult neural activity in specific layers of the prelimbic (PL) and infralimbic (IL) parts of the mPFC. These changes could underlie the emergence of fear-related disorders following an auditory fear conditioning at adult age, expressed as a lower rate of fear extinction and overgeneralization of fear to a new sound.

The lentiviral methodology was chosen to spatially circumscribe the incorporation and action of the miRNA as much as possible to the BLA. The KD virus was under a CaMKII promoter, aiming at targeting the 80% excitatory pyramidal cells of BLA, which highly express CaMKII (McDonald 1984; Ouimet et al. 1984). Pyramidal CaMKII-expressing cells activity in the amygdala is essential for conditioned fear learning and the modulation of its expression (Johansen et al. 2010; Butlet et al. 2017), and a stimulation of BLA CaMKII-projecting cells to the central amygdala may have a role in anxiety in rats (Tye et al. 2011). Moreover, CaMKII is an essential protein for the induction of NMDAR-dependent LTP in the amygdala and in the formation of synaptic plasticity (Murakoshi et al. 2018; Zalcmán et al. 2018). Hence, by targeting CaMKII-expressing pyramidal cells, we ensured to target an important class of cells for fear behavior and its related plasticity. Our analyses indicated for both ages of injection that

1
2
3 reduced tuberlin expression by approximately 14-20% and concomitant increased mTOR
4 activity does not induce obvious morphological changes in BLA area and volume (not shown),
5 although BLA dendritic arborization still develops through adolescence (Koss et al. 2014).
6
7 Although Tsc correlates with epilepsy (Mizuguchi et al. 2021), the fact that not all of the
8 amygdala cells were transduced by the KD lentiviruses, and the transfection was localized and
9 BLA-restricted, is likely to have lowered the risk for amygdala-generated general epilepsy, as
10 no change in c-Fos(+) cells was observed near the site of injection in BLA, and no overt sign
11 for major epilepsy was ever observed in any of the animals in their home cage nor at any stage
12 of the visually-monitored behavioral experiments. The sole difference observed was age-
13 related, and not virus-related, with a higher level of BLA neural activity in animals injected
14 during early adolescence (PN25), as compared to those injected at late adolescence (PN50).
15
16 As we chose to keep the same delay between surgery and perfusion (14 weeks) to ensure an
17 equivalent time of viral activity in BLA between groups, animals had a difference of 25 days of
18 age at the time of perfusion (respectively PN125 and PN150). Nevertheless, it is unlikely that
19 the observed differences in c-Fos counting were due to this 25-day lag, as the brain is fully
20 mature at these two ages. Rather, the global difference could possibly be due to a long-term
21 age-dependent differential impact of anesthesia and/or surgery, in particular early in
22 development (e.g.,(Ju et al. 2020)). Whether compensatory mechanisms have been at play,
23 to keep BLA micro-networks activity at a homeostatic level when BLA's activity was disrupted
24 by viral activity will need further investigation.

25
26
27
28
29
30
31
32
33
34
35
36
37
38
39
40
41
42
43
44
45 More importantly regarding our initial aim, changes were observed in basal neural
46 activity in mPFC, specifically in animals injected with the *Tsc2*-KD virus in the BLA at early
47 adolescence (PN25). It seems unlikely that these changes were directly related to the fear
48 conditioning, as all brains were taken directly from the colony room at least 7 weeks after the
49 last fear conditioning session, and no similar changes were observed in BLA. The increased
50 c-Fos(+) cells were seen in all, except superficial layers of PL and IL cortices, and in the deep
51 layers of IL cortex. The middle (II-III) and deep (V-VI) layers are known to be directly
52 interconnected with the BLA, with the development of BLA to mPFC connectivity preceding
53
54
55
56
57
58
59
60

1
2
3 reciprocal projections (Bouwmeester, Smits, et al. 2002; Bouwmeester, Wolterink, et al. 2002;
4 Arruda-Carvalho et al. 2017). At PN25, the connectivity between amygdala and mPFC is still
5 in development, marked by a dense sprouting of projections emerging from the posterior BLA
6 to layer V of PL and IL cortices (Cunningham et al. 2002). Reciprocally, adolescence is marked
7 by the development of projections from deep layers of mPFC to BLA, mainly to its anterior part,
8 that are significantly pruned from late adolescence to adulthood (PN45 – PN90) (Cressman,
9 Balaban, Steinfeld, Shemyakin, Graham, et al. 2010; Arruda-Carvalho et al. 2017). Knowing
10 that bidirectional cortico-cortical connections between PL and IL cortices are made through
11 deep (V-VI) and, to a lesser extent, middle (II-III) layers (Marek et al. 2018; Mukherjee and
12 Caroni 2018), and that projections from IL to BLA originate from layer II-III and V (Ferreira et
13 al. 2015), the increase in c-Fos(+) cells' density in layer II-III of IL cortex, but not in the deepest
14 layers, may suggest a dysregulation of activity in the PL-IL-BLA network. Indeed, during this
15 developmental stage, connectivity within the prefrontal cortex is also under
16 construction/refinement (van Eden and Uylings 1985; Kolb et al. 2012; Chini and Hanganu-
17 Opatz 2021), and an imbalance between excitatory and inhibitory drives may have also been
18 at play (Caballero et al. 2014; Konstantoudaki et al. 2018). Thus, *Tsc2*-KD in the posterior BLA
19 at the time of major development of its connectivity with the prefrontal cortex could have
20 stimulated the development of projections between the two structures, thus producing a long-
21 term alteration of mPFC functioning, particularly in the PL cortex, until adulthood.

22
23
24
25
26
27
28
29
30
31
32
33
34
35
36
37
38
39
40
41
42
43 At the behavioral level, we found two reliable effects of BLA *Tsc2*-KD: (1) A delayed
44 fear extinction acquisition in BLA *Tsc2*-KD animals, whatever the age at which the virus was
45 injected; (2) an overgeneralization of fear to an unknown tone stimulus selectively in animals
46 for which BLA *Tsc2*-KD was induced at early adolescence (PN25), excepting for slight
47 discrepancies between the effects of the two KD viruses (*Vir1*, *Vir2*), possibly due to off-target
48 effects. As only 20 % of BLA cells are engaged in the Pavlovian fear conditioning learning and
49 extinction (Han et al. 2007), and given the known BLA's involvement in contextual fear (Chaaya
50 et al. 2018), we could have expected changes in fear learning and fear memory. However, the
51 observed normal fear learning to the CS and the context concurs with the lack of modification
52
53
54
55
56
57
58
59
60

1
2
3 in overall BLA basal neural activity. The similar levels of freezing observed in all groups during
4 and 24h after fear conditioning, as well as 24h after extinction, rather support the hypothesis
5 of a **differential rate** in the acquisition of extinction, not a strengthened fear expression, in *Tsc2*-
6 KD animals. This **slowed extinction could** be due to a modified connectivity or cells' reactivity
7 to the CS within BLA, especially given the rather posterior location of our injection sites (Zhang
8 et al. 2020). Since no modification was observed in basal levels of neural activity in the BLA,
9 it is unlikely that the behavioral phenotype reflected a hyper-activity of BLA cells, but rather a
10 modified responsiveness of BLA cells to the CS during the acquisition of extinction.
11 Nevertheless, the fact that the mPFC-to-BLA connectivity undergoes significant pruning from
12 PN45 to PN90 suggests this process might have been similarly affected in both groups of age
13 (Cressman, Balaban, Steinfeld, Shemyakin, Graham, et al. 2010; Cressman, Balaban,
14 Steinfeld, Shemyakin, Parisot, et al. 2010), thus resulting in a similar phenotype in the two
15 groups. **Moreover, as *Tsc2* gene expression in amygdala seems constant through
16 development in human brains (Li et al. 2018), we unlikely interfered with a period of over- or
17 under-regulation of *Tsc2* gene through adolescence, but rather on important developmental
18 changes relative to adolescent period. The KD-*Tsc2* disruption could have thus impacted the
19 dynamic of connectivity development between the amygdala and the prelimbic cortex (Pattwell
20 et al. 2016) during adolescence, potentially amplifying these developmental processes and
21 creating a vulnerability ground to fear-related disorders appearance at adulthood when
22 challenged by stressful events. Whether the delayed extinction was due to the KD-*Tsc2* during
23 adolescence and/or at the time of extinction remains an open question that would need the
24 technical development for a temporary knockdown of *Tsc2*, as well as a temporary rescue of
25 *Tsc2* to address it.** Interestingly, it has recently been shown that recent recall of fear memory
26 following Pavlovian conditioning engages cells activity in the deep layers of PL cortex, whereas
27 long-term recall of fear memory may depend on activity in layers II III of PL cortex (Jacques et
28 al. 2019). Whether, in our model, specific PL or IL layers are more engaged by the CS at the
29 end of extinction, and whether the modified connectivity concerns the PL or IL afferents to
30
31
32
33
34
35
36
37
38
39
40
41
42
43
44
45
46
47
48
49
50
51
52
53
54
55
56
57
58
59
60

1
2
3 specific cells in the BLA, and/or to within BLA connectivity or cells' reactivity within the BLA,
4
5 will need further investigation.
6

7 The overgeneralization to a new auditory stimulus was selectively observed in *Tsc2*-
8
9 KD BLA animals injected early in adolescence (PN25). Generalization is often studied in
10
11 relation to context, and when studied in relation to cued-fear memory, it is often in a
12
13 discriminative setting. Here, generalization testing took place in the initial training context
14
15 where the animals had never been exposed to this new auditory stimulus, which had a higher
16
17 frequency than the original CS in order to ensure good detection. The overgeneralization was
18
19 specific to the unknown auditory stimulus, as no elevated fear was observed in these same
20
21 animals neither to a novel context (context B), nor to the context and CS during the renewal
22
23 test. The neural basis of cued fear generalization is still poorly understood (for a recent review,
24
25 see (Asok et al. 2019)). Of most interest to us is the involvement of both the amygdala (Ghosh
26
27 and Chattarji 2015)(Resnik and Paz 2015), and the mPFC, in particular the PL (Vieira et al.
28
29 2015; Concina et al. 2018), as *Tsc2*-KD animals injected at early adolescence showed higher
30
31 basal neural activity in the PL cortex. The significant correlation found between the specific
32
33 increase of basal c-Fos activity in layers II-III of PL cortex and the level of fear measured during
34
35 the new tone presentation suggests a functional link between the basal level of cells' activity
36
37 in middle layers of PL cortex and the fear-related disorder-like overgeneralization of fear.
38
39
40
41
42
43
44
45
46
47
48
49
50
51
52
53
54
55
56
57
58
59
60

Conclusion

In all, our findings indicate that early life *Tsc2* -related dysfunction in the rat's amygdala could exert a bias towards fear-related disorder occurrence later in adult life following a threat, and a long-lasting alteration in mPFC activity. The phenotype observed included delayed fear extinction and overgeneralization to a new stimulus when the down-regulation was induced at the time of development of connectivity between the amygdala and the prefrontal cortex (PN25), which resulted in long-term changes in basal neural activity in the prelimbic cortex. These changes are likely due to changes in functional connectivity between the prefrontal cortex and basolateral amygdala, as well as cue-evoked cells' reactivity to auditory stimuli in both brain regions during fear conditioning, extinction and generalization, which needs to be confirmed in future research. Our findings indicate that early life *Tsc2*-related dysfunction in the amygdala may induce long-lasting vulnerabilities leading to a bias towards FRD occurrence later in life. As it has been previously shown, animal models of TSC present higher states of anxiety, alterations in contextual fear discrimination, and an imbalance in excitatory/inhibitory transmission (Ehninger et al. 2008; Ehninger and Silva 2011; Haji et al. 2020). **Although *Tsc2* is a protein essential for a proper brain development from embryonic stage, our experimental strategy permitted to identify specific post-natal ages during which a KD-*Tsc2* may interfere with brain developmental processes and induce long-term effects on emotional behavior and connectivity between the amygdala and its associated structures.** Hence, our experimental strategy brings forward a new type of animal model to study how specific genetic conditions associated with environmental stressors could induce long-lasting changes in connectivity between the prefrontal cortex and the amygdala (Huang et al. 2016; Pagani et al. 2020), which may predispose to fear-related disorders appearance at adult age, in particular in TSC individuals suffering of GAD, phobias, or PTSD.

Acknowledgments

We thank Nathalie Samson-Desvignes for her precious help in immunohistochemistry assessment, Véronique Rousseau for her help in biochemistry experiments, and the zootechnicians for their daily engagement in animal care.

Supplementary material

Supplementary data are available at *Cerebral Cortex* online.

Funding

This work was supported by Ministère de l'Enseignement Supérieur, de la Recherche, et de l'Innovation (MESRI) to FJ; by the Programme Hubert Curien, France-Australia Science Innovation Collaboration (PHC FASIC) (Grant number 43402ZA) to FJ, LRJ, VD; by Brainscopes (Paris-Saclay University) (Grant number REC-2018-031) to CV and VD, and by the National Center of Scientific Research (CNRS) and Université Paris-Saclay to JF, CV, NEM and VD.

Notes

FJ carried out the *in vivo* experiments and analyzed the data. FJ, NEM, CV, VD designed the experiments and wrote the manuscript. PJ, MK and HV designed the viral vectors and carried out the *in vitro* experiments. MK, LJ, HV commented and edited the manuscript. LRJ and SR developed and trained FJ to microanatomy analysis. All the authors equally contributed to the interpretation of data. All the authors declare no conflicts of interest.

References

- 1
2
3
4
5 Arruda-Carvalho M, Wu WC, Cummings KA, Clem RL. 2017. Optogenetic examination of
6
7 prefrontal-amygdala synaptic development. *J Neurosci.* 37:2976–2985.
8
9 Asok A, Kandel ER, Rayman JB. 2019. The neurobiology of fear generalization. *Front Behav*
10
11 *Neurosci.* 12:1–15.
12
13 Atwoli L, Stein DJ, Koenen KC, McLaughlin KA. 2015. Epidemiology of posttraumatic stress
14
15 disorder: Prevalence, correlates and consequences. *Curr Opin Psychiatry.* 28:307–311.
16
17 Bandelow B, Michaelis S. 2015. Epidemiology of anxiety disorders in the 21st century.
18
19 *Dialogues Clin Neurosci.* 17:327–335.
20
21 Bergstrom HC, McDonald CG, Johnson LR. 2011. Pavlovian Fear Conditioning Activates a
22
23 Common Pattern of Neurons in the Lateral Amygdala of Individual Brains. *PLoS One.*
24
25 6:e15698.
26
27 Blanchard RJ, Blanchard DC. 1969. Crouching as an index of fear. *J Comp Physiol Psychol.*
28
29 67:370–375.
30
31 Boronat S, van Eeghen AM, Shinnick JE, Newberry P, Thiele EA. 2013. Stressor-related
32
33 disorders in tuberous sclerosis. *Ann Clin Psychiatry.* 25:243–249.
34
35 Bouwmeester H, Smits K, Van Ree JM. 2002. Neonatal development of projections to the
36
37 basolateral amygdala from prefrontal and thalamic structures in rat. *J Comp Neurol.*
38
39 450:241–255.
40
41 Bouwmeester H, Wolterink G, Van Ree JM. 2002. Neonatal development of projections from
42
43 the basolateral amygdala to prefrontal, striatal, and thalamic structures in the rat. *J Comp*
44
45 *Neurol.* 442:239–249.
46
47 Bremner JD, Elzinga B, Schmahl C, Vermetten E. 2007. Structural and functional plasticity of
48
49 the human brain in posttraumatic stress disorder. *Prog Brain Res.* 167:171–186.
50
51 Burghy C a, Stodola DE, Ruttle PL, Molloy EK, Jeffrey M, Oler J a, Fox ME, Hayes AS, Kalin
52
53 NH, Essex MJ, Davidson RJ, Birn RM. 2013. Developmental pathways to amygdala-
54
55 prefrontal function and internalizing symptoms in adolescence. *Nat Neurosci.* 15:1736–
56
57 1741.
58
59
60

- 1
2
3 Butler RK, Ehling S, Barbar M, Thomas J, Hughes MA, Smith CE, Pogorelov VM, Aryal DK,
4
5 Wetsel WC, Lascelles BD. 2017. Distinct neuronal populations in the basolateral and
6
7 central amygdala are activated with acute pain, conditioned fear, and fear-conditioned
8
9 analgesia. *Neurosci Lett.* 661:11–17.
10
11 Caballero A, Flores-Barrera E, Cass DK, Tseng KY. 2014. Differential regulation of
12
13 parvalbumin and calretinin interneurons in the prefrontal cortex during adolescence. *Brain*
14
15 *Struct Funct.* 219:395–406.
16
17 Cassell MD, Wright DJ. 1986. Topography of projections from the medial prefrontal cortex to
18
19 the amygdala in the rat. *Brain Res Bull.* 17:321–333.
20
21 Chaaya N, Battle AR, Johnson LR. 2018. An update on contextual fear memory mechanisms:
22
23 Transition between Amygdala and Hippocampus. *Neurosci Biobehav Rev.* 92:43–54.
24
25 Chaby LE, Lasseter HC, Geier C, Jeromin A. 2020. Determining effects of adolescent stress
26
27 exposure on risk for posttraumatic stress disorder in adulthood. *Curr Opin Behav Sci.*
28
29 36:79–89.
30
31 Chini M, Hanganu-Opatz IL. 2021. Prefrontal Cortex Development in Health and Disease:
32
33 Lessons from Rodents and Humans. *Trends Neurosci.* 44:227–240.
34
35 Choi YJ, Di Nardo A, Kramvis I, Meikle L, Kwiatkowski DJ, Sahin M, He X. 2008. Tuberous
36
37 sclerosis complex proteins control axon formation. *Genes Dev.* 22:2485–2495.
38
39 Cisler JM, Sigel BA, Steele JS, Smitherman S, Vanderzee K, Pemberton J, Kramer TL, Kilts
40
41 CD. 2016. Changes in functional connectivity of the amygdala during cognitive reappraisal
42
43 predict symptom reduction during trauma-focused cognitive-behavioral therapy among
44
45 adolescent girls with post-traumatic stress disorder. *Psychol Med.* 46:3013–3023.
46
47 Cloitre M, Stolbach B, Herman J, van der Kolk B, Pynoos R, Wang J, Petkova E. 2009. A
48
49 Developmental Approach to Complex PTSD: Childhood and Adult Cumulative Trauma as
50
51 Predictors of Symptom Complexity. *J Trauma Stress.* 22:399–408.
52
53 Concina G, Cambiaghi M, Renna A, Sacchetti B. 2018. Coherent activity between the prelimbic
54
55 and auditory cortex in the slow-gamma band underlies fear discrimination. *J Neurosci.*
56
57 38:8313–8328.
58
59
60

- 1
2
3 Cressman VL, Balaban J, Steinfeld S, Shemyakin A, Graham P, Parisot N, Moore H. 2010.
4
5 Prefrontal cortical inputs to the basal amygdala undergo pruning during late adolescence
6
7 in the rat. *J Comp Neurol.* 518:2693–2709.
8
9 Cressman VL, Balaban J, Steinfeld S, Shemyakin A, Parisot N, Moore H. 2010. Pruning During
10
11 Late Adolescence in the Rat. *J Comp Neurol.* 518:2693–2709.
12
13 Cunningham MG, Bhattacharyya S, Benes FM. 2002. Amygdalo-cortical sprouting continues
14
15 into early adulthood: Implications for the development of normal and abnormal function
16
17 during adolescence. *J Comp Neurol.* 453:116–130.
18
19 de Vries PJ, Belousova E, Benedik MP, Carter T, Cottin V, Curatolo P, Dahlin M, D’Amato L,
20
21 Beaure d’Augères G, Ferreira JC, Feucht M, Fladrowski C, Hertzberg C, Jozwiak S,
22
23 Lawson JA, Macaya A, Marques R, Nabbout R, O’Callaghan F, Qin J, Sander V, Sauter
24
25 M, Shah S, Takahashi Y, Touraine R, Youroukos S, Zonnenberg B, Kingswood JC,
26
27 Jansen AC. 2020. Tuberous Sclerosis Complex-Associated Neuropsychiatric Disorders
28
29 (TAND): New Findings on Age, Sex, and Genotype in Relation to Intellectual Phenotype.
30
31 *Front Neurol.* 11:1–12.
32
33
34 de Vries PJ, Wilde L, de Vries MC, Moavero R, Pearson DA, Curatolo P. 2018. A clinical update
35
36 on tuberous sclerosis complex-associated neuropsychiatric disorders (TAND). *Am J Med*
37
38 *Genet Part C Semin Med Genet.* 178:309–320.
39
40 Ehninger D, Han S, Shilyansky C, Zhou Y, Li W, David J. 2008. Reversal of learning deficits in
41
42 a *Tsc2*^{+/-} mouse model of tuberous sclerosis. *14:843–848.*
43
44 Ehninger D, Silva AJ. 2011. Increased levels of anxiety-related behaviors in a *Tsc2* dominant
45
46 negative transgenic mouse model of tuberous sclerosis. *Behav Genet.* 41:357–363.
47
48 Fenster RJ, Lebois LAM, Ressler KJ, Suh J. 2018. Brain circuit dysfunction in post-traumatic
49
50 stress disorder: from mouse to man. *Nat Rev Neurosci.* 19:535–551.
51
52 Ferreira AN, Yousuf H, Dalton S, Sheets PL. 2015. Highly differentiated cellular and circuit
53
54 properties of infralimbic pyramidal neurons projecting to the periaqueductal gray and
55
56 amygdala. *Front Cell Neurosci.* 9:1–15.
57
58 Gee DG, Humphreys KL, Flannery J, Goff B, Telzer EH, Shapiro M, Hare TA, Bookheimer SY,
59
60

- 1
2
3 Tottenham N. 2013. A developmental shift from positive to negative connectivity in human
4 amygdala-prefrontal circuitry. *J Neurosci*. 33:4584–4593.
5
6
7 Ghosh S, Chattarji S. 2015. Neuronal encoding of the switch from specific to generalized fear.
8 *Nat Neurosci*. 18:112–120.
9
10
11 Gründemann J, Lüthi A. 2015. Ensemble coding in amygdala circuits for associative learning.
12 *Curr Opin Neurobiol*. 35:200–206.
13
14
15 Ha S, Sohn I-J, Kim N, Sim HJ, Cheon K-A. 2015. Characteristics of Brains in Autism Spectrum
16 Disorder: Structure, Function and Connectivity across the Lifespan. *Exp Neurobiol*.
17 24:273–284.
18
19
20
21
22 Haji N, Riebe I, Aguilar-Valles A, Artinian J, Laplante I, Lacaille JC. 2020. Tsc1
23 haploinsufficiency in Nkx2.1 cells upregulates hippocampal interneuron mTORC1 activity,
24 impairs pyramidal cell synaptic inhibition, and alters contextual fear discrimination and
25 spatial working memory in mice. *Mol Autism*. 11:1–19.
26
27
28
29
30 Han J-H, Kushner SA, Yiu AP, Cole CJ, Matynia A, Brown RA, Neve RL, Guzowski JF, Silva
31 AJ, Josselyn SA. 2007. Neuronal Competition and Selection During Memory Formation.
32 *Science* (80-). 316:457–460.
33
34
35
36
37 Haruvi-Lamdan N, Horesh D, Zohar S, Kraus M, Golan O. 2020. Autism Spectrum Disorder
38 and Post-Traumatic Stress Disorder: An unexplored co-occurrence of conditions. *Autism*.
39 24:884–898.
40
41
42
43 Henigsberg N, Kalember P, Petrović ZK, Šečić A. 2019. Neuroimaging research in
44 posttraumatic stress disorder – Focus on amygdala, hippocampus and prefrontal cortex.
45 *Prog Neuro-Psychopharmacology Biol Psychiatry*. 90:37–42.
46
47
48
49 Hermans EJ, Battaglia FP, Atsak P, De Voogd LD, Fernández G, Rozenaal B. 2014. How
50 the amygdala affects emotional memory by altering brain network properties. *Neurobiol*
51 *Learn Mem*. 112:2–16.
52
53
54
55 Hoeffler CA, Klann E. 2010. mTOR signaling: At the crossroads of plasticity, memory and
56 disease. *Trends Neurosci*. 33:67–75.
57
58
59
60 Hollocks MJ, Lerh JW, Magiati I, Meiser-Stedman R, Brugha TS. 2019. Anxiety and depression

1
2
3 in adults with autism spectrum disorder: A systematic review and meta-analysis. *Psychol*
4
5 *Med.* 49:559–572.

6
7 Huang WC, Chen Y, Page DT. 2016. Hyperconnectivity of prefrontal cortex to amygdala
8
9 projections in a mouse model of macrocephaly/autism syndrome. *Nat Commun.* 7:1–15.

10
11 Hwang S, White S, Nolan Z, Sinclair S, Blair RJR. 2014. Neurodevelopmental changes in the
12
13 responsiveness of systems involved in top down attention and emotional responding.
14
15 *Neuropsychologia.* 62:277–285.

16
17 Im K, Ahtam B, Haehn D, Peters JM, War SK, Sahin M, Grant PE. 2016. Altered Structural
18
19 Brain Networks in Tuberous Sclerosis Complex. *Cereb Cortex.* 26:2046–2058.

20
21 Jacques A, Chaaya N, Hettiarachchi C, Carmody ML, Beecher K, Belmer A, Chehrehasa F,
22
23 Bartlett S, Battle AR, Johnson LR. 2019. Microtopography of fear memory consolidation
24
25 and extinction retrieval within prefrontal cortex and amygdala. *Psychopharmacology*
26
27 (Berl). 236:383–397.

28
29 Jacques A, Wright A, Chaaya N, Overell A, Bergstrom HC, McDonald C, Battle AR, Johnson
30
31 LR. 2018. Functional neuronal topography: A statistical approach to micro mapping
32
33 neuronal location. *Front Neural Circuits.* 12:1–14.

34
35 Johansen JP, Hamanaka H, Mon MH, Behnia R, Deisseroth K, Blair HT. 2010. Optical
36
37 activation of lateral amygdala pyramidal cells instructs associative fear learning. *Proc Natl*
38
39 *Acad Sci U S A.* 107:12692–12697.

40
41 Johnson FK, Delpech J-C, Thompson GJ, Wei L, Hao J, Herman P, Hyder F, Kaffman A. 2018.
42
43 Amygdala hyper-connectivity in a mouse model of unpredictable early life stress. *Transl*
44
45 *Psychiatry.* 8:49.

46
47 Ju X, Ryu MJ, Cui J, Lee Y, Park S, Hong B, Yoo S, Lee WH, Shin YS, Yoon SH, Kweon GR,
48
49 Kim YH, Ko Y, Heo JY, Chung W. 2020. The mTOR Inhibitor Rapamycin Prevents
50
51 General Anesthesia-Induced Changes in Synaptic Transmission and Mitochondrial
52
53 Respiration in Late Postnatal Mice. *Front Cell Neurosci.* 14:1–10.

54
55 Kaiser RH, Clegg R, Goer F, Pechtel P, Beltzer M, Vitaliano G, Olson DP, Teicher MH,
56
57 Pizzagalli DA. 2018. Childhood stress, grown-up brain networks: Corticolimbic correlates
58
59
60

- 1
2
3 of threat-related early life stress and adult stress response. *Psychol Med.* 48:1157–1166.
4
5 Kerns CM, Kendall PC, Berry L, Souders MC, Franklin ME, Schultz RT, Miller J, Herrington J.
6
7 2014. Traditional and atypical presentations of anxiety in youth with autism spectrum
8
9 disorder. *J Autism Dev Disord.* 44:2851–2861.
10
11 Khazipov R, Zaynutdinova D, Ogievetsky E, Valeeva G, Mitrukhina O, Manent JB, Represa A.
12
13 2015. Atlas of the postnatal rat brain in stereotaxic coordinates. *Front Neuroanat.* 9:1–5.
14
15 Kim JE, Lyoo IK, Estes AM, Renshaw PF, Shaw DW, Friedman SD, Kim DJ, Yoon SJ, Hwang
16
17 J, Dager SR. 2010. Laterobasal amygdalar enlargement in 6- to 7-year-old children with
18
19 autism spectrum disorder. *Arch Gen Psychiatry.* 67:1187–1197.
20
21 Klengel T, Binder EB. 2015. Epigenetics of Stress-Related Psychiatric Disorders and Gene x
22
23 Environment Interactions. *Neuron.* 86:1343–1357.
24
25 Koenen KC, Amstadter AB, Nugent NR. 2009. Gene-environment Interaction in Posttraumatic
26
27 Stress Disorder: An Update. *J Trauma Stress.* 22:416–426.
28
29 Kolb B, Mychasiuk R, Muhammad A, Li Y, Frost DO, Gibb R. 2012. Experience and the
30
31 developing prefrontal cortex. *Proc Natl Acad Sci U S A.* 109:17186–17196.
32
33 Konstantoudaki A, Chalkiadaki K, Vasileiou E, Kalemaki K, Karagogeos D, Sidiropoulou K.
34
35 2018. Prefrontal cortical-specific differences in behavior and synaptic plasticity between
36
37 adolescent and adult mice. *J Neurophysiol.* 119:822–833.
38
39 Kopp CMC, Muzykewicz DA, Staley BA, Thiele EA, Pulsifer MB. 2008. Behavior problems in
40
41 children with tuberous sclerosis complex and parental stress. *Epilepsy Behav.* 13:505–
42
43 510.
44
45 Koss WA, Belden CE, Hristov AD, Juraska JM. 2014. Dendritic remodeling in the adolescent
46
47 medial prefrontal cortex and the basolateral amygdala of male and female rats. *Synapse.*
48
49 68:61–72.
50
51 Kriebel M, Ebel J, Battke F, Griesbach S, Volkmer H. 2020. Interference With Complex IV as
52
53 a Model of Age-Related Decline in Synaptic Connectivity. *Front Mol Neurosci.* 13:1–14.
54
55 Kriebel M, Metzger J, Trinks S, Chugh D, Harvey RJ, Harvey K, Volkmer H. 2011. The cell
56
57 adhesion molecule neurofascin stabilizes axo-axonic GABAergic terminals at the axon
58
59
60

1
2
3 initial segment. *J Biol Chem.* 286:24385–24393.

4
5 Ledoux JE. 1996. *The Emotional Brain : The mysterious underpinnings of emotional life.* New
6
7 York : Simon & Schuster.

8
9 LeDoux JE. 2000. Emotion Circuits in the Brain. *Annu Rev Neurosci.* 23:155–184.

10
11 Li Y, Barkovich MJ, Karch CM, Nillo RM, Fan C, Broce IJ, Tan CH, Cuneo D, Hess CP, Dillon
12
13 WP, Glenn OA, Glastonbury CM, Olney N, Yokoyama JS, Bonham LW, Miller B, Kao A,
14
15 Schmansky N, Fischl B, Andreassen OA, Jernigan T, Dale A, Barkovich AJ, Desikan RS,
16
17 Sugrue LP. 2018. Regionally specific TSC1 and TSC2 gene expression in tuberous
18
19 sclerosis complex. *Sci Rep.* 8:1–10.

20
21 Li Y, Corradetti MN, Inoki K, Guan KL. 2004. TSC2: Filling the GAP in the mTOR signaling
22
23 pathway. *Trends Biochem Sci.* 29:32–38.

24
25 Liberzon I, Sripada CS. 2007. The functional neuroanatomy of PTSD: a critical review. *Prog*
26
27 *Brain Res.* 167:151–169.

28
29 Marcotte L, Aronica E, Baybis M, Crino PB. 2012. Cytoarchitectural alterations are widespread
30
31 in cerebral cortex in tuberous sclerosis complex. *Acta Neuropathol.* 123:685–693.

32
33 Marek R, Xu L, Sullivan RKP, Sah P. 2018. Excitatory connections between the prelimbic and
34
35 infralimbic medial prefrontal cortex show a role for the prelimbic cortex in fear extinction.
36
37 *Nat Neurosci.* 21:654–658.

38
39 Márquez C, Poirier GL, Cordero MI, Larsen MH, Groner A, Marquis J, Magistretti PJ, Trono D,
40
41 Sandi C. 2013. Peripuberty stress leads to abnormal aggression, altered amygdala and
42
43 orbitofrontal reactivity and increased prefrontal MAOA gene expression. *Transl*
44
45 *Psychiatry.* 3:e216–e216.

46
47 Maximo JO, Cadena EJ, Kana RK. 2014. The implications of brain connectivity in the
48
49 neuropsychology of autism. *Neuropsychol Rev.* 24:16–31.

50
51 McDonald AJ. 1984. Neuronal organization of the lateral and basolateral amygdaloid nuclei in
52
53 the rat. *J Comp Neurol.* 222:589–606.

54
55 Mizuguchi M, Ohsawa M, Kashii H, Sato A. 2021. Brain Symptoms of Tuberous Sclerosis
56
57 Complex: Pathogenesis and Treatment. *Int J Mol Sci.* 22:6677.

- 1
2
3 Morey RA, Gold AL, LaBar KS, Beall SK, Brown VM, Haswell CC, Nasser JD, Wagner HR,
4
5 McCarthy G. 2012. Amygdala volume changes in posttraumatic stress disorder in a large
6
7 case-controlled veterans group. *Arch Gen Psychiatry*. 69:1169–1178.
8
9 Mukherjee A, Caroni P. 2018. Infralimbic cortex is required for learning alternatives to prelimbic
10
11 promoted associations through reciprocal connectivity. *Nat Commun*. 9:2727.
12
13 Murakoshi H, Shin ME, Parra-bueno P, Szatmari EM, Shibata ACE, Yasuda R. 2018. Kinetics
14
15 of endogenous CaMKII required for synaptic plasticity revealed by optogenetic kinase
16
17 inhibitor. *Neuron*. 94:37–47.
18
19 Neves LT, Neves PFR, Paz LV, Zancan M, Milanese BB, Lazzari GZ, da Silva RB, de Oliveira
20
21 MMBP, Venturin GT, Greggio S, da Costa JC, Rasia-Filho AA, Mestriner RG, Xavier LL.
22
23 2019. Increases in dendritic spine density in BLA without metabolic changes in a rodent
24
25 model of PTSD. *Brain Struct Funct*. 224:2857–2870.
26
27
28 Nimmo-Smith V, Heuvelman H, Dalman C, Lundberg M, Idring S, Carpenter P, Magnusson C,
29
30 Rai D. 2020. Anxiety Disorders in Adults with Autism Spectrum Disorder: A Population-
31
32 Based Study. *J Autism Dev Disord*. 50:308–318.
33
34 Ouimet CC, McGuinness TL, Greengard P. 1984. Immunocytochemical localization of
35
36 calcium/calmodulin-dependent protein kinase II in rat brain. *Proc Natl Acad Sci U S A*.
37
38 81:5604–5608.
39
40 Pagni M, Bertero A, Trakoshis S, Ulysse L, Locarno A, Miseviciute L, De Felice A, Canella C,
41
42 Supekar K, Galbusera A, Menon V, Tonini R, Deco G, Lombardo M, Pasqualetti M, Gozzi
43
44 A. 2020. A cross-species link between mTOR-related synaptic pathology and functional
45
46 hyperconnectivity in autism. *bioRxiv*.
47
48
49 Pattwell SS, Liston C, Jing D, Ninan I, Yang RR, Witztum J, Murdock MH, Dincheva I, Bath
50
51 KG, Casey BJ, Deisseroth K, Lee FS. 2016. Dynamic changes in neural circuitry during
52
53 adolescence are associated with persistent attenuation of fear memories. *Nat Commun*.
54
55 7:1–9.
56
57 Pavliša G, Papa J, Pavić L, Pavliša G. 2006. Bilateral MR volumetry of the amygdala in chronic
58
59 PTSD patients. *Coll Antropol*. 30:565–568.
60

- 1
2
3 Paxinos G, Watson C. 2009. *The Rat Brain in Stereotaxic Coordinates*. Academic P. ed.
4
5 London.
- 6
7 Preibisch S, Saalfeld S, Tomancak P. 2009. Globally optimal stitching of tiled 3D microscopic
8
9 image acquisitions. *Bioinformatics*. 25:1463–1465.
- 10
11 Rauch SL, Shin LM, Phelps EA. 2006. Neurocircuitry Models of Posttraumatic Stress Disorder
12
13 and Extinction: Human Neuroimaging Research-Past, Present, and Future. *Biol*
14
15 *Psychiatry*. 60:376–382.
- 16
17 Reis LB, Filippi-chiela EC, Ashton-prolla P, Visioli F. 2021. The paradox of autophagy in
18
19 Tuberous Sclerosis Complex. *Genet Mol Biol*. 44:e20200014.
- 20
21 Resnik J, Paz R. 2015. Fear generalization in the primate amygdala. *Nat Neurosci*. 18:188–
22
23 190.
- 24
25 Rodriguez-Seijas C, Gadow KD, Rosen TE, Kim H, Lerner MD, Eaton NR. 2020. A
26
27 transdiagnostic model of psychiatric symptom co-occurrence and autism spectrum
28
29 disorder. *Autism Res*. 13:579–590.
- 30
31 Rosen TE, Mazefsky CA, Vasa RA, Lerner MD. 2018. Co-occurring psychiatric conditions in
32
33 autism spectrum disorder. *Int Rev Psychiatry*. 30:40–61.
- 34
35 Rumball F, Happé F, Grey N. 2020. Experience of Trauma and PTSD Symptoms in Autistic
36
37 Adults: Risk of PTSD Development Following DSM-5 and Non-DSM-5 Traumatic Life
38
39 Events. *Autism Res*. 13:2122–2132.
- 40
41 Saha R, Knapp S, Chakraborty D, Horovitz O, Albrecht A, Kriebel M, Kaphzan H, Ehrlich I,
42
43 Volkmer H, Richter-Levin G. 2017. GABAergic Synapses at the Axon Initial Segment of
44
45 Basolateral Amygdala Projection Neurons Modulate Fear Extinction.
46
47 *Neuropsychopharmacology*. 42:473–484.
- 48
49 Scherf KS, Smyth JM, Delgado MR. 2013. The amygdala: An agent of change in adolescent
50
51 neural networks. *Horm Behav*. 64:298–313.
- 52
53 Schindelin J, Arganda-Carreras I, Frise E, Kaynig V, Longair M, Pietzsch T, Preibisch S,
54
55 Rueden C, Saalfeld S, Schmid B, Tinevez J-Y, White DJ, Hartenstein V, Eliceiri K,
56
57 Tomancak P, Cardona A. 2012. Fiji: an open-source platform for biological-image
58
59
60

1
2
3 analysis. *Nat Methods*. 9:676–682.

4
5 Sharma S, Powers A, Bradley B, Ressler KJ. 2016. Gene × Environment Determinants of
6
7 Stress- and Anxiety- Related Disorders. *Annu Rev Psychol*. 67:239–261.

8
9 Shin LM, Handwerker K. 2009. Is Posttraumatic Stress Disorder A Stress-Induced Fear
10
11 Circuitry Disorder? *J Trauma Stress*. 22:409–415.

12
13 Sierra-Mercado D, Padilla-Coreano N, Quirk GJ. 2011. Dissociable roles of prelimbic and
14
15 infralimbic cortices, ventral hippocampus, and basolateral amygdala in the expression
16
17 and extinction of conditioned fear. *Neuropsychopharmacology*. 36:529–538.

18
19 Sigmundi RA, Bouton ME, Bolles RC. 1980. Conditioned freezing in the rat as a function of
20
21 shock intensity and CS modality. *Bull Psychon Soc*. 15:254–256.

22
23 Top DN, Stephenson KG, Doxey CR, Crowley MJ, Kirwan CB, South M. 2016. Atypical
24
25 Amygdala Response to Fear Conditioning in Autism Spectrum Disorder. *Biol Psychiatry*
26
27 *Cogn Neurosci Neuroimaging*. 1:308–315.

28
29 Tottenham N, Gabard-Durnam L. 2017. The developing amygdala: a student of the world and
30
31 a teacher of the cortex. *Curr Opin Psychol*. 17:55–60.

32
33 Tsoory M, Cohen H, Richter-Levin G. 2007. Juvenile stress induces a predisposition to either
34
35 anxiety or depressive-like symptoms following stress in adulthood. *Eur*
36
37 *Neuropsychopharmacol*. 17:245–256.

38
39 Tye KM, Prakash R, Kim S, Fenno LE, Grosenick L, Zarabi H, Thompson KR, Gradinaru V,
40
41 Ramakrishnan C. 2011. Amygdala circuitry mediating reversible and bidirectional control
42
43 of anxiety. *Nature*. 471:358–362.

44
45 Uematsu A, Matsui M, Tanaka C, Takahashi T, Noguchi K, Suzuki M, Nishijo H. 2012.
46
47 Developmental Trajectories of Amygdala and Hippocampus from Infancy to Early
48
49 Adulthood in Healthy Individuals. *PLoS One*. 7:e46970.

50
51 Van De Werd HJJM, Rajkowska G, Evers P, Uylings HBM. 2010. Cytoarchitectonic and
52
53 chemoarchitectonic characterization of the prefrontal cortical areas in the mouse. *Brain*
54
55 *Struct Funct*. 214:339–353.

56
57 van Eden CG, Uylings HBM. 1985. Cytoarchitectonic development of the prefrontal cortex in
58
59
60

1
2
3 the rat. *J Comp Neurol.* 241:253–267.
4

5 VanTieghem M, Tottenham N. 2018. Neurobiological programming of early life stress:
6
7 Functional development of amygdala-prefrontal circuitry and vulnerability for stress-
8
9 related psychopathology. *Curr Top Behav Neurosci.* 38:117–136.
10

11 Vieira PA, Corches A, Lovelace JW, Westbrook KB, Mendoza M, Korzus E. 2015. Prefrontal
12
13 NMDA receptors expressed in excitatory neurons control fear discrimination and fear
14
15 extinction. *Neurobiol Learn Mem.* 119:52–62.
16

17
18 Whitaker AM, Gilpin NW, Edwards S. 2014. Animal models of post-traumatic stress disorder
19
20 and recent neurobiological insights. *Behav Pharmacol.* 25:398–409.
21

22 Zalcman G, Federman N, Romano A. 2018. CaMKII Isoforms in Learning and Memory:
23
24 Localization and Function. *Front Mol Neurosci.* 11:1–14.
25

26 Zhang X, Kim J, Tonegawa S. 2020. Amygdala Reward Neurons Form and Store Fear
27
28 Extinction Memory. *Neuron.* 105:1077-1093.e7.
29

30 Zimmermann K, Richardson R, Baker K. 2019. Maturation Changes in Prefrontal and
31
32 Amygdala Circuits in Adolescence: Implications for Understanding Fear Inhibition during
33
34 a Vulnerable Period of Development. *Brain Sci.* 9:65.
35
36
37
38
39
40
41
42
43
44
45
46
47
48
49
50
51
52
53
54
55
56
57
58
59
60

Figure 1

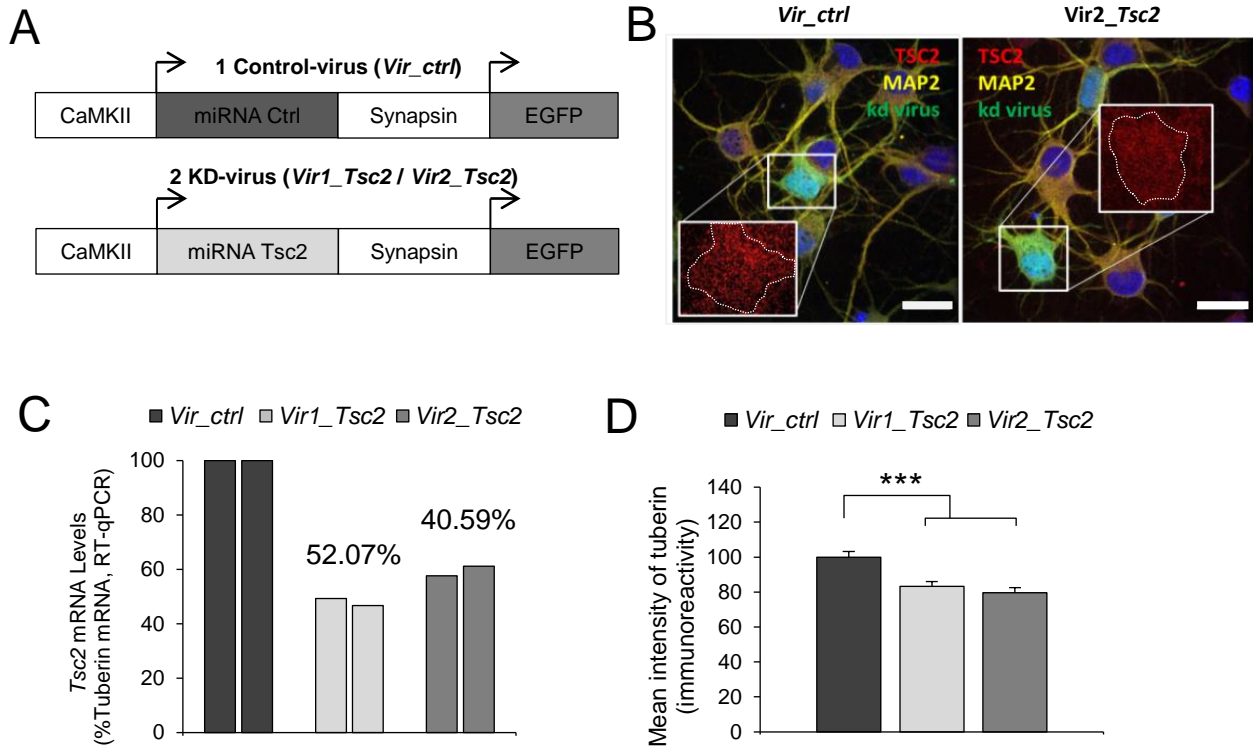
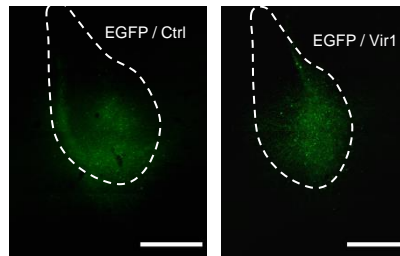
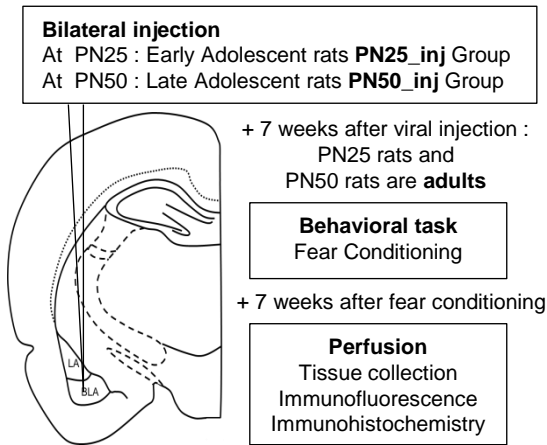
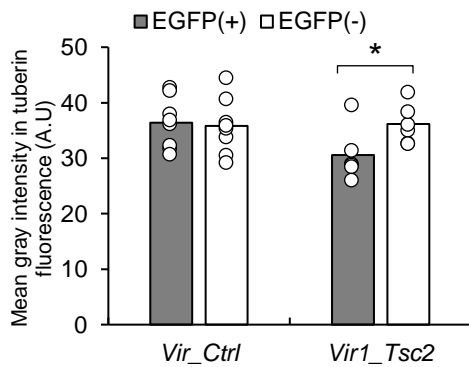


Figure 2

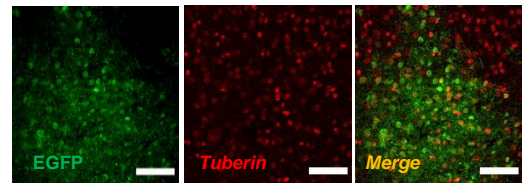
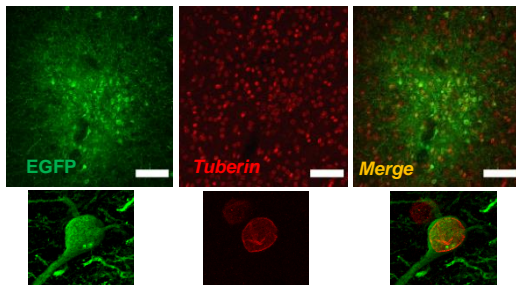
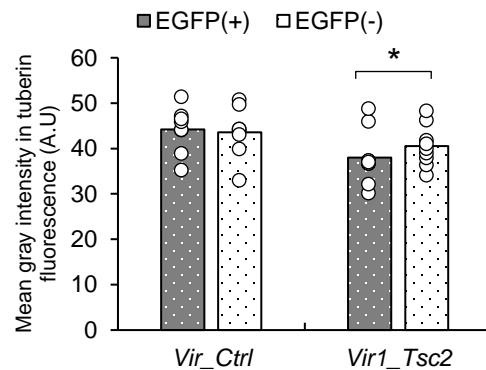
A



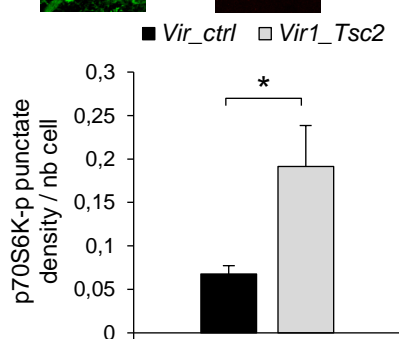
B



C



D



E

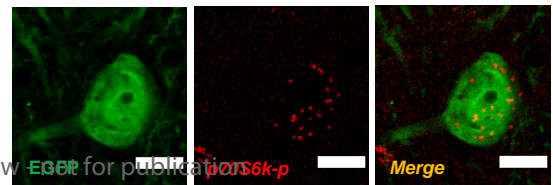
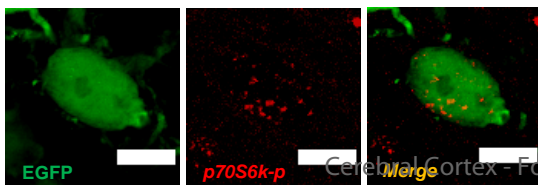
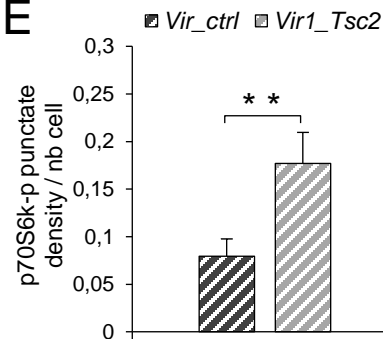
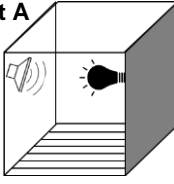
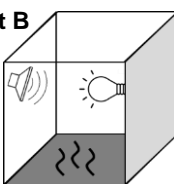
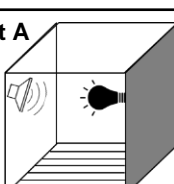
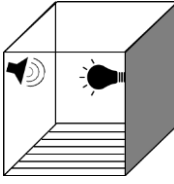




Figure 3

A

| | | |
|-----------------------------------|-------------------------------------|--|
| Day 1 Habituation | 5 CS — 30 s 4 kHz | Context A  |
| Day 2 Fear Learning | 7 CS — 30 s 7 US — 0.5 s, 0.5 mA |  |
| Day 3 Fear Extinction | 20 CS — 30 s 4 kHz | Context B  |
| Day 4 Extinction Recall | 5 CS — 30 s 4 kHz |  |
| Day 5 Renewal | 5 CS — 30 s 4 kHz | Context A  |
| Generalization | 5 new tone — 30 s 11 kHz |  |

B

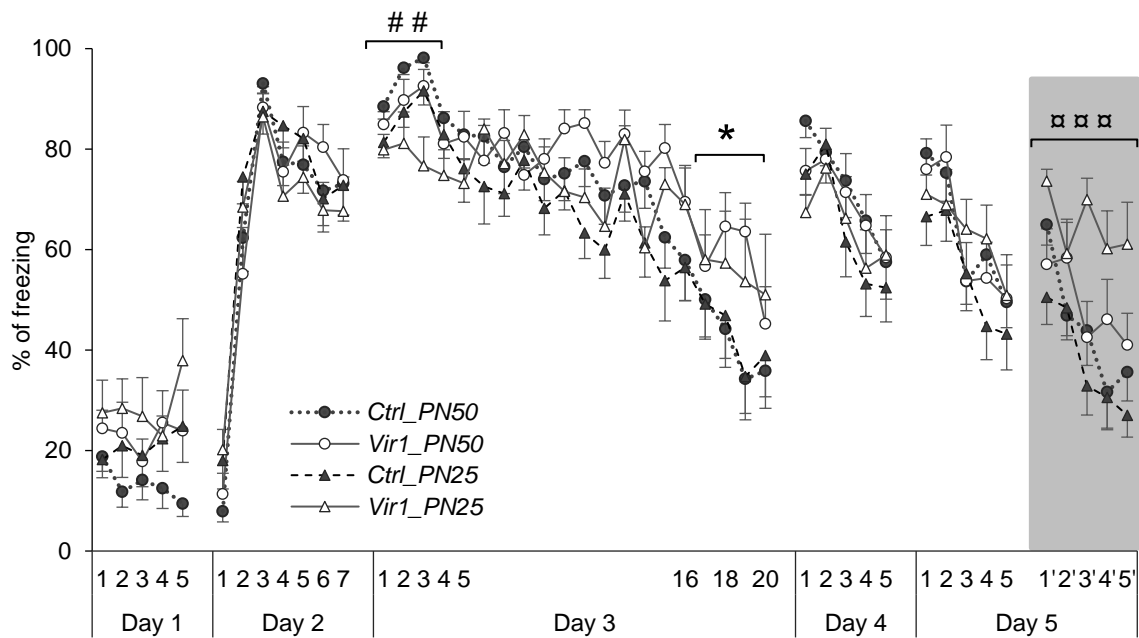


Figure 4

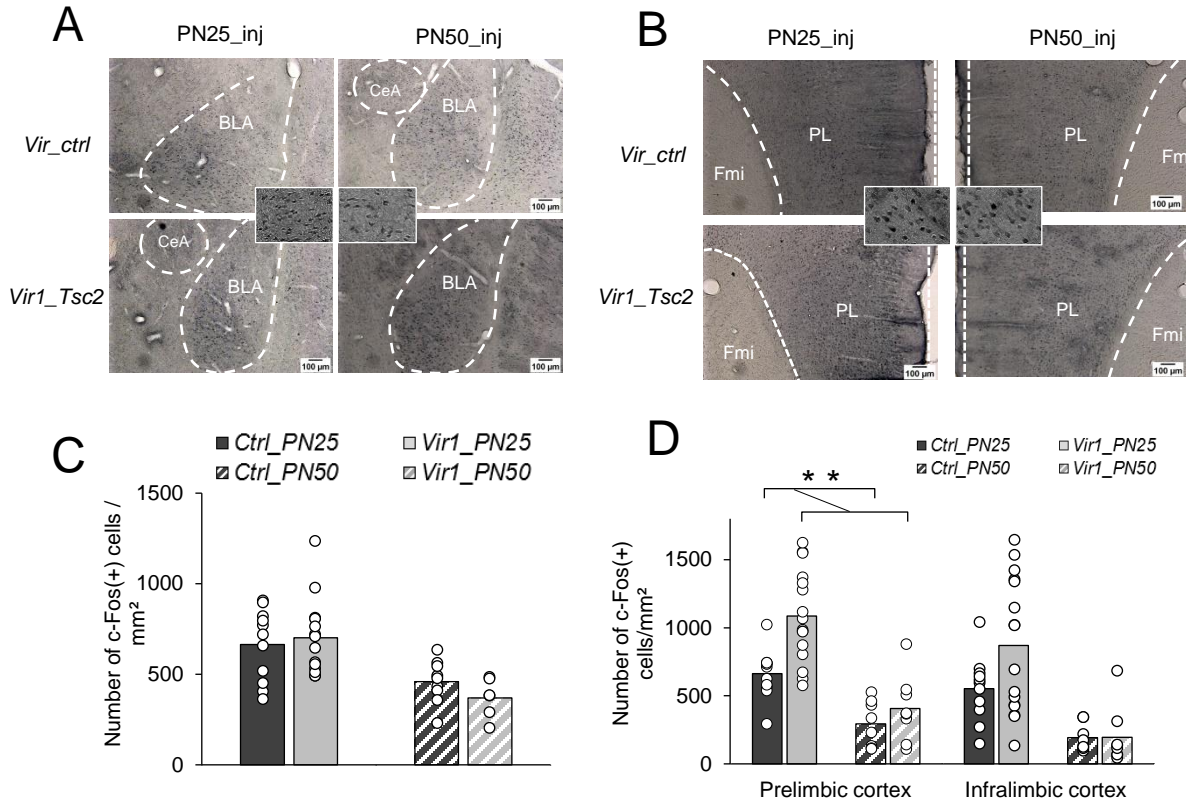


Figure 5

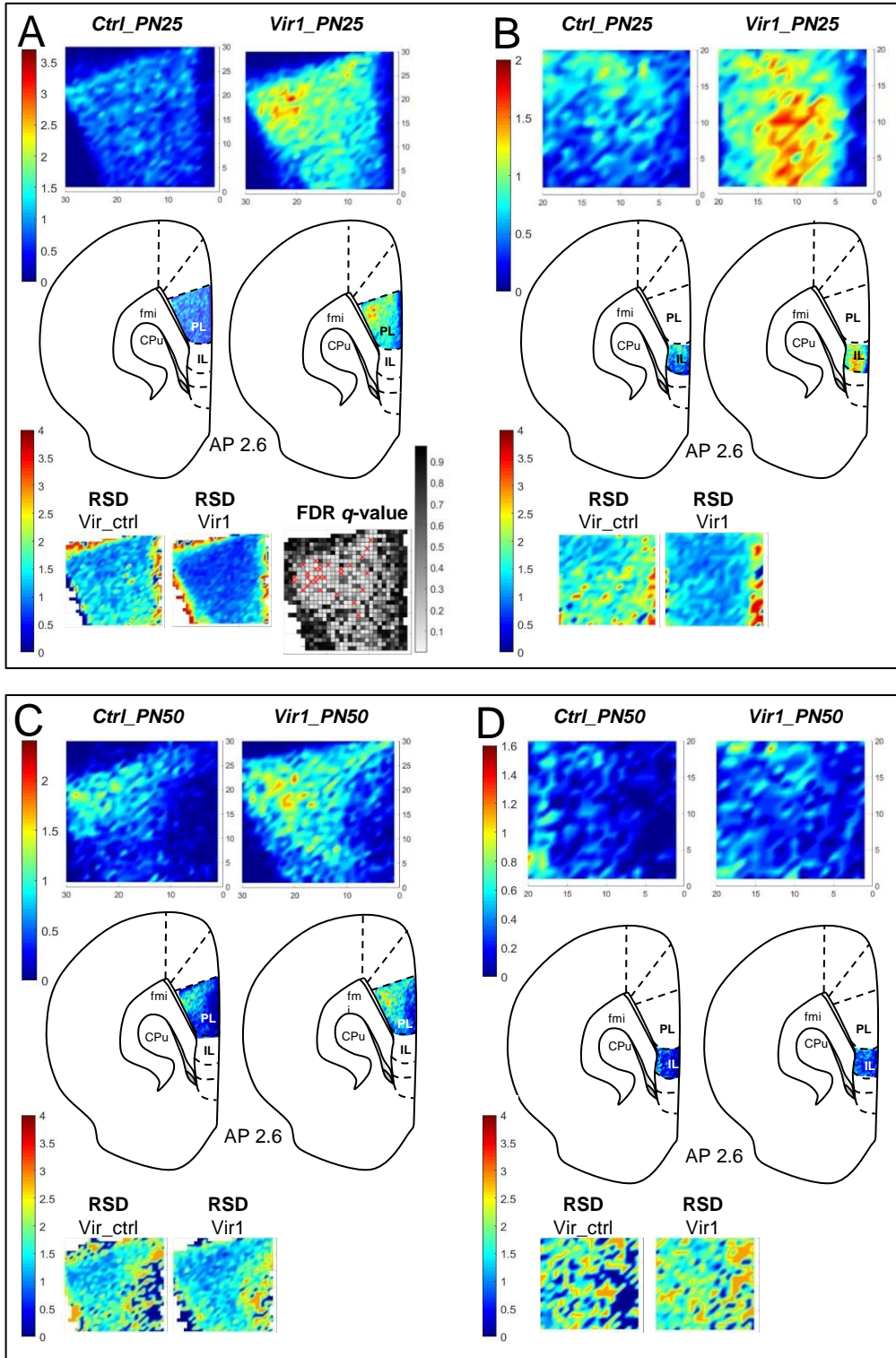
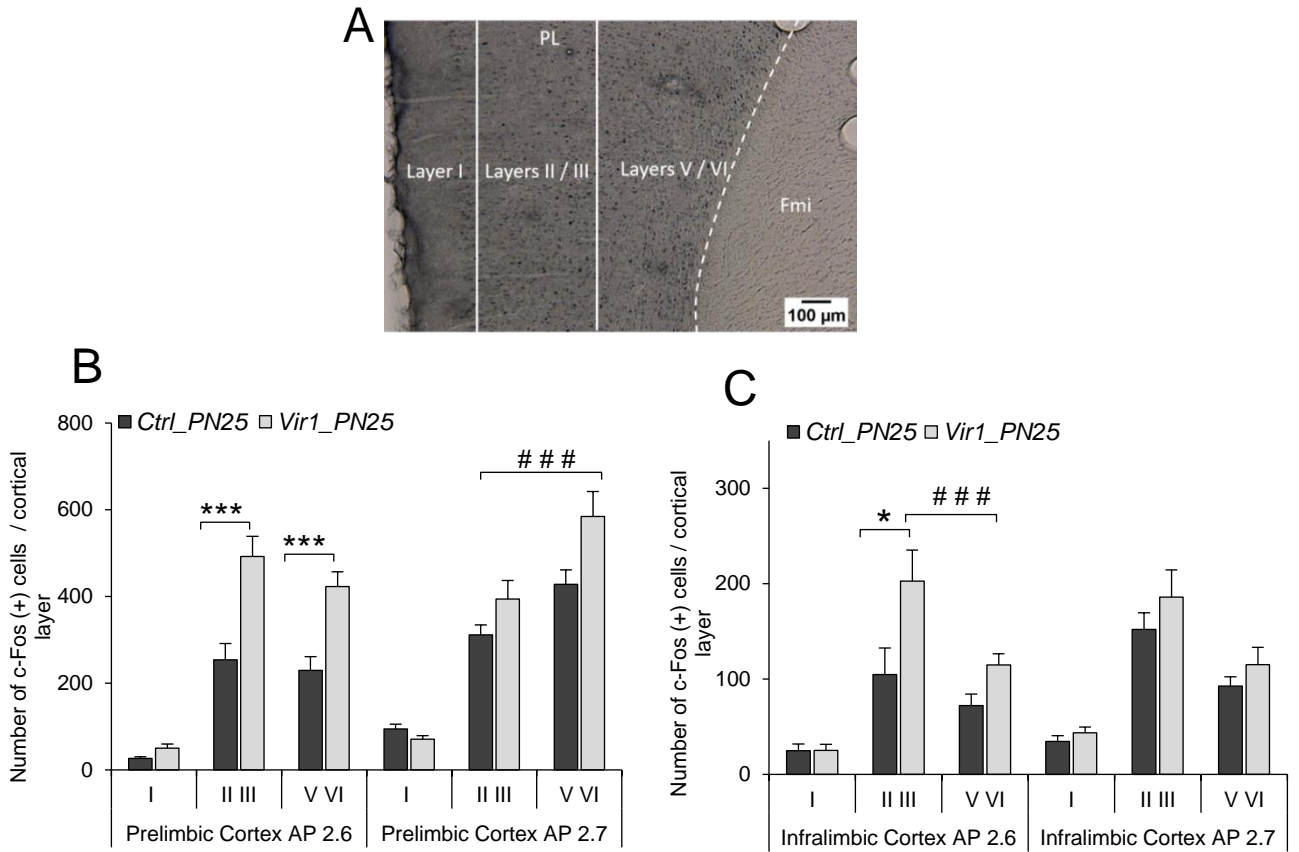
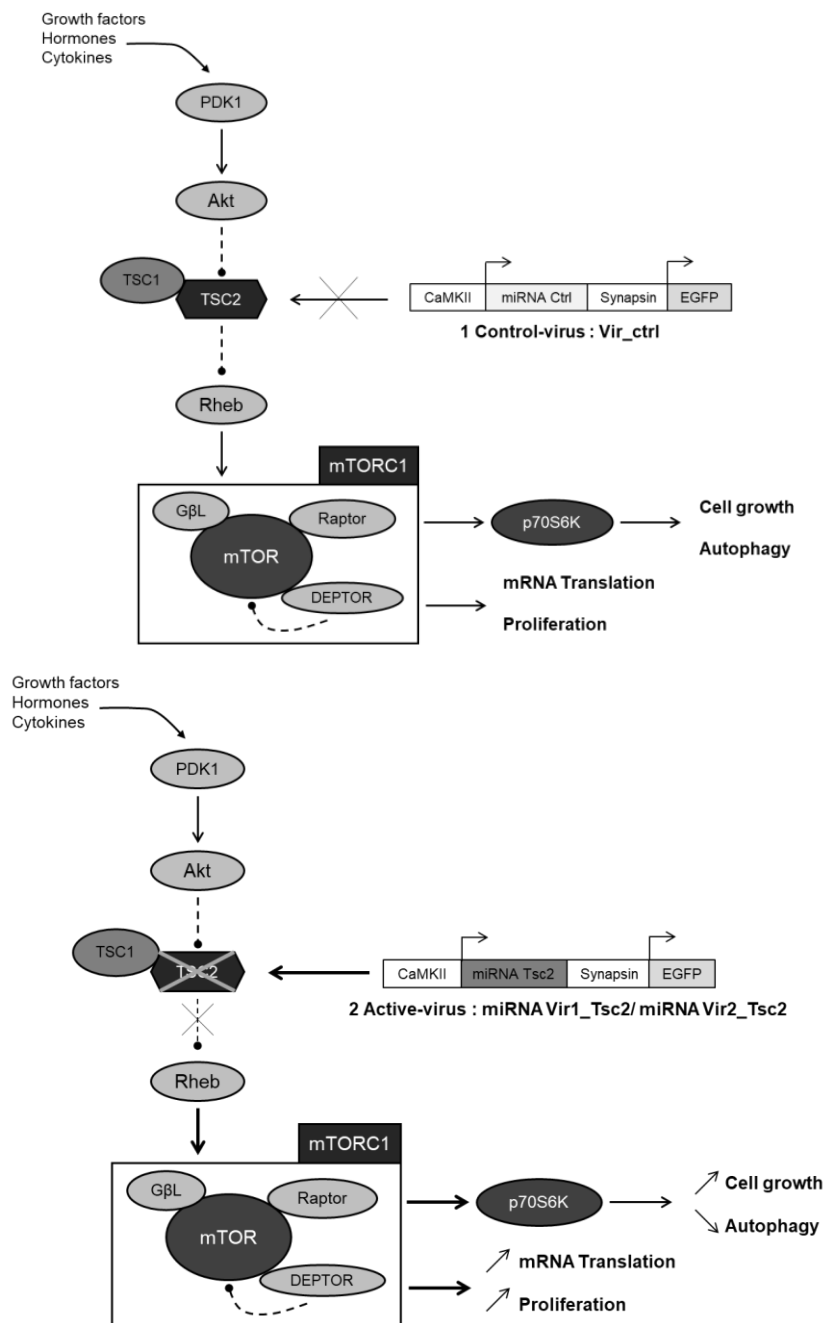


Figure 6

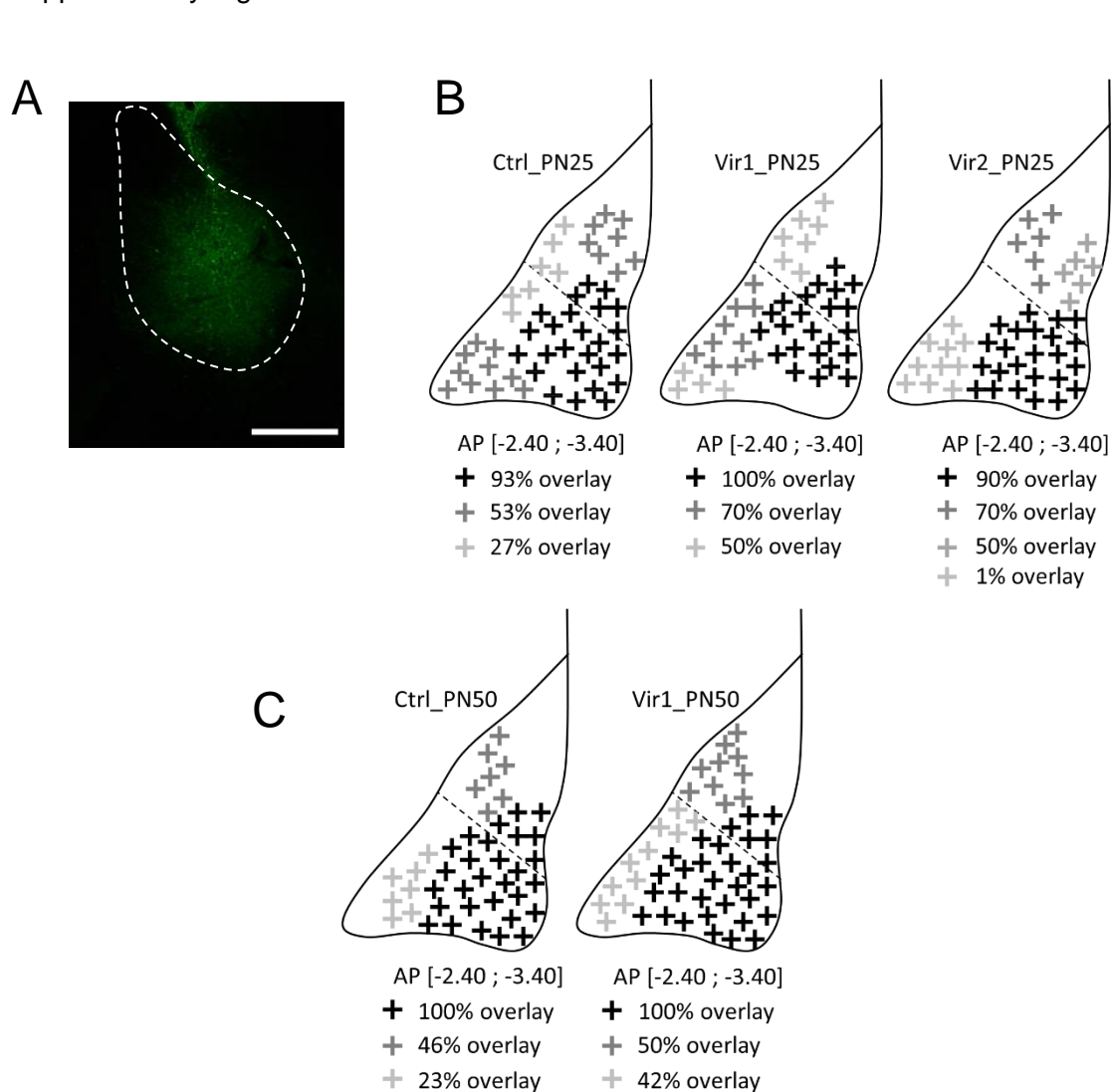


Supplementary Figure 1



Supplementary Figure 1. Lentiviral-vector mechanisms of action. Diagrams show the *Tsc2*/mTOR signaling pathway in baseline condition in presence of the control vector (*Vir_ctrl*, up) that expresses a control miRNA and EGFP, and in presence of the knock-down vectors *Vir1_Tsc2* or *Vir2_Tsc2* (down) that expresses both EGFP and a miRNA targeting the *Tsc2* protein. *Tsc2* plays as a negative regulator of mammalian Target of Rapamycin (mTOR), a serine/threonine kinase participating in the formation of the protein complex mTORC1. When activated, the mTORC1 complex promotes protein synthesis and proliferation, as well as cell growth and decreases autophagy processes through the activation of p70-S6 Kinase 1 (p70S6K). Hence, by reducing *Tsc2* protein expression in transduced cells, the lentiviral constructions (*Vir1_Tsc2* and *Vir2_Tsc2*) induce a constitutive activation of the mTORC1 pathway.

Supplementary Figure 2



Supplementary Figure 2. Ex vivo characterization of viral transduction efficiency following injection in the basolateral amygdala. (A) Sample image showing lentiviral transduction efficiency in BLA cells from PN25 rats injected with *Vir2_Tsc2*. Scale bar = 100 μ m. (B) Diagrams depicting the viral EGFP distribution in BLAs of animals injected at PN25 with *Vir_ctrl*, *Vir1_Tsc2*, or *Vir2_Tsc2* observed at antero-posteriority from -2.40 to -3.40 millimeter posterior to Bregma ([-2.40; -3.40]). Percentages represent the proportion of animals presenting an overlying viral EGFP signal in distinct zones of the BLA, illustrated by different “+” symbols. Dotted line delineates the separation between the lateral amygdala (above) and the basal amygdala (below). (C) Diagrams depicting the viral EGFP distribution in BLAs of animals injected at PN50 with *Vir_ctrl* or *Vir1_Tsc2* observed at antero-posteriority from -2.40 to -3.40 millimeter posterior to Bregma ([-2.40; -3.40]). Percentages represent the proportion of animals presenting an overlying EGFP fluorescence in distinct zones. Dotted line delineates the separation between the lateral amygdala (above) and the basal amygdala (below).

Supplementary Table 1

A

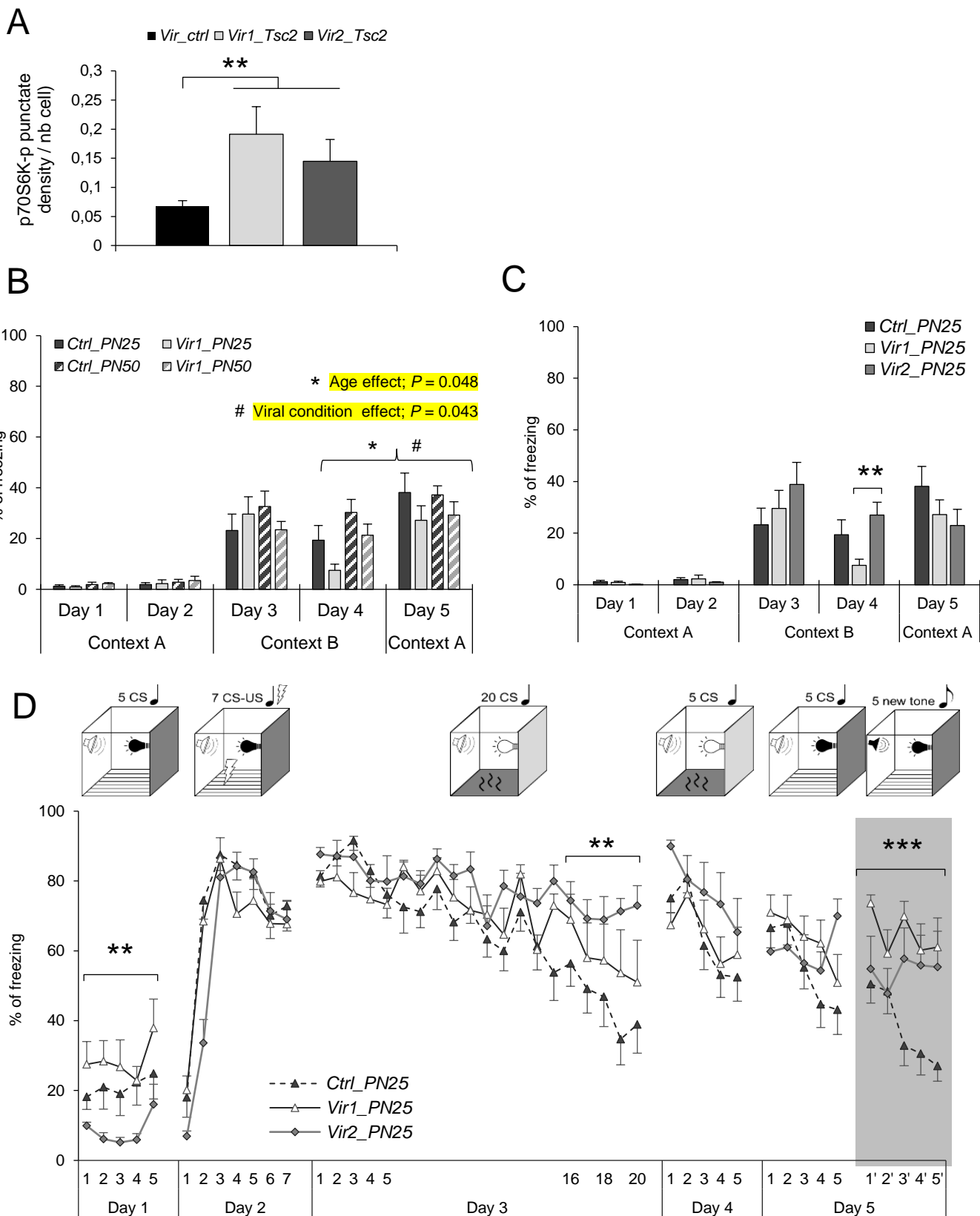
| Three-Way ANOVA Fear conditioning. Percentage of freezing to context (=Day) | Day (within subject) | Viral Condition (between subject) | Age (between subject) | Day x Viral condition | Day x Age | Viral condition x Age | Day x Viral Condition x Age |
|---|--|--|--|--------------------------------|--|--------------------------------|---------------------------------|
| All contexts Day 1 to Day 5 | F(4,164) = 43.746, P < 0.001 | F(1,41) = 2.286, P = 0.138 | F(1,41) = 1.725, P = 0.196 | F(4,164) = 1.52, P = 0.199 | F(4,164) = 1.619, P = 0.172 | F(1,41) = 0.120, P = 0.731 | F(4,164) = 0.711, P = 0.585 |
| Day 1 (context A) | X | F(1,41) = 0.0042, P = 0.949 | F(1,41) = 2.1700, P = 0.148 | X | X | F(1,41) = 0.1726, P = 0.680 | X |
| Day 2 (context A) | X | F(1,46) = 0.1642, P = 0.687 | F(1,46) = 0.8067, P = 0.374 | X | X | F(1,46) = 0.0081, P = 0.929 | X |
| Day 3 (context B) | X | F(1,46) = 0.0533, P = 0.819 | F(1,46) = 0.0766, P = 0.783 | X | X | F(1,46) = 1.6912, P = 0.200 | X |
| Day 4 (context B) | X | F(1,46) = 4.2697, P = 0.044 | F(1,46) = 6.0024, P = 0.018 | X | X | F(1,46) = 0.0850, P = 0.772 | X |
| Day 5 (context A) | X | F(1,46) = 2.4120, P = 0.127 | F(1,46) = 0.0094, P = 0.923 | X | X | F(1,46) = 0.059, P = 0.809 | X |
| Day 2 context A vs Day 3 context B | F(1,46) = 63.0015, P < 0.001 | F(1,46) = 0.0215, P = 0.884 | F(1,46) = 0.2122, P = 0.647 | F(1,46) = 0.0077, P = 0.930 | F(1,46) = 0.0917, P = 0.763 | F(1,46) = 1.6316, P = 0.208 | F(1,46) = 1.6137, P = 0.210 |
| Day 4 context B vs Day 5 context A | F(1,46) = 21.2168, P < 0.001 | F(1,46) = 4.3165, P = 0.043 | F(1,46) = 1.8292, P = 0.183 | F(1,46) = 0.0270, P = 0.870 | F(1,46) = 4.1221, P = 0.048 | F(1,46) = 0.0950, P = 0.759 | F(1,46) = 3.06e-6, P = 0.999 |

B

| Three-Way ANOVA Fear conditioning. Percentage of freezing to tone (=Trial) | Trial (within subject) | Viral Condition (between subject) | Age (between subject) | Trial x Viral condition | Trial x Age | Viral condition x Age | Trial x Viral Condition x Age |
|---|---|--|---|--------------------------------|--|--|----------------------------------|
| Day 1 - Habituation | F(4,164) = 0.724, P = 0.577 | F(1,41) = 3.3754, P = 0.073 | F(1,41) = 2.0272, P = 0.162 | F(4,164) = 0.622, P = 0.647 | F(4,164) = 1.589, P = 0.180 | F(1,41) = 0.049, P = 0.825 | F(4,164) = 0.713, P = 0.584 |
| Day 2 - Fear learning | F(6,276) = 124.638, P < 0.001 | F(1,46) = 0.2676, P = 0.607 | F(1,46) = 0.0726, P = 0.789 | F(6,276) = 0.953, P = 0.436 | F(6,276) = 2.825, P = 0.025 | F(1,46) = 0.493, P = 0.486 | F(6,276) = 0.638, P = 0.640 |
| Day 3 - Extinction 1-5 | F(4,184) = 7.771, P < 0.001 | F(1,46) = 3.125, P = 0.084 | F(1,46) = 6.289, P = 0.016 | F(4,184) = 1.041, P = 0.376 | F(4,184) = 0.528, P = 0.661 | F(1,46) = 0.163, P = 0.688 | F(4,184) = 0.409, P = 0.745 |
| Day 3 - Extinction 16-20 | F(4,184) = 9.790, P < 0.001 | F(1,46) = 4.222, P = 0.046 | F(1,46) = 0.0099, P = 0.921 | F(4,184) = 1.580, P = 0.201 | F(4,184) = 0.462, P = 0.692 | F(1,46) = 0.043, P = 0.835 | F(4,184) = 0.0449, P = 0.700 |
| Day 4 - Extinction Recall | F(4,184) = 16.338, P < 0.001 | F(1,46) = 0.0642, P = 0.801 | F(1,46) = 1.7856, P = 0.188 | F(4,184) = 1.076, P = 0.363 | F(4,184) = 0.981, P = 0.407 | F(1,46) = 0.112, P = 0.738 | F(4,184) = 0.183, P = 0.918 |
| Day 5 - Renewal | F(4,184) = 27.994, P < 0.001 | F(1,46) = 0.482, P = 0.491 | F(1,46) = 0.462, P = 0.500 | F(4,184) = 0.288, P = 0.847 | F(4,184) = 2.018, P = 0.109 | F(1,46) = 0.721, P = 0.400 | F(4,184) = 1.054, P = 0.374 |
| Day 5 - Generalization | F(4,184) = 10.374, P < 0.001 | F(1,46) = 14.03, P < 0.001 | F(1,46) = 1.18, P = 0.284 | F(4,184) = 1.340, P = 0.257 | F(4,184) = 0.379, P = 0.824 | F(1,46) = 7.25, P = 0.010 | F(4,184) = 2.160, P = 0.075 |

Supplementary Table 1: Detailed statistical analysis of the fear conditioning experiment. (A) The table shows the F and P values obtained following two-way ANOVAs (Age x Viral condition) comparing the percent freezing to context (before the appearance of the first tone) for each testing day (day 1 to day 5), and planned three-way ANOVAs with repeated measures (day) comparing percent of freezing to context at Day 2 vs Day 3, or Day 4 vs Day 5 between rats injected with *Vir_ctrl* or *Vir1_Tsc2* at PN25 or PN50. Characters in bold highlight significant differences. **(B)** The table shows the F and P values obtained following three-Way ANOVAs with repeated Measure (trials) comparing the percent freezing to tone during each testing day (day 1 to day 5) between rats injected with *Vir_ctrl* or *Vir1_Tsc2* at PN25 or PN50. Characters in bold highlight significant differences.

Supplementary Figure 3



1
2
3
4 **Supplementary Figure 3. *Vir2_Tsc2* had similar effects than *Vir1_Tsc2* on p70S6K-p density and fear**
5 **behavior in PN25_injected rats. (A)** Semi-quantitative analysis of p70S6K-p fluorescent punctate in EGFP(+)
6 cells of PN25_inj rats with *Vir_Ctrl*, *Vir1*, or *Vir2_Tsc2*. Histograms show the density of punctate counted in cells co-
7 expressing viral EGFP per number of cells. Note the significant elevation of p70S6K-p protein expression in BLA
8 cells transduced by the KD-virus (*Vir1_Tsc2*, $n = 9$ amygdalae; *Vir2_Tsc2*, $n = 14$ amygdalae) compared to BLA
9 cells transduced with the control vector (*Vir_ctrl*, $n = 13$ amygdalae; Helmert contrast test *Vir_Ctrl* vs [*Vir1*,*Vir2*], $**P = 0.017$) **(B)** Enhanced reactivity to the initial learning context during renewal session in rats injected at PN25.
10 Percentage of freezing to context alone, measured before the first CS for each experimental group (*Vir_ctrl*
11 PN25_inj, $n = 15$; *Vir1_Tsc2* PN25_inj, $n = 10$; *Vir_ctrl* PN50_inj, $n = 13$; *Vir1_Tsc2* PN50_inj, $n = 12$) over the 5
12 days of the experiment (see protocol in **Fig. 3A**, **statistical details in Supplementary Table 1A**). Comparisons
13 between Day 4 and Day 5 revealed a significant Day x Age interaction (3-Way RM ANOVA (Day (4-5) x Viral
14 Condition x Age); (Day (4-5) x Age interaction); $*P = 0.048$). Bonferroni *post hoc* analyses revealed that
15 PN25_injected rats had a higher level of freezing in Context A on Day 5 compared to Day 4 in context B (PN25_inj
16 Day 4 vs Day 5, Bonferroni *post hoc* test; $P_{bonf} < 0.001$), suggesting an enhanced reactivity for PN25_inj rats
17 compared to PN50_inj rats (PN50_inj rats, Day 4 vs Day 5, $P_{bonf} = 0.434$) when animals were returned to the
18 initial training context. Moreover, a significant Viral condition effect was revealed, (Viral condition effect, $^{\#}P = 0.043$),
19 suggesting that animals injected with *Vir1_Tsc2* froze less than *Vir_ctrl* injected ones, whatever the age of
20 injection. **(C)** Contextual fear compared between rats injected with *Vir_ctrl*, *Vir1_Tsc2* and *Vir2_Tsc2* at PN25. In
21 order to evaluate putative off-target effects, freezing responses to the context alone of PN25_inj animals were
22 compared in three Viral Conditions (*Vir_ctrl*, $n = 15$; *Vir1_Tsc2*, $n = 10$; *Vir2_Tsc2*, $n = 10$). *Vir2_Tsc2* animals
23 injected at PN25 showed a higher level of fear to the extinction context on Day 4, 24 hours after extinction Day.
24 (Helmert Contrast test *Vir1_Tsc2* vs *Vir2_Tsc2*, $**P = 0.018$; See **Table S2A** for context detailed statistics) **(D)** Rats
25 injected with the second KD virus (*Vir2_Tsc2*) at PN25 also showed retarded fear extinction and fear
26 overgeneralization to a new tone. Percent freezing was measured as in **Fig. 3B** (*Vir_ctrl* $n = 15$, *Vir1_Tsc2* $n = 10$
27 or *Vir2_Tsc2* $n = 10$). See **Table S2B** for freezing to tone detailed statistics. Helmert contrast analysis showing a
28 significant higher level of freezing for rats injected with *Vir1_Tsc2* compared to *Vir2_Tsc2* during habituation (Day
29 1, $**P = 0.008$), and a higher level of freezing for both active viral conditions compared to control at the end of the
30 extinction session on Day 3 ($**P = 0.016$), as already shown for *Vir1_Tsc2* in **Fig. 3B**. They also presented a higher
31 level of freezing to the new tone during generalization testing on day 5 (highlighted in gray) for both *Vir1_Tsc2* and
32 *Vir2_Tsc2* injected animals as well ($***P < 0.001$), reflecting an overgeneralization of cued fear in rats injected with
33 active vectors at PN25.
34
35
36
37
38
39
40
41
42
43
44
45
46
47
48
49
50
51
52
53

Supplementary Table 2

A

| Helmert contrast test Percentage of freezing to context | CTRL vs <i>Vir1</i> , <i>Vir2</i> | <i>Vir1</i> vs <i>Vir2</i> |
|---|--------------------------------------|---|
| Day 1 (context A) | $t(32) = 1.093$, $P = 0.282$ | $t(32) = 1.041$, $P = 0.306$ |
| Day 2 (context A) | $t(32) = 0.352$, $P = 0.727$ | $t(32) = 0.906$, $P = 0.372$ |
| Day 3 (context B) | $t(32) = -1.301$, $P = 0.203$ | $t(32) = -0.832$, $P = 0.412$ |
| Day 4 (context B) | $t(32) = 0.359$, $P = 0.722$ | $t(32) = -2.493$, $P = 0.018$ |
| Day 5 (context A) | $t(32) = 1.550$, $P = 0.131$ | $t(32) = 0.358$, $P = 0.722$ |
| Day 2 context A vs Day 3 context B | $t(32) = -1.235$, $P = 0.226$ | $t(32) = -0.703$, $P = 0.487$ |
| Day 4 context B vs Day 5 context A | $t(32) = 1.212$, $P = 0.235$ | $t(32) = -0.959$, $P = 0.345$ |

B

| Helmert contrast test Percentage of freezing to tone | CTRL vs <i>Vir1</i> , <i>Vir2</i> | <i>Vir1</i> vs <i>Vir2</i> |
|--|--|--|
| Day 1 Habituation | $t(32) = 0.447$, $P = 0.658$ | $t(32) = 2.818$, $P = 0.008$ |
| Day 2 Fear learning | $t(32) = 1.298$, $P = 0.203$ | $t(32) = 0.607$, $P = 0.548$ |
| Day 3 Extinction 1-5 | $t(32) = 0.827$, $P = 0.414$ | $t(32) = -1.444$, $P = 0.158$ |
| Day 3 Extinction 16-20 | $t(32) = -2.539$, $P = 0.016$ | $t(32) = -1.293$, $P = 0.205$ |
| Day 4 Extinction Recall | $t(32) = -1.273$, $P = 0.212$ | $t(32) = -1.830$, $P = 0.077$ |
| Day 5 Renewal | $t(32) = -1.063$, $P = 0.296$ | $t(32) = 0.395$, $P = 0.695$ |
| Day 5 Generalization | $t(32) = -4.587$, $P < 0.001$ | $t(32) = 1.695$, $P = 0.100$ |

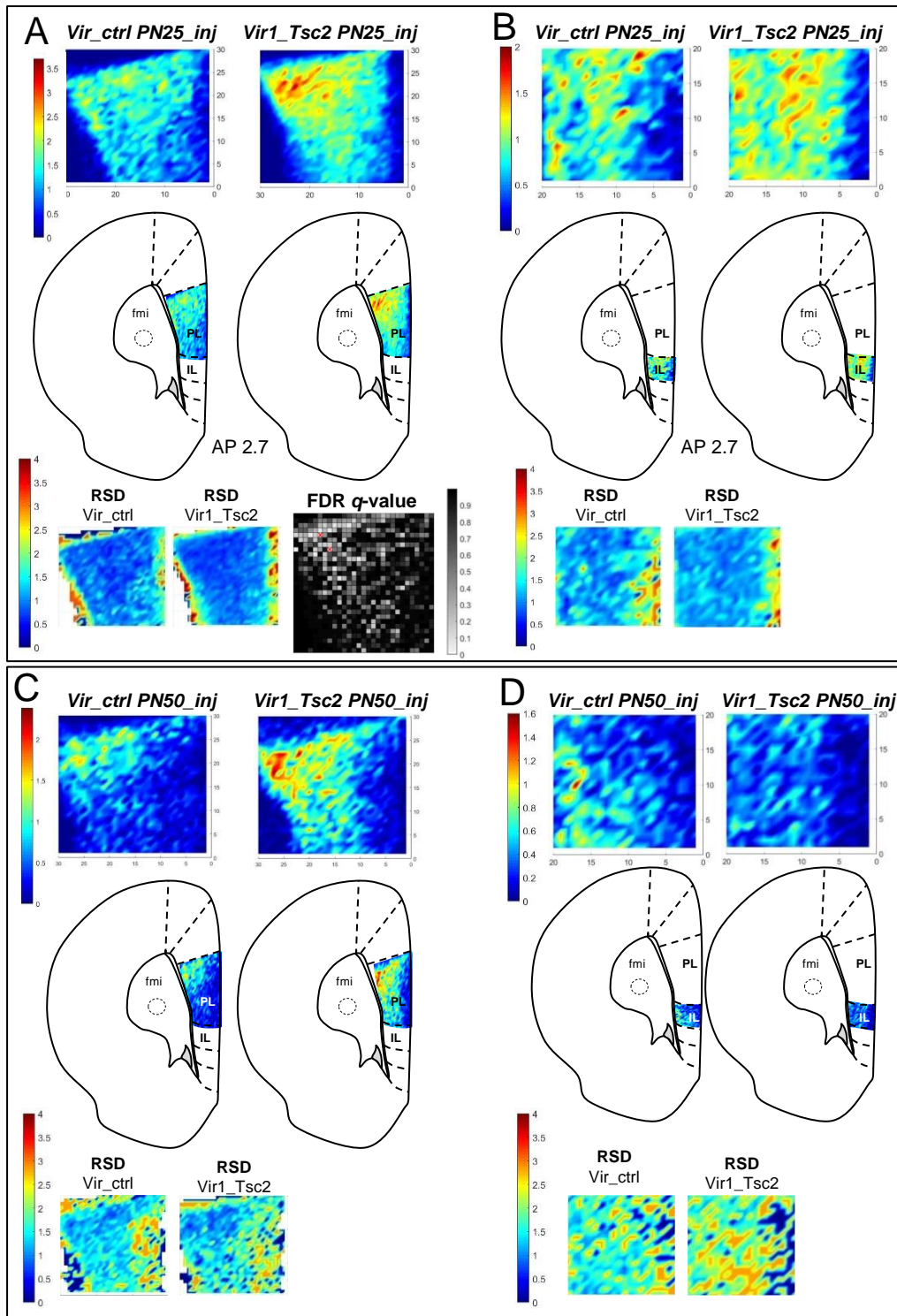
Supplementary Table 2. Helmert contrast analysis of percent freezing to context or to tones in rats injected at PN25. (A) Statistical table shows the t and P values obtained following a Helmert contrast test comparing the percent freezing at each context (before the presentation of the first tone) for each testing day (day 1 to day 5), and comparing the percent freezing to context day 2 vs day 3, or day 4 vs day 5, for animals injected with *Vir_ctrl* vs [*Vir1_Tsc2* and *Vir2_Tsc2*] (first column), and between *Vir1_Tsc2* and *Vir2_Tsc2* animals (second column). Characters in bold highlight significant differences. **(B)** Statistical table shows the t and P values obtained following a Helmert contrast test comparing the percent freezing to tone at each testing day for animals injected with *Vir_ctrl* vs [*Vir1_Tsc2* and *Vir2_Tsc2*] animals (first column), and between *Vir1_Tsc2* and *Vir2_Tsc2* animals (second column). Characters in bold highlight significant differences.

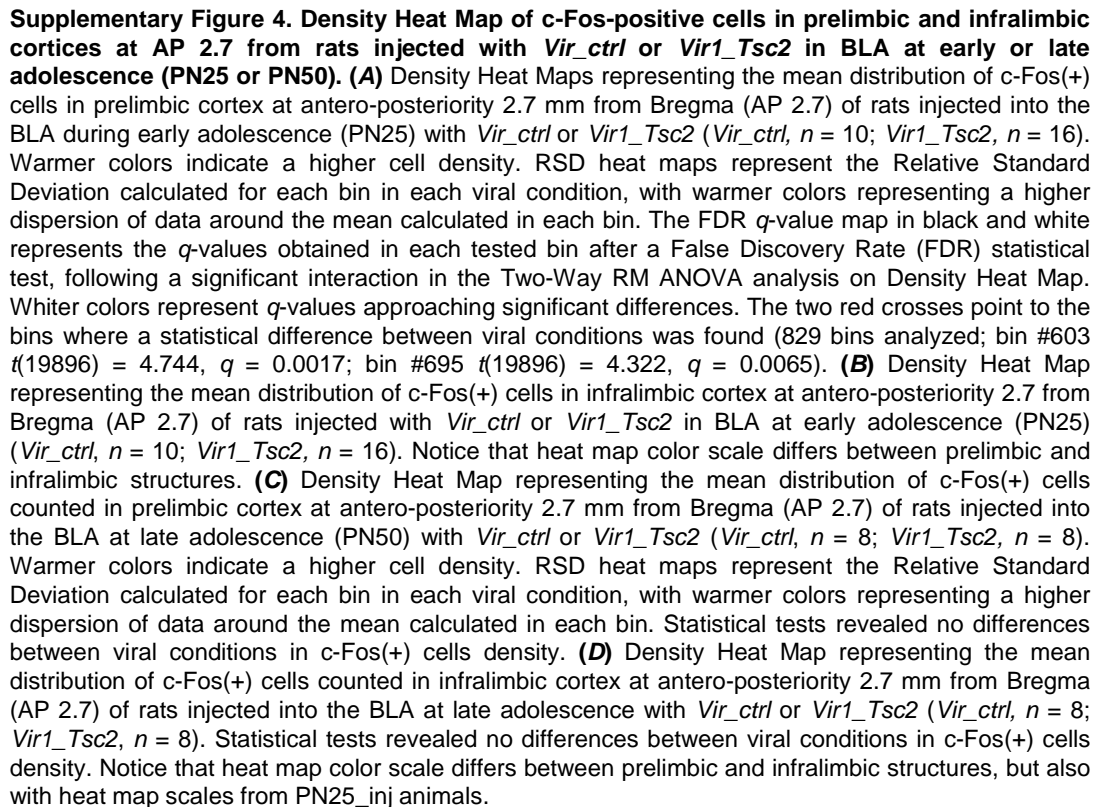
Supplementary Table 3

| Two-Way Repeated Measures ANOVA: Density Heat Map | XY Coordinates (within subject) | Viral Condition (between subject) | XY Coordinates x Viral Condition |
|---|--|--|---|
| PN25_injected animals | | | |
| Prelimbic cortex AP 2.6 | F(829,18238) = 5.39, P < 0.0001 | F(1,22) = 20.49, P = 0.0002 | F(829,18238) = 1.49, P < 0.0001 |
| Infralimbic cortex AP 2.6 | F(399,8778) = 2.251, P < 0.0001 | F(1,22) = 4.682, P = 0.0416 | F(399,8778) = 1.191, P = 0.0062 |
| Prelimbic cortex AP 2.7 | F(828,19872) = 6.23, P < 0.0001 | F(1,24) = 2.789, P = 0.1079 | F(828,19872) = 1.42, P < 0.0001 |
| Infralimbic cortex AP 2.7 | F(399,9576) = 3.273, P < 0.0001 | F(1,24) = 0.9255, P = 0.3456 | F(399,9576) = 0.9738, P = 0.6344 |
| PN50_injected animals | | | |
| Prelimbic cortex AP 2.6 | F(851,11914) = 2.739, P < 0.0001 | F(1,14) = 2.049, P = 0.1743 | F(851,11914) = 0.928, P = 0.9276 |
| Infralimbiccortex AP 2.6 | F(395,5530) = 1.763, P < 0.0001 | F(1,14) = 0.6347, P = 0.4389 | F(395,5530) = 0.9346, P = 0.8118 |
| Prelimbic cortex AP 2.7 | F(864,12096) = 3.235, P < 0.0001 | F(1,14) = 1.06, P = 0.3206 | F(864,12096) = 1.045, P = 0.1845 |
| Infralimbic cortex AP 2.7 | F(393,5502) = 1.561, P < 0.0001 | F(1,14) = 0.2877, P = 0.6001 | F(393,5502) = 0.9726, P = 0.6380 |

Supplementary Table 3. Statistical analysis of c-Fos(+) Density Heat Maps from adult rats injected at PN25 or PN50. F and P values were obtained from a Two-Way RM ANOVA analyzing XY Coordinates (Within factor) x Viral Condition (Between factor) from Density Heat Maps of c-Fos(+) cells counted in prelimbic and infralimbic cortices at both APs (2.6 and 2.7 mm from Bregma) for PN25 or PN50_injected rats. Characters in bold highlight significant values.

Supplementary Figure 4



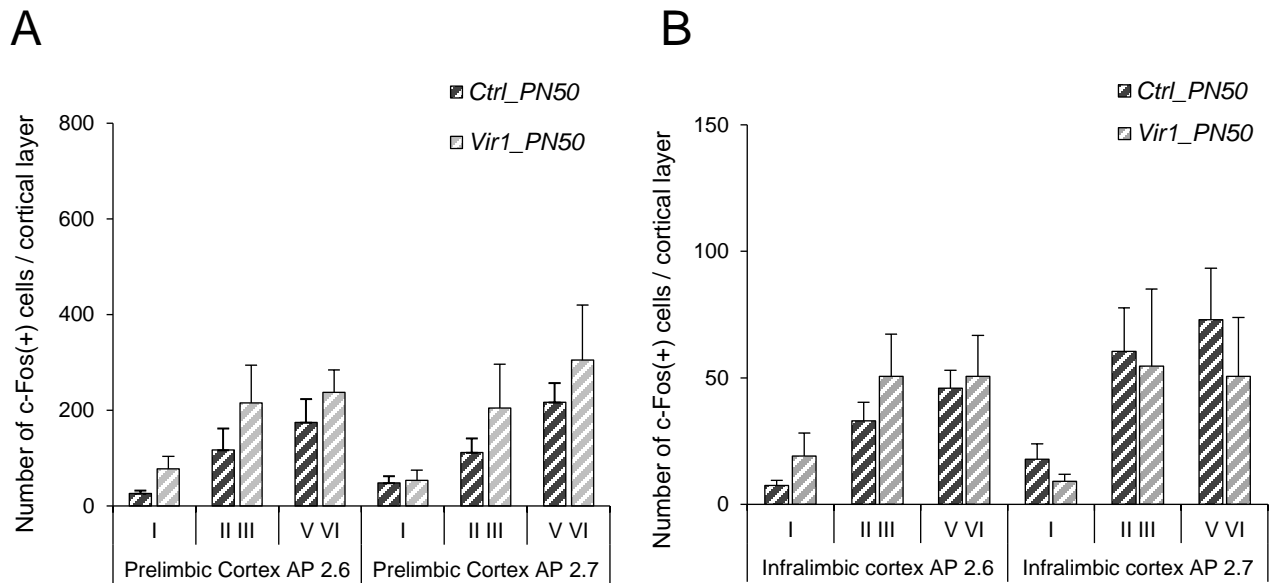
1
2
3 **Supplementary Figure 4. Density Heat Map of c-Fos-positive cells in prelimbic and infralimbic**
4 **cortices at AP 2.7 from rats injected with *Vir_ctrl* or *Vir1_Tsc2* in BLA at early or late**
5 **adolescence (PN25 or PN50). (A)** Density Heat Maps representing the mean distribution of c-Fos(+) 
6 cells in prelimbic cortex at antero-posteriority 2.7 mm from Bregma (AP 2.7) of rats injected into the
7 BLA during early adolescence (PN25) with *Vir_ctrl* or *Vir1_Tsc2* (*Vir_ctrl*, $n = 10$; *Vir1_Tsc2*, $n = 16$).
8 Warmer colors indicate a higher cell density. RSD heat maps represent the Relative Standard
9 Deviation calculated for each bin in each viral condition, with warmer colors representing a higher
10 dispersion of data around the mean calculated in each bin. The FDR q -value map in black and white
11 represents the q -values obtained in each tested bin after a False Discovery Rate (FDR) statistical
12 test, following a significant interaction in the Two-Way RM ANOVA analysis on Density Heat Map.
13 Whiter colors represent q -values approaching significant differences. The two red crosses point to the
14 bins where a statistical difference between viral conditions was found (829 bins analyzed; bin #603
15 $t(19896) = 4.744$, $q = 0.0017$; bin #695 $t(19896) = 4.322$, $q = 0.0065$). **(B)** Density Heat Map
16 representing the mean distribution of c-Fos(+) cells in infralimbic cortex at antero-posteriority 2.7 from
17 Bregma (AP 2.7) of rats injected with *Vir_ctrl* or *Vir1_Tsc2* in BLA at early adolescence (PN25)
18 (*Vir_ctrl*, $n = 10$; *Vir1_Tsc2*, $n = 16$). Notice that heat map color scale differs between prelimbic and
19 infralimbic structures. **(C)** Density Heat Map representing the mean distribution of c-Fos(+) cells
20 counted in prelimbic cortex at antero-posteriority 2.7 mm from Bregma (AP 2.7) of rats injected into
21 the BLA at late adolescence (PN50) with *Vir_ctrl* or *Vir1_Tsc2* (*Vir_ctrl*, $n = 8$; *Vir1_Tsc2*, $n = 8$).
22 Warmer colors indicate a higher cell density. RSD heat maps represent the Relative Standard
23 Deviation calculated for each bin in each viral condition, with warmer colors representing a higher
24 dispersion of data around the mean calculated in each bin. Statistical tests revealed no differences
25 between viral conditions in c-Fos(+) cells density. **(D)** Density Heat Map representing the mean
26 distribution of c-Fos(+) cells counted in infralimbic cortex at antero-posteriority 2.7 mm from Bregma
27 (AP 2.7) of rats injected into the BLA at late adolescence with *Vir_ctrl* or *Vir1_Tsc2* (*Vir_ctrl*, $n = 8$;
28 *Vir1_Tsc2*, $n = 8$). Statistical tests revealed no differences between viral conditions in c-Fos(+) cells
29 density. Notice that heat map color scale differs between prelimbic and infralimbic structures, but also
30 with heat map scales from PN25_inj animals.
31
32
33
34
35
36
37
38
39
40
41
42
43
44
45
46
47
48
49
50
51
52
53

Supplementary Table 4

| Two-Way Repeated Measures ANOVA : Cortical Layers | Layer (within subject) | Viral Condition (between subject) | Layer x Viral Condition |
|---|---|---|---|
| PN25_injected animals | | | |
| Prelimbic cortex AP 2.6 | F(2,44) = 79.054, P < 0.001 | F(1,22) = 24.962, P < 0.001 | F(2,44) = 7.729, P = 0.001 |
| Infralimbic cortex AP 2.6 | F(2,44) = 37.457, P < 0.001 | F(1,22) = 4.682, P = 0.042 | F(2,44) = 5.395, P = 0.024 |
| Prelimbic cortex AP 2.7 | F(2,48) = 93.591, P < 0.001 | F(1,24) = 2.789, P = 0.108 | F(2,48) = 4.147, P = 0.031 |
| Infralimbic cortex AP 2.7 | F(2,48) = 50.920, P < 0.001 | F(1,24) = 0.925, P = 0.346 | F(2,48) = 0.457, P = 0.547 |
| PN50_injected animals | | | |
| Prelimbic cortex AP 2.6 | F(2,28) = 21.542, P < 0.001 | F(1,14) = 2.047, P = 0.174 | F(2,28) = 0.498, P = 0.613 |
| Infralimbic cortex AP 2.6 | F(2,28) = 21.730, P < 0.001 | F(1,14) = 0.635, P = 0.439 | F(2,28) = 0.652, P = 0.529 |
| Prelimbic cortex AP 2.7 | F(2,28) = 27.395, P < 0.001 | F(1,14) = 1.060, P = 0.321 | F(2,28) = 1.517, P = 0.241 |
| Infralimbic cortex AP 2.7 | F(2,28) = 8.494, P = 0.006 | F(1,14) = 0.293, P = 0.597 | F(2,28) = 0.231, P = 0.694 |

Supplementary Table 4: Statistical analysis comparing the number of c-FOS(+) cells in different layers of prefrontal or infralimbic cortices depending on the viral condition for both ages of injection at both antero-posteriority from Bregma. F and p values were obtained following a Two-Way RM ANOVA comparing cells distribution in cortical LayerS (I, II III and V VI, Within factor) and viral condition (Between factor) at both APs for PN25 (up) or PN50_inj (down) rats. Characters in bold highlight significant effects.

Supplementary Figure 5



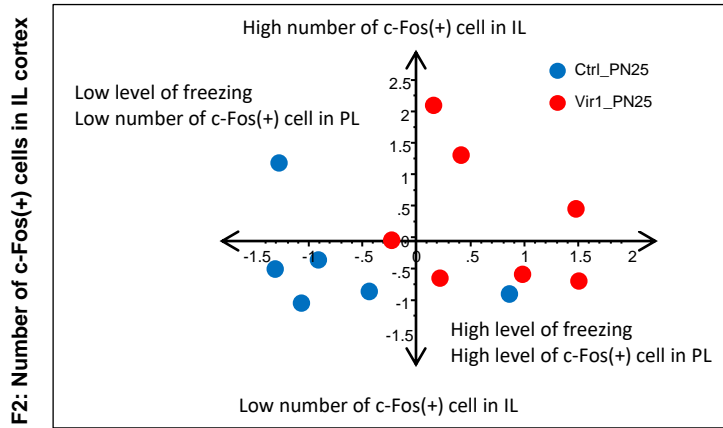
Supplementary Figure 5. Number of c-Fos(+) cells in different cortical layers of prelimbic and infralimbic cortices in rats injected in the BLA at late adolescence (PN50). (A) Number of c-Fos(+) cells are not significantly modified within the cortical layers of prelimbic cortex in rats injected with *Vir1_Tsc2* at late adolescence (PN50). The histogram show the number of c-Fos(+) cells sorted depending on the origin belonging layer at Bregma 2.6 and 2.7 mm from most superficial (Layer I) to deeper (Layers V VI) layers. No differences were observed between layers at both tested antero-posteriority. (B) Number of c-Fos(+) cells are not significantly modified within the cortical layers of infralimbic cortex in rats injected with *Vir1_Tsc2* at late adolescence (PN50). The histograms show the number of c-Fos(+) cells in infralimbic cortex sorted depending on their origin belonging layers at 2.6 mm and 2.7 mm from Bregma. (*Vir1_ctrl*, $n = 8$; *Vir1_Tsc2*, $n = 8$).

Supplementary Figure 6

A

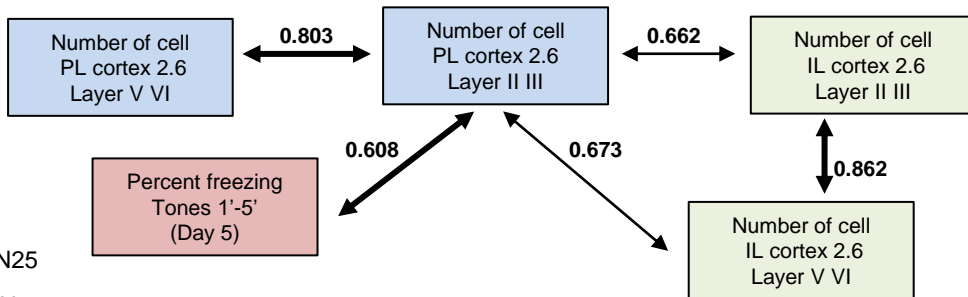
| Variables | Nb c-Fos(+) cell PL II III | Nb c-Fos(+) cell PL V VI | % freezing tones 1'-5' Generalization (Day 5) | % freezing tones 16-20 Extinction (Day 3) | Nb c-Fos(+) cell IL II III | Nb c-Fos(+) cell IL V VI |
|-----------|----------------------------|--------------------------|---|---|----------------------------|--------------------------|
| Factor 1 | 0.760 | 0.911 | 0.766 | 0.459 | 0.170 | 0.360 |
| Factor 2 | 0.514 | 0.169 | 0.274 | 0.556 | 0.952 | 0.870 |

B



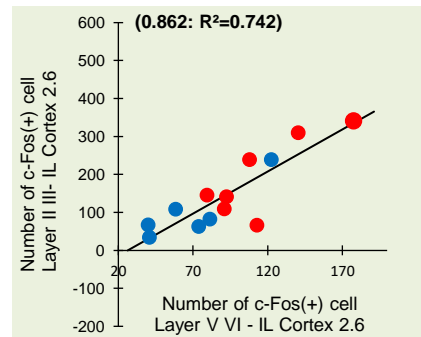
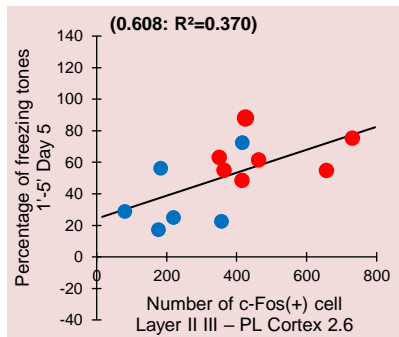
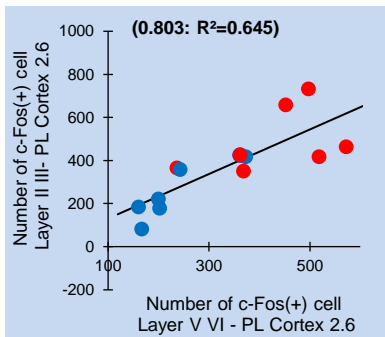
F1: Number of c-Fos(+) cells in PL cortex / Freezing to tones 1'-5' Generalization testing

C



● Ctrl_PN25

● Vir1_PN25



1
2
3 **Supplementary Figure 6. Principal Component Analysis and linear regression comparing freezing behavior and c-Fos**
4 **counting in mPFC of PN25_injected animals. (A)** Table recapitulating the weights of the six variables on the two principal
5 factors extracted by Principal Component Analysis (PCA). The six variables are: Number of c-Fos(+) cells in PL or IL cortices
6 in layers II III or V VI at AP 2.6, and percent freezing at the end of extinction (Day 3, Tones 16-20) or during generalization
7 testing (Day 5, Tones 1'-5'). Animals used in this analysis were injected at PN25 with either *Vir_ctrl* or *Vir1_Tsc2* (*n Vir_ctrl*
8 *PN25_inj* = 6; *n Vir1_Tsc2 PN25_inj* = 7). Orange-highlighted cells correspond to the variables presenting strong correlation
9 (>0.75) on one factor, and low correlation on the other factor, which is used to interpret the factors. **(B)** Scatter plot
10 representing the distribution of individual factor scores in an orthogonal graphical representation (x: factor 1, y: factor 2) of the
11 PCA. Animals injected at PN25 with *Vir1_Tsc2* (red dots) showed rightward shift of their distribution, as compared to rats
12 injected with the control vector (blue dots), illustrating their higher level of freezing during generalization correlated with higher
13 number of c-Fos(+) cells in PL cortex. **(C)** Correlation matrix following Principal Component Analysis. The diagram represents
14 the significant correlations (> 0.60) among pairs of variables. Arrows in the diagram show the significant R values (Pearson
15 correlation test, $P < 0.05$) between two tested variables. The three plots below illustrate the linear regression calculated for the
16 three most relevant correlations (thicker arrows, bold characters) and their related R values (left, 0.803, $P = 0.001$; middle,
17 0.608, $P = 0.027$; right, 0.862, $P = 0.0002$, Pearson Correlation test). In each plot, the black line represents the model of a R^2
18 =1. Dots represent individual PN25_inj animals of *Vir_ctrl* (blue) and *Vir1_Tsc2* (red) groups.
19
20
21
22
23
24
25
26
27
28
29
30
31
32
33
34
35
36
37
38
39
40
41
42
43
44
45
46
47
48
49
50
51
52
53
54
55
56